PB-230 046

REACTION OF HYDROGEN SULFIDE WITH FULLY CALCINED DOLOMITE

DISSERTATION FOR THE DOCTOR OF PHILOSOPHY

by

MELVYN PELL

1971

Reproduced by
NATIONAL TECHNICAL
INFORMATION SERVICE
U S Department of Commerce
Springfield VA 22151

MDCCCXLVII

Department of Chemical Engineering
THE CITY COLLEGE
THE CITY UNIVERSITY OF NEW YORK
NEW YORK, NEW YORK 10031

Grant AP00945
Air Programs Office
Environmental Protection Agency

PB 230 046

REACTION OF HYDROGEN SULFIDE
WITH FULLY CALCINED DOLOMITE

by

MELVYN PELL

A dissertation submitted to the Graduate
Faculty in Engineering in partial fulfillment
for the degree of Doctor of Philosophy, The
City University of New York.

1971

Reproduced by
NATIONAL TECHNICAL
INFORMATION SERVICE
U S Department of Commerce
Springfield VA 22151

COPYRIGHT BY
MELVYN PELL
1971

This manuscript has been read and accepted for the Graduate Faculty in Engineering in satisfaction of the dissertation requirement for the degree of Doctor of Philosophy.

May 14, 1971 Arthur M. Squires
Date Chairman of Examining Committee

Date Executive Officer

Prof. Arthur M. Squires (Chairman)
Prof. Robert A. Graff
Prof. Robert Pfeffer
Prof. Amos Turk
Supervisory Committee

The City University of New York

Abstract

Calcined dolomite is a candidate acceptor for H_2S in processes for gasifying or pyrolyzing sulfurous fuels, such as coal and residual oil, to provide sulfur-free fuels for use in power stations. Preferably, the processes would be satellite to power-generating apparatus.

Differential kinetic data are given for the reaction

$$[CaO+MgO] + H_2S = [CaS+MgO] + H_2O$$

between 475° and 900°C at H_2S partial pressures between 0.003 and 0.2 atmospheres. Data were obtained gravimetrically for both spherical and powder samples of stone.

to iii

Sphere data at 950°C disclose that the reaction is controlled by ash-layer diffusion at this temperature. The solid [CaS+MgO] produced at 950°C displays an internal effective diffusivity approximately 6% of the diffusivity in open space. This should be a fair approximation for the effective diffusivity for [CaS+MgO] prepared at lower temperatures.

Sphere data at lower temperature discloses that the reaction generally occurs homogeneously throughout the solid and that the rate is proportional to the quantity of unreacted CaO remaining in the sample. Although a gradient in concentration of CaS was observed near the surface of a

6 mm sphere reacted partially at 625°C, negligible gradient in CaS concentration would be expected in a particle of powder size.

The main features of data obtained for a powder of size -80+325 mesh appear to be explained by the assumption that activated adsorption of H_2S by unreacted CaO hinders the rate, the adsorption being in general not at equilibrium. An expression for the rate appears to require at least three kinetic constants: an adsorption rate constant, a desorption rate constant, and a reaction rate constant. The activation energy of the reaction kinetic constant is estimated to be 23 kcal/g-mole.

Some effects of steam concentration, hydrogen concentration, and sintering on the activity of calcined dolomite are discussed. (M)

Acknowledgements

I thank Prof. Arthur M. Squires and Prof. Robert A. Graff for their guidance and interest in this research.

Thanks are also due to John Bodnaruk and George DiIorio of the Chemical Engineering Shop for their assistance in constructing and setting up the experimental apparatus.

Special thanks are due my wife, Ellen, for her encouragement and patience.

Grant Number AP-00945 from the Air Pollution Control Office of the Environmental Protection Agency supported the major part of this work.

Presentations and Publications

Portions of this research appear in papers presented at meetings of the American Institute of Chemical Engineers:

A.M. Squires, R.A. Graff, and M. Pell, "Desulfurization of Fuels by Calcined Dolomite: I. Introduction and First Results", presented at Washington, D.C., November, 1969; Chem. Eng. Progr. Symposium Series, in press.

M. Pell, R.A. Graff, and A.M. Squires, "Desulfurization of Fuels by Calcined Dolomite: II. Reaction of CaO with H_2S", presented at Chicago, Illinois, December, 1970; Chem. Eng. Progr. Technical Manual, in press.

Table of Contents

Page

Abstract ii

Acknowledgements iv

Presentations and Publications v

Table of Contents vi

List of Tables xi

List of Figures xiii

1.0 Introduction 1

2.0 Object of Research 5

3.0 Significance of Research 6

4.0 Technical Background 8

  4.01 Calcined Dolomite and [CaS+MgO] 8

  4.02 Work of Gesellschaft für Kohlentechnik 10

  4.03 Consolidation Coal Company CO_2 Acceptor Gasification Process 12

  4.04 Squires' Fuel Desulfurization Processes 14

    4.04.1 Low Temperature Regeneration 15

    4.04.2 Process Example 16

5.0 Thermodynamic and Experimental Conditions 20

  5.01 Thermodynamic Equilibria 20

  5.02 Experimental Conditions 21

Table of Contents (continued)

Page

5.02.1 Desulfurization 21

5.02.2 Regeneration 22

5.02.3 Calcination 23

6.0 Experimental Techniques 25

6.01 Equipment 25

6.02 Procedures 32

6.03 Dolomite Feed Supply 33

6.03.1 Preparation of Samples 35

6.03.2 Capacity of Samples 36

7.0 Experimental Results 38

7.01 Runs with Powder Seeking a Kinetic Model 39

7.02 Nonequilibrium Adsorption Model 49

7.02.1 Introduction to Model 49

7.02.2 Derivation of Equations for Nonequilibrium Model 52

7.02.3 Equivalence with Equilibrium Case 54

7.02.4 Determination of Kinetic Constants 55

7.02.5 Testing the Model 56

7.03 Runs with Spheres 63

7.03.1 Dependence of Rate Upon CaO Concentration 68

7.03.2 Diffusion and Thermal Effects 72

Table of Contents (continued) Page

7.03.3 Kinetic Data for Spheres 75

7.03.4 Correlation of Reaction Rate and Time for Calcination 79

7.03.5 Effect of Cycling 81

7.04 Inspections of Sectioned Spheres 82

7.04.1 Spheres Disclosing Reaction Homogeneity 82

7.04.2 Spheres Disclosing Control by Ash-Layer Diffusion 84

7.05 Diffusion in Spheres 88

7.05.1 Equation for Determining Effective Diffusivity 88

7.05.2 Determination of Effective Diffusivity in [CaS+MgO] 91

7.05.3 Thiele Utilization Factor in Particles Reacting Homogeneously 95

7.06 Effect of Hydrogen Concentration 97

7.07 Effect of Water 100

7.08 Effect of Calcination Conditions Upon Reactivity 105

7.09 Reaction of Calcium Sulfide with Steam and Carbon Dioxide 114

7.10 Miscellaneous Observations 121

7.10.1 Changing Conditions During a Run 121

7.10.2 An Interrupted Run 123

Table of Contents (continued)

Page

7.10.3 Recarbonation of Calcium Oxide 124

7.10.4 The Mysterious Wiggle 126

7.10.5 Pan Discoloration 126

8.0 Discussion of Results 127

8.01 Discussion of Model 127

8.01.1 Deviation at Low Concentrations and High Temperatures 127

8.01.2 Variability of Results 130

8.01.3 H_2S Adsorption 133

8.01.4 A Possible Model Invoking Multiple Reactivities 133

8.02 Other Work on the Reaction of Hydrogen Sulfide with CaO 136

8.02.1 Work in Russia 136

8.02.2 Work of Vestal and Johnston 138

8.03 Calcination and Recarbonation of Dolomite 141

8.03.1 Dolomite 141

8.03.2 Calcination and Sintering of Dolomite 142

8.03.3 Recarbonation of Dolomite 144

8.04 Ability of the Solid to Survive the Fuel Desulfurization Reaction Cycle 146

8.05 Further Kinetic Experiments 151

List of Tables

Page

1. Analysis of Dolomite Number BCR 1337. 34
2. Analysis of Greenfield Dolomite Number 82-2R. 34
3. Kinetic Data for Powder Samples. 45
4. Coefficients of Arrhenius Expressions for Kinetic Constants. 61
5. Kinetic Constants Obtained from Trial and Error Analysis. 62
6. Absorption of Sulfur from H_2S by Spheres of Fully Calcined Dolomite. 73
7. Variation in Time Required to Calcine Various Dolomites. 80
8. Distribution of Sulfur in Sectioned Spheres. 86
9. Effective Diffusivity of H_2S in Sulfided Calcined Dolomite. 94
10. Effect of Hydrogen on Reaction Rate. 98
11. Effect of H_2O on Reaction Rate. 104
12. Summary of Data from Study of Sintering. 111
13. Regeneration Data. 119
14. Raw Data: Time and Change in Weight for Powder. 170
15. Raw Data: Time and Change in Weight for Spheres. 186

List of Tables (continued)

		Page
16.	Raw Data: Time and Change in Weight for Runs in which Temperature was Changed in Midrun.	192
17.	Raw Data: Time and Change in Weight for Regeneration.	194
18.	Raw Data: Time and Change in Weight for Recarbonation.	196
19.	Weight Loss During Calcination of Powder Samples.	198

List of Figures

Page

1. Carbonizing and desulfurizing coal in a system suitable for installation as a satellite to power generation. 17

2. Reactor to obtain differential weight data. 27

3. System to supply gas mixture to reactor of Figure 2. 29

4. Burner at bottom of furnace tube. 31

5. Log (1 - x) plot for Run 80-9 at 700°C, 5% H_2S, on Greenfield powder, -80+325 mesh. 41

6. Log (1 - x) plots for runs on Greenfield powder at 550°C with 0.3% and 20% H_2S. 42

7. "Final" rates versus concentration of H_2S. 44

8. Potential energy diagram broadly appropriate to our postulated reaction model. 50

9. Reaction rate constant, K_3. 58

10. Desorption rate constant, K_2. 59

11. Adsorption equilibrium constant, K_e. 60

12. Comparison of log (1 - x) plot for run at 475°C with curve regenerated from K's. 64

13. Comparison of log (1 - x) plots for duplicate runs at 550°C with curve regenerated from K's. 64

14. Comparison of log (1 -x) plot for run at 625°C with curve regenerated from K's. 65

15. Comparison of log (1 - x) plots for duplicate runs at 700°C with curve regenerated from K's. 66

List of Figures (continued)

		Page
16.	Data of Run 76-5, conducted at 625°C on 7.6 mm sphere of Glasshouse stone.	70
17.	Data of Run 72-2, conducted at 700°C on 6.5 mm sphere of Glasshouse stone.	71
18.	Arrhenius plot of data from five runs performed on the same spherical sample.	76
19.	Arrhenius plot of data from runs on a number of spherical samples of stone.	77
20.	Fractional conversion of CaO to CaS as a function of position along traverse through spherical samples of stone.	85
21.	Run 80-4 with an 8 mm sphere of Greenfield stone, at 950°C, 5% H_2S.	92
22.	Runs with Greenfield powder at 550°C, 10% H_2S, with and without water added.	102
23.	Runs with Greenfield powder, at 550°C, 0.3% H_2S, with and without water added.	103
24.	Typical nonisothermal recarbonation data.	108
25.	Temperature at which 80% conversion is attained in a nonisothermal recarbonation vs. the hold temperature.	110
26.	Plot of (1 - x) vs. time for the reaction of CaS with steam and CO_2.	117
27.	Arrhenius plot of rate data for reaction of CaS with steam and CO_2.	118
28.	Recarbonation of [CaO+MgO] at 550°C, 10% CO_2.	125

List of Figures (continued) Page

29. Run 94-4 on Greenfield powder at 900°C, 0.3% H_2S. 129

30. Comparison of a representative log (1 - x) curve regenerated from K's with hypothetical curves in which both K_1 and K_2 have been raised or lowered by a factor of 10. 132

31. First order rate constant for the reaction of calcined dolomite with H_2S. Data of Vestal and Johnston are plotted together with our data for spheres. 144

32. Data of Run 2-2-2, conducted at 900°C, 1% H_2S on Greenfield powder. 167

1.0 Introduction

Air pollution is one of the severe problems facing our industrial society. Sulfur in the form of sulfur dioxide is a major pollutant with respect to health, and power plants are a major source of sulfur dioxide.

Numerous processes have been proposed to remove sulfur dioxide from power plant stack gases or to remove sulfur from fuels before they are burned. The history of efforts to remove SO_2 from stack gases is not encouraging. Large installations for limestone scrubbing of flue gas are now under construction at costs in the vicinity of $35 to $40 per kilowatt. Independent plant for desulfurizing coal or residual oil is expensive and poor in thermal efficiency.

The team formed at the City College to attack this problem believes the best hope to lie in fuel-treating processes which are satellite to power generation itself. Such processes could provide low-sulfur fuels to power generation and recover a sulfur byproduct. If at least a portion of the fuel is available as a clean gas, the designer could incorporate gas-turbine plant in the power-generating equipment, thereby affording a saving in both capital and operating costs. Process air for use in fuel-treating steps could be "borrowed" at high pressure from the discharge of the gas turbine's compressor. The exact heating value of the clean gas would not matter very much, and within wide limits the proportion of the sulfurous fuel's heating value which turns up in the gas would not matter either. These considerations would afford the designer of fuel-treating apparatus considerable flexibility not available in design of independent plant for desulfurizing fuels. The designer could be somewhat careless about rejecting heat, since the power-generating equipment can use the heat, indeed in unlimited amounts if the heat is at a high temperature level.

Gasification with air and pyrolysis (preferably under a significant partial pressure of H_2) are candidate steps for incorporation in such power-satellite fuel-treating processes. These steps release sulfur in the fuel in form of H_2S.

Both fully calcined and half-calcined dolomite have the power to accept sulfur from H_2S:

Desulfurization Reactions

$$[CaO+MgO] + H_2S = [CaS+MgO] + H_2O \qquad (A)$$

$$[CaCO_3+MgO] + H_2S = [CaS+MgO] + H_2O + CO_2 \qquad (B)$$

Either [CaO+MgO] or [$CaCO_3$+MgO] is a candidate for use in conjunction with gasification or pyrolysis to render fuel products low in sulfur. Removal of sulfur at a high temperature level is preferable to removal by a wet system at low temperature, because the latter inevitably leads to loss of heat at a temperature too low for practical use. An acceptor process, too, has the unique capability, when it includes a pyrolysis step, of supplying a portion of the treated fuel in form of a low-sulfur coke.

Reaction (B) can be conducted in reverse to regenerate half-calcined dolomite and to obtain H_2S in concentrated form:

Regeneration Reaction

$$[CaS+MgO] + H_2O + CO_2 = [CaCO_3+MgO] + H_2S \qquad (C)$$

Reaction (C) is followed by a calcination step when fully-calcined dolomite is desired for use in reaction (A). The concentrated H_2S can be converted to elemental sulfur in a conventional Claus system.

The City College team has initiated a program of study of the kinetics of reactions (A), (B), and (C). This thesis is a report on work upon reaction (A).

2.0 Object of the Research

From a broad point of view, the object of the research is two-fold: (1) to provide data which will contribute toward the close design of fuel-desulfurization processes of the aforementioned type; and (2) to acquire insights into reaction mechanisms, which may prove valuable in carrying the practical development of such processes past expected difficulties.

This thesis will concentrate on reaction (A), the reaction of fully calcined dolomite with H_2S, conducted at atmospheric pressure. Some work was done on reaction (C), the regeneration of $CaCO_3$, and on factors affecting both calcination of $CaCO_3$ and recarbonation of CaO.

Future work by others will take up reactions (B) and (C), and will study each of the three reactions over a wide range of pressure.

3.0 Significance of the Research

The research may contribute towarding finding means for eliminating sulfur oxides from power-station stack gases at significantly lower costs than now appear possible.

For new power stations, there is a good possibility that sulfur oxides can be eliminated by means which also reduce the overall cost of electricity (1,2). Raw fuel would be gasified, the fuel gas would be cleaned, and the clean fuel would be committed to an advanced power cycle specifically engineered to take advantage of the superior qualities of the clean fuel. Alternatively, fuel would be pyrolyzed, gaseous products of pyrolysis would be cleaned and committed to a gas turbine, and a solid product would be desulfurized and shipped to another site or stored against peaks in demand for power.

The kinetic data reported in this study will be of use to a designer of practical equipment to remove H_2S from fuel gases. Knowledge of effects of gas composition to be described herein can provide the designer of pilot or process equipment with insight into the problems which may arise in operation.

The kinetic model to be introduced is unique in its approach to nonequilibrium adsorption phenomena. We are not aware of work which has developed such a model as an outcome of noncatalytic solid-gas reaction studies.

4.0 Technical Background

4.01 Calcined Dolomite and [CaS+MgO]

Dolomite is a true chemical species, $CaCO_3 \cdot MgCO_3$.

We express half- and fully calcined dolomite by the formulas [$CaCO_3$+MgO] and [CaO+MgO] respectively, to indicate that each solid comprises an intimate intermingling of microscopic crystallites of MgO and the respective calcium compound.

There is no volume change, nor indeed any change of particle shape, when dolomite is calcined gently to produce [$CaCO_3$+MgO]. The same may be said if dolomite is calcined to produce [CaO+MgO] at a temperature below about 1000°C.

Haul (3) gave surface area and porosity data for [$CaCO_3$+MgO] and [CaO+MgO] derived from a "dolomite" of unspecified analysis. The table below gives a comparison of Haul's porosity data at 800°C with "ideal" porosities calculated from molar volumes of the relevant chemical species. The calculation assumes that no shrinkage occurs as CO_2 is expelled from dolomite and that all internal porosity is accessible. Practically no shrinkage should occur when a true dolomite is calcined at 800°C, and Haul's data suggest that at least some of the pores in the calcined materials may not be accessible.

"Ideal" Porosities of Some Solids Derived From Dolomite

	"Ideal" Porosity	Haul's Value at 800°C
[CaO+MgO]	36.2 cm^3/g-"mole"	23.2 cm^3/g-"mole"
[$CaCO_3$+MgO]	16.2	10.8
[CaS+MgO]	27.4	--

Basis of "ideal" porosities: $CaCO_3 \cdot MgCO_3$ = 64.2 cm^3/g-mole; no shrinkage as the various solids are produced; MgO = 11.05 cm^3/g-mole, CaO = 16.9, $CaCO_3$ = 36.9, CaS = 25.8.

Haul reported surface areas of [CaO+MgO] and [$CaCO_3$+MgO] at 800°C to be 56.2 and 6.7 m^2/g respectively. He did not report surface areas for the latter solid at any other temperature. Surface areas of [CaO+MgO] were reported to decline over the temperature interval 800° to 1000°C, the area at 1000°C being about 5 m^2/g. Measurements by TVA (4) confirm that the surface area of [CaO+MgO] at about 1000°C is generally in the range from about 3 to about 8 m^2/g.

The foregoing table notes the "ideal" porosity of [CaS+MgO], which stands between that for [CaO+MgO] and [$CaCO_3$+MgO].

Reflection upon these data leads one to the hope that dolomite might maintain a high degree of porosity if it is used in a process in which it is converted from $CaCO_3$ to CaO to CaS and back to $CaCO_3$ by means of reactions (A) and (C) coupled with a calcination step at a temperature below 1000°C. If this is so, the stone might be expected to maintain its reactivity and capacity over a number of reaction cycles.

4.02 Work of Gesellschaft für Kohlentechnik

During the 1920's, Gesellschaft für Kohlentechnik (now Bergbau-Forschung) developed a process which used calcined dolomite to promote the shift reaction (5).

$$H_2O + CO = CO_2 + H_2 \qquad (D)$$

$$[CaO+MgO] + H_2O + CO_2 = [CaCO_3+MgO] + H_2 \qquad (E)$$

It was found that MgO in calcined dolomite was catalytic for reaction (D). The process was conducted in a fixed bed until reaction (E) caused the dolomite to be used up, whereupon breakthrough of CO occurred. The dolomite was then calcined at 950°C, and the bed was put back into production.

In a large pilot unit, after more than a score of calcinations at 950°C, each followed by a recarbonation at 500°C, both the catalytic activity of MgO and the activity of CaO toward CO_2 were essentially unimpaired.

This experience provides further grounds for hope that dolomite might be suitable for use as an acceptor in a cyclic process to remove H_2S from a fuel gas.

The Gesellschaft für Kohlentechnik showed that the best natural stone should have an atomic ratio of calcium to magnesium close to the ideal of 1:1. Stones low in magnesium did not give good utilization of CaO and showed poor resistance to sintering during a calcination step.

Runs were also made to determine the maximum calcination temperature which would not cause deactivation of the CaO. Best results were obtained below 1000°C.

4.03 Consolidation Coal Company CO_2 Acceptor Gasification Process

In the Consolidation Coal Company (Consol) acceptor process (6), calcined dolomite acts on devolatilized coal char in a fluidized bed gasified with steam. The endothermic gasification reaction

$$C + H_2O = CO + H_2 \qquad (F)$$

is driven by the exothermic absorption of CO_2 by the calcined dolomite. In addition, shift reaction (D) and desulfurization (A) occur. The fluidized bed is run at about 870°C (1600°F) and 20 atmospheres. Solids consisting mostly of [$CaCO_3$+MgO] and [CaS+MgO] are withdrawn for regeneration in a second fluidized bed.

In order to regenerate CaO from CaS as well as from $CaCO_3$, Consol controls conditions in the regeneration fluidized bed so that the following reaction occurs:

$$1/4\ CaS + 3/4\ CaSO_4 = CaO + SO_2 \qquad (G)$$

Consol's CO_2 acceptor process inherently requires the regeneration bed to operate at about 1060° (1940°F).

A major point proven in Consol's work is that dolomite is suitable for use in fluidized beds for a large number of reaction cycles without serious attrition taking place. After a number of cycles, Consol found that the attrition rate became less than 0.5% per cycle and was often immeasurably small.

At the high temperature of Consol's regeneration bed, the acceptor suffers drastic loss of capacity for absorbing CO_2 and presumably also suffers loss of reactivity. After 20 cycles between regeneration at 1060°C and recarbonation at 870°C, one of the better dolomites tested absorbed only 40% as much carbon dioxide as the stoichiometric amount corresponding to its CaO content. We may presume that its chemical reactivity, both toward CO_2 and H_2S, had also declined. The greater loss of reactivity in Consol's work by comparison with the negligible loss experienced by Gesellschaft für Kohlentechnik is plausibly due to the higher temperature employed by Consol in regeneration, 1060° versus 950°C.

Nevertheless, it is of interest to note that Consol's work appears to establish that the reactivity of CaO in calcined dolomite is sufficient for commercial usefulness, in spite of Consol's high temperature during regeneration. Consol assumes approach to equilibrium for reaction (A) in process design.

4.04 Squires' Fuel Desulfurization Processes

Squires (1,7,8) has proposed a class of fuel-treating processes intended for installation ancillary to large power stations. The processes treat a sulfurous fuel at high pressure in presence of an agent to capture sulfur, and provide at least a portion of the fuel's heating value in form of dilute fuel gases for use in a combustion to drive a gas turbine.

The processes would reject heat at a temperature economically useful for power generation. Air for the processes would be provided from air compresssors of the type which manufacturers furnish for gas-turbine use; i.e., the compressors would be large axial-flow machines with little or no intercooling. Such compressors are far cheaper than intercooled compressors of types common in industry. Exhaust gases from the gas turbine of a Squires process would be supplied to a conventional steam boiler. There is advantage in making the gas-turbine component of the power from the station as large as possible, to take maximum advantage of the improved efficiency and lowered capital cost afforded when a gas turbine "tops" the conventional steam cycle.

The cited features of a Squires process -- fuel processing at high pressure in presence of an agent to capture sulfur, gas turbine, steam cycle topped by a gas turbine and receiving waste heat from fuel processing, process air furnished by the gas turbine's compressor or another compressor of the same type -- combine synergistically to make an overall process which is extremely attractive from a design point of view.

4.04.1 Low Temperature Regeneration of $CaCO_3$ from CaS

A Squires process might use calcined dolomite as an acceptor for sulfur via reaction (A), the acceptor being regenerated via reaction (C) followed by a calcination. Reaction (C) would be conducted at a temperature below about 700°C; the highest temperature of the process is achieved in the calcination step, which typically may be no greater than about 950°C. Hopefully, this procedure will combine the resistance to attrition found in Consolidation Coal's work with the excellent resistance to deactivation encountered by Gesellschaft für Kohlentechnik.

4.04.2 Process Example

Figure 1 sketches an illustrative Squires process wherein a unitary operation may carbonize coal and desulfurize the products by action of hydrogen and a solid acceptor for sulfur.

In this example, the fuel-processing vessel operates at 21 atm and houses three fluidized-solids zones:

- A "hydrocarbonizing" zone, at 760°C, converts finely ground coal into gaseous products and coke pellets of 3 to 15 mm. The H_2 partial pressure is 4.4 atm.
- A desulfurizing zone, contiguous with the hydrocarbonizing zone and also at 760°C, removes sulfur both from gaseous products of carbonization and from coke by action of H_2 (at 5.8 atm) and calcined dolomite acting as sulfur acceptor. In this zone, CaO in the acceptor is converted partly to CaS and partly to $CaCO_3$.
- A calcination zone, at about 950°C, decomposes $CaCO_3$.

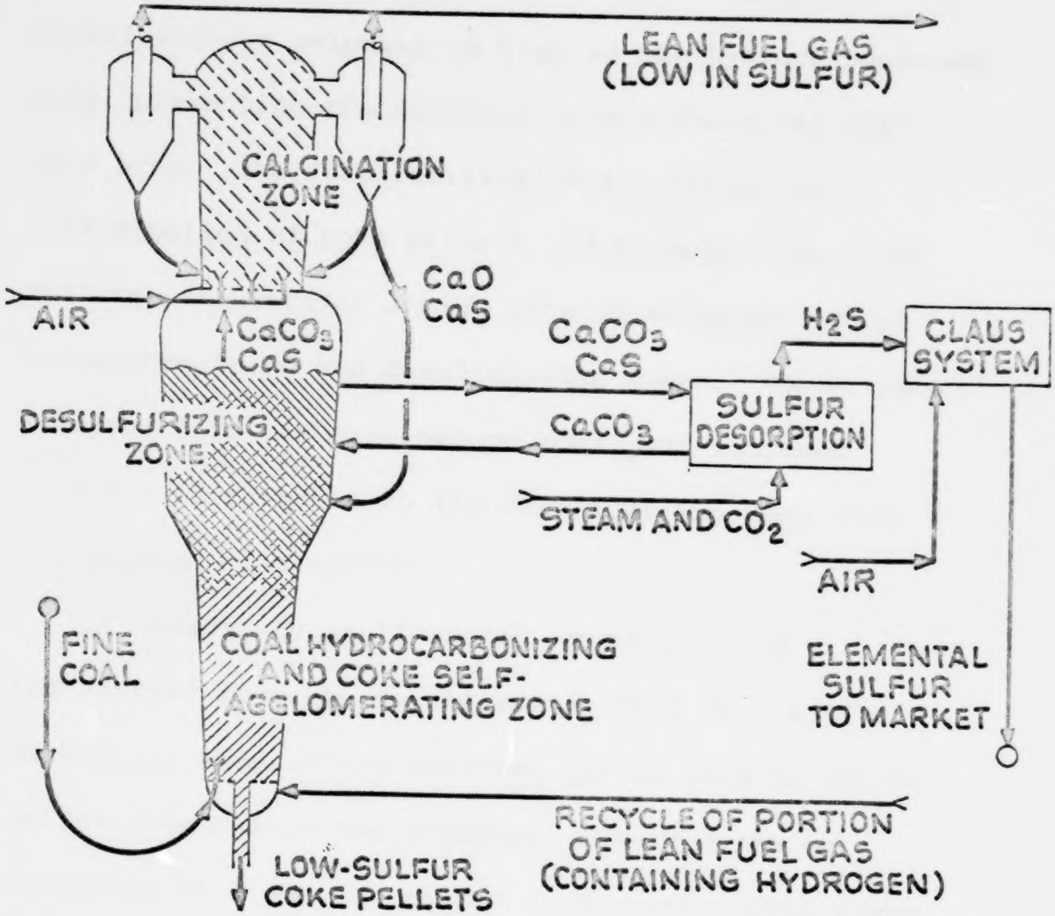
LEAN FUEL GAS
(LOW IN SULFUR)
CALCINATION
ZONE
AIR
CaO
CaS
CaCO3
CaS
CaCO3
CaS
H2S
CLAUS
SYSTEM
DESULFURIZING
ZONE
SULFUR
DESORPTION
CaCO3
STEAM AND CO2
AIR
FINE
COAL
COAL HYDROCARBONIZING
AND COKE SELF-
AGGLOMERATING ZONE
ELEMENTAL
SULFUR
TO MARKET
RECYCLE OF PORTION
OF LEAN FUEL GAS
(CONTAINING HYDROGEN)
LOW-SULFUR
COKE PELLETS

Figure 1. Carbonizing and desulfurizing coal in a system suitable for installation as a satellite to power generation.

The acceptor is much finer than the coke pellets. Fluidizing-gas velocity is high in the hydrocarbonizing zone, preventing the acceptor from sinking far into this zone. The desulfurizing zone contains an intermingling of coke pellets and acceptor, and coke pellets circulate at a high rate of exchange between hydrocarbonizing and desulfurizing zones. Gases convey acceptor into the calcination zone, and calcined acceptor is returned to the desulfurizing zone from the dipleg of a cyclone.

A relatively small amount of acceptor is transferred from the desulfurizing zone to a sulfur desorption step, where reaction (C) is used to desorb sulfur from CaS in the acceptor. The H_2S can be converted to elemental sulfur in a conventional Claus system.

Partial combustion of volatile matter by air provides heat to the calcination zone, and this heat in turn drives the carbonization process below. Cooling and recarbonation of CaO returned to the desulfurizing zone develops heat therein, which is transmitted by the direct contact between desulfurizing and hydrocarbonizing zones. The air flow of Figure 1 is only 11% of the stoichiometric air for complete combustion of the coal, and the gases undergoing treatment have only a tiny fraction of the volume which must be handled in a stack-gas cleaning operation.

5.0 Thermodynamics and Experimental Conditions

5.01 Thermodynamic Equilibria

Equilibrium for reaction (A) is favorable for the absorption of sulfur over a wide range of temperature. The equilibrium is given by the expression:

$$\log_{10}[H_2O]/[H_2S] = 3519.2/T - 0.268 \qquad (1)$$

where the brackets signify mole fraction and temperature T is in °K. This is a least squares fit of data from Uno (9), Rosenqvist (10), and Curran, Fink, and Gorin (6).

Equilibrium for the conversion of MgO to MgS is unfavorable at all reaction conditions of interest to this work, and MgO does not participate in the reactions.

Equilibrium for reaction (B) may be found by combining the foregoing expression (1) with the equilibrium decomposition pressures of $CaCO_3$ given by Hill and Winter (11) to obtain:

$$\log_{10}[H_2O][CO_2]P/[H_2S] = 7.253 - 5280.5/T \qquad (2)$$

where pressure P is in atmospheres.

Hydrogen sulfide can dissociate to a significant extent at our reaction temperature. The JANAF Tables (12) list values for the K_p of formation of H_2S from H_2 and S_2 gas. These may be used to calculate equilibrium dissociation concentrations.

5.02 Experimental Conditions

5.02.1 Desulfurization

Using equation (1), one finds that the equilibrium ratio of $[H_2O]/[H_2S]$ exceeds 1000 below about 800°C. Since water was materially excluded from most of our runs, reaction (A) can be considered to be irreversible.

The dissociation of H_2S can cause questions as to actual gas concentrations and can cause operating problems, for sulfur would condense on cool surfaces in the apparatus. In some early experiments, sulfur condensed on the balance suspension wire, significantly affecting the weight record at high conversions. Hydrogen was added to all desulfurization runs at a concentration sufficient to prevent the equilibrium S_2 concentration from exceeding 0.05%. In addition, hydrogen prevented the possibility that CaS might be oxidized to $CaSO_4$ by traces of water.

Reaction (A) was investigated over the temperature range from 475° to 950°C. Ash-layer diffusion was encountered at 950°C, and kinetic data was not obtained at temperatures above 900°C. The rate was rather slow at 475°C, and only low conversions were obtained. These temperatures should bracket operating conditions of process interest.

The investigated range of H_2S partial pressure was from 0.003 atm to 0.20 atm. For a process operating at 20 atmospheres, these pressures correspond to molar concentrations of 0.015% and 1% respectively. In practice, since most of the reaction volume will be needed to remove final amounts of H_2S, this is expected to be the concentration range of greatest interest.

5.02.2 Regeneration

When reaction (C) is to be used in a process to regenerate half-calcined dolomite, it must be carried out at elevated pressure and at a temperature below about 700°C. This is necessary to obtain a concentration of H_2S in dry gas adequate for feed to a Claus without undue consumption of steam. For example, the equilibrium constant for reaction (C) at 550°C is 0.15 atm^{-1}.

Our apparatus was not capable of operation at high pressure. For our experimental work on reaction (C), the poor equilbrium at atmospheric pressure was overcome by feeding gas containing no H_2S at a high rate. The temperatures employed were determined by rate considerations rather than by the need to achieve a high concentration of H_2S.

5.02.3 Calcination

The regeneration procedure calls for a calcination step to follow reaction (C), and this step is preferably conducted at a temperature below 1000°C. At the highest CO_2 pressure available to us, one atmosphere, calcination begins at about 900°. A temperature of 925° was chosen as being representative of typical process conditions. Decomposition was observed to commence as the reactor temperature passed 900°. Decomposition continued for some time after the thermocouple measured 925°. The sample was kept under CO_2 until the calcination was complete.

Exploratory experiments were made in which the solid was held for varying time intervals at temperatures as high as 975°C to look for the effects of sintering. Exploratory experiments also examined the effect of substituting N_2 for CO_2 during calcination.

6.0 Experimental Techniques

Each of the reactions to be studied produces a change in weight of the solid. This suggests that reaction rate can be conveniently determined by continuously weighing the solid during reaction. In the apparatus used here, a stream of the gas to be reacted was passed over a sample of the solid suspended from the arm of an automatic recording balance. A sufficient gas flow was maintained to prevent a substantial change in gas composition. The first experiments used a sample in the form of a sphere; interpretation of kinetic results is simpler for a sphere than for any other shape, and study of a sphere quickly sheds light on the mode of reaction. Once questions related to diffusion and reaction mode were satisfied, the work was continued with powders.

6.01 Equipment

Figures 2, 3, and 4 illustrate schematically the experimental arrangement, which in many respects closely resembled apparatus used by McKewan to study kinetics of the reduction of iron oxides by H_2 and CO (13).

Figure 2 shows the automatic recording balance (Ainsworth RV-AU-1) from which the sample was suspended in a Vycor reaction tube positioned in a Lindberg 54356 furnace. The furnace is capable of maintaining a flat zone of ± 2^{o}F over a 12 inch central length. The balance is equipped to measure automatically a total change in sample weight up to 400 mg to an accuracy of 0.1 mg. For a 5 mm particle undergoing reaction (A), this accuracy corresponds to 0.7% conversion.

Temperature was measured by a thermocouple in a Vycor well about one inch from the sample. For most of the runs a sheathed chromel alumel (KX) thermocouple was used. On several runs a platinel thermocouple was introduced along with the KX couple or instead of it. They agreed within a few degrees. There was some concern about possible drifting of the KX thermocouple as the temperature was cycled between 900+^{o}C and room temperature, and platinel was tested. However, because of construction difficulties, the platinel couples generally broke after only one or two runs. Since the change in rate due to an error of several degrees in temperature was small compared to the variance observed

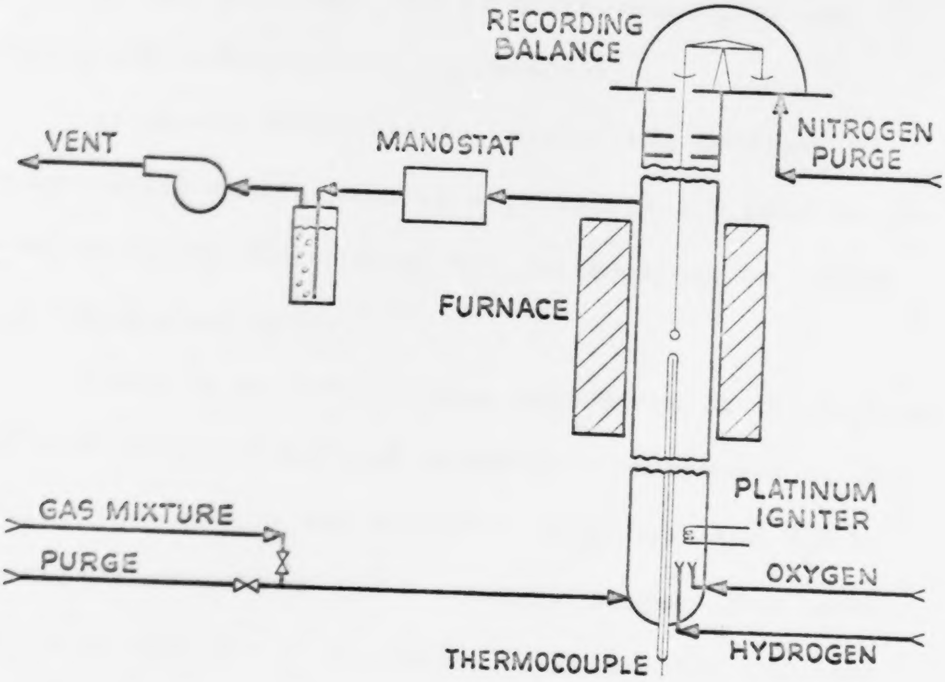
RECORDING
BALANCE
VENT
MANOSTAT
NITROGEN
PURGE
FURNACE
PLATINUM
IGNITER
GAS MIXTURE
PURGE
OXYGEN
THERMOCOUPLE
HYDROGEN

Figure 2. Reactor to obtain differential rate data by following the change in weight of a sample of stone suspended from an automatic recording balance.

in the rate, and since any great drift in couple readings would be disclosed by drift in temperature at which calcination occurred, use of KX thermocouples was continued with periodic replacement.

It may be advisable to improve the accuracy of temperature measurement if experiments are refined so that a larger fraction of the variance can be traced to temperature error.

Gases to be reacted were introduced at the bottom of the furnace tube, and products were removed at the top. The balance was protected from heat and H_2S by a series of baffles and a nitrogen purge. The Vycor furnace tube was 51 mm inside diameter; the reactant gas flow was 500 cm^3 (STP)/min; and the Reynolds number for flow past the stone sphere was of the order of unity.

Figure 3 shows the system for preparing the gas mixture to be reacted. Each gas component was metered through its own individual capillary flowmeter, with 1% accuracy. Low-pressure pancake regulators maintained constant pressure to the flowmeters. A manostat was provided on the combined stream of the several gases, so that atmospheric pressure can be maintained at the

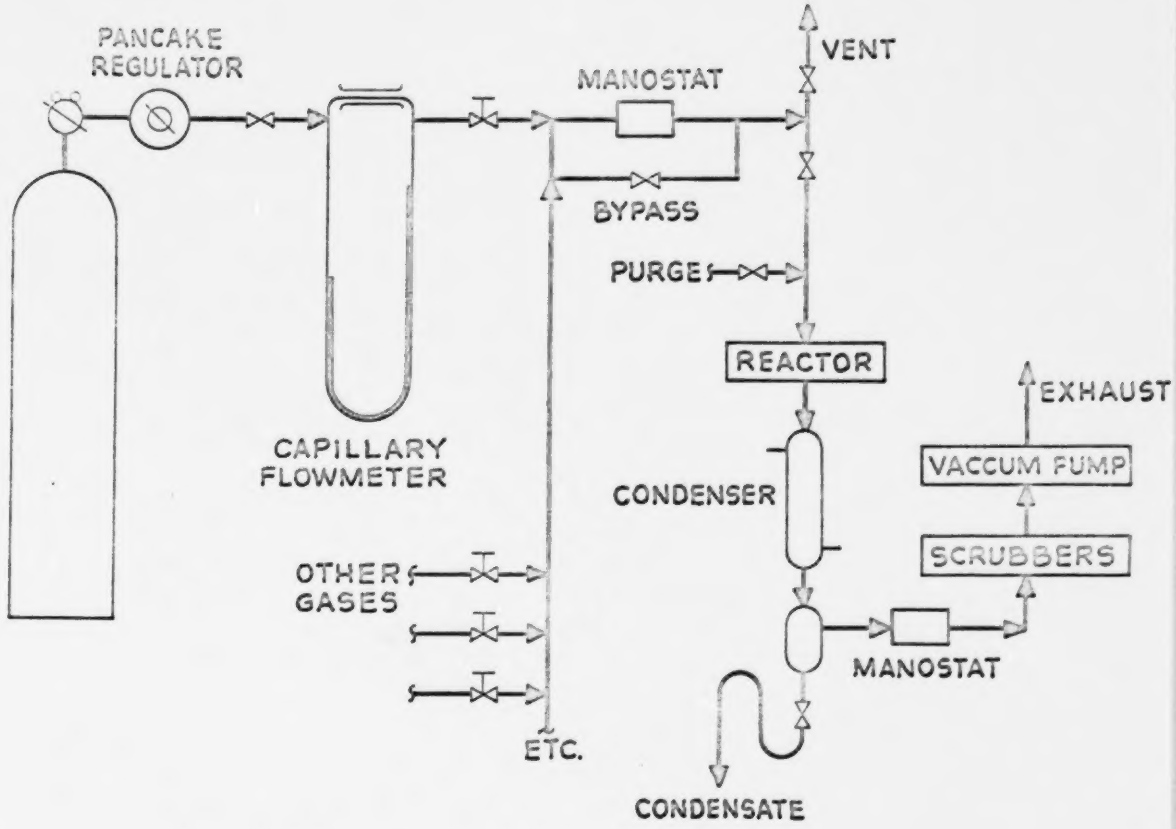
PANCAKE REGULATOR
CAPILLARY FLOWMETER
MANOSTAT
BYPASS
VENT
PURGE
REACTOR
EXHAUST
CONDENSER
VACCUM PUMP
SCRUBBERS
OTHER GASES
ETC.
MANOSTAT
CONDENSATE

Figure 3. System to supply gas mixture to reactor of Figure 2.

several capillary flowmeters when the furnace tube is maintained at a sub-atmospheric pressure. The manostat was bypassed in my experiments, which were conducted by atmospheric pressure.

Reaction steam was provided on one of two ways. The first was to produce water chemically by burning hydrogen with oxygen at the bottom of the furnace tube with the apparatus depicted in Figure 4. This technique makes it possible to supply steam at a steady and accurate rate. All runs of reaction (C) and Run 90-2 for reaction (A) were made with the burner supplying steam. Other runs for reaction (A) used a simple bubbler immersed in a constant temperature bath to provide steam, because a question arose as to whether some H_2S might be dissociating in the flame.

Gases from the furnace tube were cooled, and a trap for water was provided for operations during which steam was present. A scrubber for H_2S was provided. Gases were discharged from the system via a vacuum pump. A manostat downstream of the furnace tube maintained the desired pressure therein.

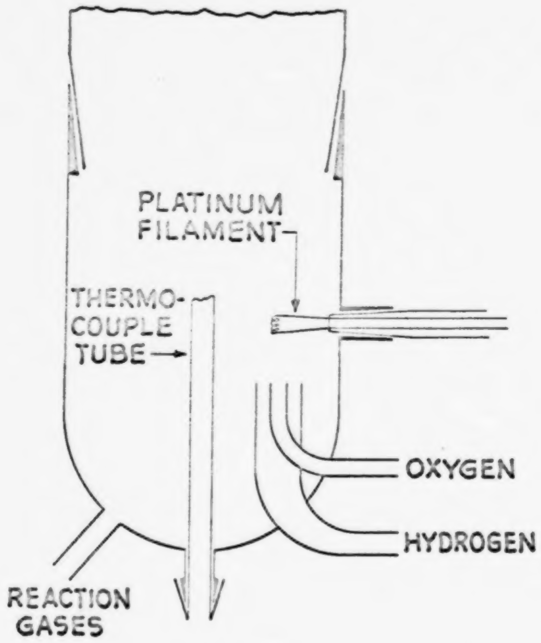
PLATINUM
FILAMENT
THERMO-
COUPLE
TUBE
OXYGEN
HYDROGEN
REACTION
GASES

Figure 4. Burner at bottom of furnance tube.

6.02 Procedures

Calcination of a fresh sample of stone was conducted nonisothermally. The stone was heated in the furnace in an atmosphere of CO_2, the temperature increasing at about 10° to $15^\circ C$ per minute. Decompostion of $MgCO_3$ occurred over a temperature interval between about 400° and $850^\circ C$, and decomposition of $CaCO_3$ occurred between about 900° and $925^\circ C$. The sample was held at a nominal temperature of $925^\circ C$ until the weight became constant. Nitrogen was then substituted for CO_2, and after about 15 minutes the sample was cooled to a temperature selected for a test of reaction (A).

Reaction (A) was preferably conducted until substantially complete conversion had been achieved -- i.e., until no further weight change was occurring. In some low-temperature runs, the temperature was raised toward the end of the run in order to achieve complete conversion in a reasonable time.

When we wished to regenerate the sulfurized stone by means of reaction (C), we brought the sample under nitrogen to a temperature selected for this reaction. A mixture of steam and CO_2 was then substituted for the nitrogen, and reaction (C) allowed to proceed.

If reaction (C) was to be followed by a calcination, the stone was heated under CO_2 to 925°C and held at this temperature until the weight became constant. The stone was then ready for a repetition of the reaction cycle, reaction (A) followed by reaction (C) followed by still another calcination.

6.03 Dolomite Feed Supply

The dolomite used in the first experiments was Glasshouse stone from the quarry of Charles Pfizer Co. at Gibsonberg, Ohio. The Air Pollution Control Office has selected stones from this quarry for other studies (specifically stones designated BCR 1337 and BCR 1920). Pfizer supplied samples directly. Based upon weight loss measurments during calcination, the stone has a Ca/Mg atomic ratio between about 0.95 and 1.0. An analysis of a BCR 1337 stone is given in Table 1. This should approximate our dolomite.

Table 1. Analysis of Glasshouse Dolomite Number BCR 1337

Analysis performed after ignition by Bituminous Coal Research Institute

Atomic Ratio, Ca/Mg = 0.9 Loss on Ignition = 47.5%

Component	Weight Percent
MgO	45.0
CaO	53
Al_2O_3	0.15
Fe_2O_3	0.25
K_2O	<0.1
Others	<0.03

Table 2. Analysis of Greenfield Dolomite Number 82-2R

Analysis performed by Lucius Pitkin Inc., New York City

Atomic Ratio, Ca/Mg = 1.09 Particle Density = 2.64 gm/cc

Component	Weight Percent
Magnesium	12.32
Calcium	22.04
Iron	0.37
Silicon	0.X
Aluminum	0.X
Others	<0.0X

The dolomite used in all runs numbered 80 or higher was from the Greenfield formation in Ohio and was supplied courtesy of Davon Incorporated from their Plum Run quarry. All of the powder runs were made from the same sample of -80+350 mesh material whose analysis is given in Table 2. X-ray diffraction study confirmed the presence of pure dolomite rather than a possible mixture of $MgCO_3$ and $CaCO_3$.

6.03.1 Preparation of Samples

In making spheres, the stone was first cut roughly in the form of a cube. It was then shaped into a sphere by use of a lapidary bead mill. This device, which can be obtained from a lapidary equipment supply store, consists of a lower plate with a groove in it and a flat upper plate which can be attached to a drill press. The stone was ground with wet #80 silicon carbide grit. As the upper plate was turned, the stone was rounded by an action similar to that observed by rolling a piece of clay between one's hand and a table. After grinding, the sphere was washed, dried, weighed and its diameter measured. Roundness to within 0.01 mm was obtained.

The spheres were suspended from the balance by platinum wire and were held in basket formed by several strands of wire. The wire basket was not cleaned between runs since it did not exhibit signs of adhering material.

The powder samples were prepared by breaking a large rock with a hammer and then grinding the pieces in a mortar and pestle. The material was sieved, and the -80+350 mesh cut was used for this research.

For each run with powder the sample was evenly spread onto a tared platinum pan about 18 by 21 mm and weighed. Between runs, the pan was washed in dilute HCl and rinsed with water. It was dried before reuse. The pan was washed because it was not possible to remove the last traces of powder by simply turning the pan over and shaking.

6.03.2 Capacity of Samples

In a run in which reaction (A), whereby H_2S is absorbed by CaO, appeared to go to completion, the weight gain at the end of the run was taken to be the capacity of the sample of stone. In all such cases, the capacity closely approximated the capacity as indicated from the weight loss during the calcination of $CaCO_3$. Where reaction (A) was not carried to completion, the weight loss during calcination of $CaCO_3$ was used to judge the sample's capacity.

In work with powder samples, the weight loss during calcination of $MgCO_3$ exceeded the theoretical loss due to release of CO_2. We judge that small amounts of stone were lost due to explosive release of CO_2, probably at sharp edges of individual particles. The loss probably amounted on the average to about 6% of the sample, and would not affect the capacity of the sample as judged by the procedure outlined above. Data on weight loss during calcination of powder samples are summarized in Section 10.04.

7.0 Experimental Results

All of the valid raw experimental data obtained in this research are tabulated in Section 10.03.

The work may be divided broadly into two phases. The first used spheres to delineate the mode of reaction and to determine values of effective diffusivity within the solid. The second delved more deeply into the kinetic mechanism and used a powdered sample.

Although the sphere work was done first, it is more readily understood in light of knowledge obtained from the powder investigation, which will be presented first.

Work with spheres had established that the reaction is controlled by ash-layer diffusion at 950°C in spheres of Greenfield dolomite having a diameter of about eight mm. The solid [CaS+MgO] produced at 950°C displays an internal effective diffusivity approximately 6% of the diffusivity in open space. The effect of diffusion upon reaction in a spherical particle varies as the square of the radius. Calculations using the diffusivity result obtained from spheres show that concentration gradient effects within an 80-mesh particle will be negligibly small. In such a particle, the reaction will occur homogeneously throughout the particle even at 900°C.

Powder had several advantages for our later work: (1) Its homogeneity removed one source of variability, caused by differences among samples of stone. (2) Questions concerning reactant diffusion and transfer of heat were eased, since a powder sample may be spread in a thin layer on a pan. (3) Spheres are time-consuming to make.

7.01 Runs with Powder Seeking a Kinetic Model

All powder runs were made with samples taken from a single supply of powdered Greenfield dolomite, -80+325 mesh.

The effect of H_2S concentration upon reaction rate was studied in forty-four runs conducted at six temperatures.

Results at temperatures above 700°C followed a simple model, in which the rate is first order in H_2S and proportional to the quantity of CaO remaining in the sample. That is:

$$-\frac{1}{W}\frac{dW}{dt} = K\,[H_2S] \tag{3}$$

where the brackets signify concentration in g-moles/liter (actual), W is the weight of unconverted CaO remaining in the sample at time t, and K is a kinetic constant. For this model, plots of log (1 - x) versus time, where x is the fractional conversion of CaO to CaS, are substantially linear. The slopes of these plots are substantially proportional to H_2S concentration. Figure 5 presents a typical log (1 - x) plot consistent with this model.

At 550°C, however, charts of log (1 - x) versus time are not linear. Many runs exhibited a high initial reaction rate, falling away to much slower rates at high conversions of CaO to CaS. The tendency for the reaction to flag at high conversions is more pronounced at higher concentrations of H_2S. Figure 6 illustrates these facts, giving (1 - x) plots for runs at 550°C with 0.3% and 20% H_2S.

An explanation for the shape of the curves in Figure 6 might include the hypothesis that CaO in the sample displays a range of reactivity. The most active CaO would be presumed to react first, leaving less active CaO to react at later stages of a run.

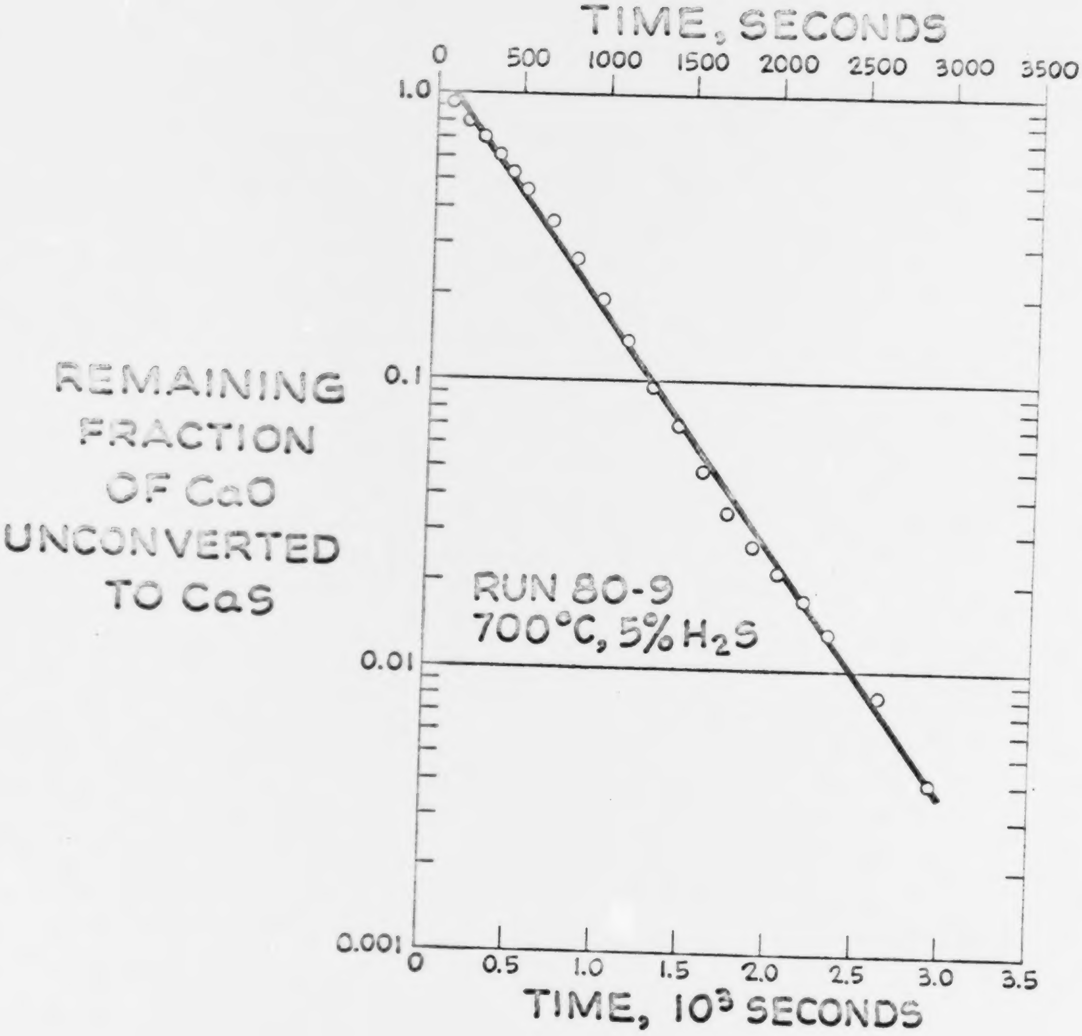

Figure 5. Log (1 - x) plot for run 80-9, at 700°C, 5% H_2S, on Greenfield powder, -80+325 mesh.

The linear plot is consistent with model which is first order in concentration of CaO in the solid.

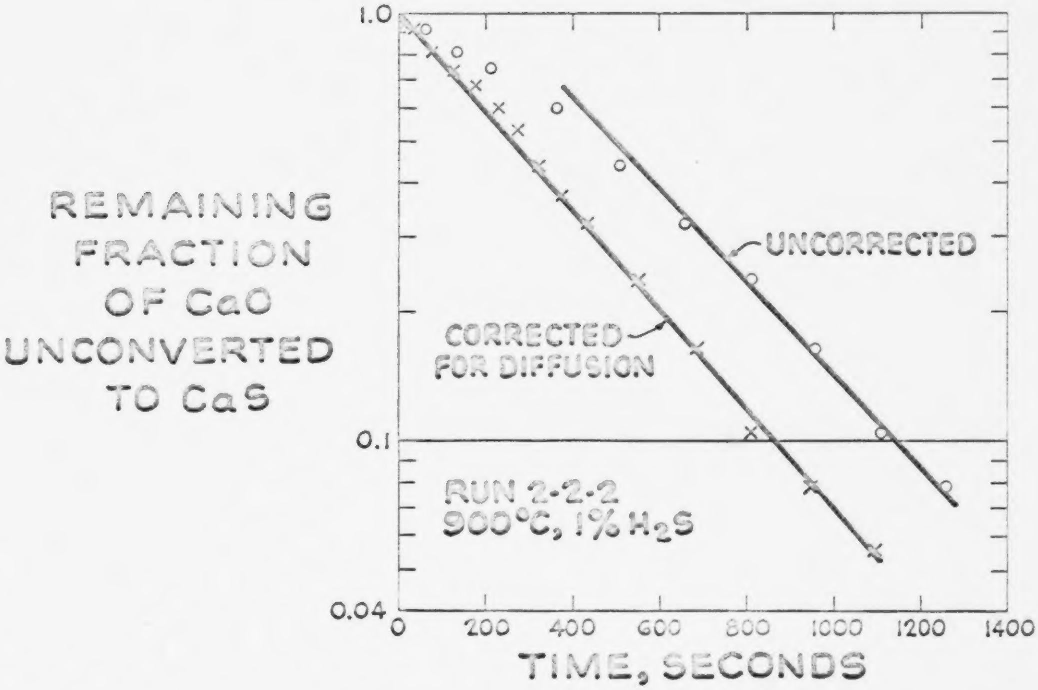

Figure 6. Log (1 - x) plots for runs on Greenfield powder at 550°C with 0.3% and 20% H_2S.

A model based upon this hypothesis, along with the assumption that the reaction is first order in H_2S, cannot explain the situation revealed by Figure 6. In absence of other effects, such a model would require the two curves to coincide if the time coordinate is normalized by multiplying this coordinate by the concentration of H_2S. Such a normalization of the two curves fails to bring them into coincidence.

In order to summarize the rate data for analysis, we estimated a "final" rate for each run from the "linear" portion of the (1 - x) plot, like the range we have indicated for each run in Figure 6 by a straight line.

Table 3 summarizes the bulk of the data for the powder runs. For each run, Table 3 notes the range of conversion covered by the linear portion of the (1 - x) plot, and tabulates the slope of this portion of the plot.

Figure 7 plots the "final" rates versus concentration of H_2S at the several temperatures studied. The curves of this figure show that the rate is not first order with respect to H_2S at low temperatures. Clearly, a

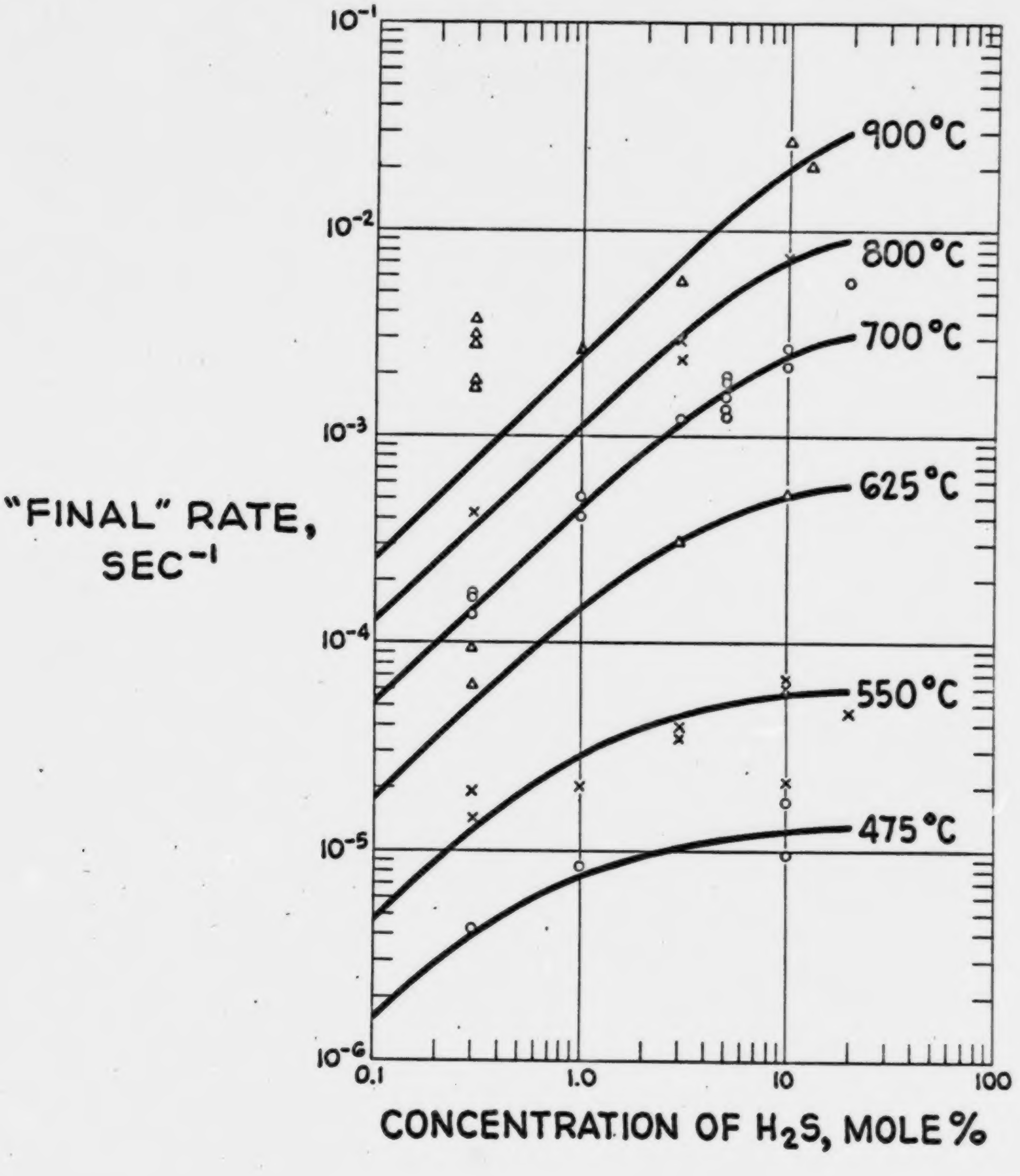

Figure 7. "Final" rates versus concentration of H_2S. Curves were generated from K's given in Table 5.

Data from runs at 900°C were corrected for gas-film diffusion; see Section 10.01.

Table 3. Kinetic Data for Powder Samples:

"Final" Rates Determined from Straight-Line Portions of Plots of Log (1 - x) versus Time

Run Ref. No.	Temp. °C.	Reaction Gas, mol%				"Final" Rate, sec^{-1}	Range Covered by Straight-Line Portion of (1 - x) Plot	
		H_2S	H_2	N_2	H_2O		(1 - x) initial	(1 - x) final
92-1	900*	12.5	25.0	62.5	-	2.01×10^{-2}	.68	.01
92-7	900	10.0	40.0	50.0	-	2.75×10^{-2}	.65	.01
86-6	900	3.0	15.0	82.0	-	5.69×10^{-3}	.6	.02
2-2-2	900	1.0	7.5	91.5	-	2.66×10^{-3}	.38	.05
94-1	900	0.3	15	84.7	-	1.76×10^{-3}	.15	< .01
94-4	900	0.3	40	59.7	-	3.62×10^{-3}	.55	.01
94-3	900	0.3	40	59.7	-	3.12×10^{-3}	.6	< .01
94-2	900	0.3	40	59.7	-	1.73×10^{-3}	1.0	0.1
92-3	900	0.3	7.5	92.2	-	2.88×10^{-3}	.26	< .01
86-4	800	10.0	10.0	80.0	-	7.4×10^{-3}	.9	.02
84-4	800	3.0	7.5	89.5	-	2.98×10^{-3}	.54	< .01
84-9	800	3.0	7.5	89.5	-	2.33×10^{-3}	.10	.02
84-9	800	0.3	7.5	92.2	-	4.24×10^{-4}	.47	.21

*Runs at 900°C corrected for diffusion effects at low conversions. See section 10.01 for a discussion of this correction.

Table 3. continued

Run Ref. No.	Temp. °C.	Reaction Gas, mol% H_2S	H_2	N_2	H_2O	"Final" Rate, sec^{-1}	Range Covered by Straight-Line Portion of (1 - x) Plot (1 - x) initial	(1 - x) final
86-2	700	20.0	7.5	72.5	-	5.7×10^{-3}	.7	< .01
94-8	700	10.0	7.5	82.5	-	2.7×10^{-3}	1.0	.01
86-1	700	10.0	7.5	82.5	-	2.17×10^{-3}	.9	< .01
80-8	700	5.0	7.5	87.5	-	1.845×10^{-3}	.95	< .01
80-9	700	5.0	7.5	87.5	-	1.94×10^{-3}	.90	< .01
80-10	700	5.0	7.5	87.5	-	1.32×10^{-3}	.35	< .01
90-2	700	5.0	7.5	62.5	25.0	1.547×10^{-3}	.76	.05
86-7	700	5.0	7.5	87.5	-	1.253×10^{-3}	1.0	.02
84-3	700	3.0	7.5	89.5	-	1.215×10^{-3}	.43	< .01
84-7	700	1.0	7.5	91.5	-	5.06×10^{-4}	.70	.20
90-8	700	1.0	7.5	91.5	-	4.16×10^{-4}	1.0	.03
92-4	700	0.3	7.5	92.2	-	1.37×10^{-4}	.82	.31
84-6	700	0.3	7.5	92.2	-	1.679×10^{-4}	.45	.06
94-6	700	0.3	7.5	67.2	25.0	1.675×10^{-4}	.8	.29

Table 3. continued

Run Ref. No.	Temp. °C.	Reaction Gas, mol% H_2S	H_2	N_2	H_2O	"Final" Rate, sec^{-1}	Range Covered by Straight-Line Portion of (1 - x) Plot (1 - x) initial	(1 - x) final
92-8	625	10.0	7.5	82.5	-	5.34×10^{-4}	0.17	.04
2-2-1	625	3.0	7.5	89.5	-	3.16×10^{-4}	.35	.023
92-5	625	0.3	7.5	92.2	-	6.4×10^{-5}	.72	.50
2-1-4	625	0.3	7.5	92.2	-	9.7×10^{-5}	1.0	.3
90-4	550	20.0	7.5	72.5	-	4.58×10^{-5}	.45	.33
94-9	550	10.0	7.5	82.5	-	6.26×10^{-5}	.52	.44
90-1	550	10.0	7.5	82.5	-	6.75×10^{-5}	.50	.39
86-3	550	10.0	7.5	82.5	-	2.14×10^{-5}	.74	.62
84-8	550	3.0	7.5	89.5	-	3.50×10^{-5}	.76	.65
84-5	550	3.0	7.5	89.5	-	3.97×10^{-5}	.80	.625
86-8	550	1.0	7.5	91.1	-	2.03×10^{-5}	.81	.69
92-6	550	0.3	7.5	92.2	-	1.925×10^{-5}	.85	.71
84-6	550	0.3	7.5	92.2	-	1.475×10^{-5}	.95	.755
94-9	475	10.0	7.5	82.5	-	9.77×10^{-6}	.72	.67
86-5	475	10.0	7.5	82.5	-	1.735×10^{-5}	.83	.74
2-1-5	475	1.0	7.5	91.5	-	8.5×10^{-6}	.8	.75
92-2	475	0.3	7.5	92.2	-	4.22×10^{-6}	.936	.887

more complex concentration dependence is involved.

From the shape of the curves in Figure 7, our first thought was that an equilibrium adsorption mechanism was operating. The rate expression would then be:

$$-\frac{1}{W}\frac{dW}{dt} = \frac{K\,[H_2S]}{1 + K_e\,[H_2S]} \qquad (4)$$

where K_e is the equilibrium constant for adsorption. Such a mechanism would explain Figure 7. It would not explain the peculiarly rapid initial rate of the lower curve of Figure 6 since a plot of log (1 - x) versus time should be linear.

As noted earlier, our procedure is to calcine under CO_2. After calcination is complete, we purge the CO_2 with nitrogen and we cool the sample under nitrogen to the run temperature. At the start of a run, the CaO may be presumed to have nothing on its surface. As the reaction proceeds, the rate slows, and this suggests that something is adsorbing upon the surface and inactivating the surface.

A notion that adsorbed water might be the culprit did not pan out, since runs with added water showed that this species does not inhibit the rate.

7.02 Nonequilibrium Adsorption Model

7.02.1 Introduction to Model

A pause is in order to consider the difference between our system and the commonly encountered catalytic systems where adsorption is a factor. One difference is that catalysts have a constant surface area, whereas our experimental system steadily loses active surface, CaO, as the reaction proceeds. Another difference is that our solid is reacting with the gas. In catalyst systems, a gas reacts with itself or with another gas. When the catalytic reaction involves only adsorbed species, it is said to follow a Langmuir-Hinshelwood mechanism. When the reaction occurs between a gas-phase molecule and an adsorbed molecule, it follows a Langmuir-Rideal mechanism (14).

Our system appears to behave according to a mechanism which may be regarded as a variant of the Langmuir-Rideal mechanism. We postulate that gas-phase H_2S reacts with the solid without undergoing adsorption, while adsorbed H_2S does not react. Figure 8 depicts broadly a potential energy diagram appropriate to the postulated mechanism. When a molecule of H_2S is adsorbed upon the surface, it must pass over a higher

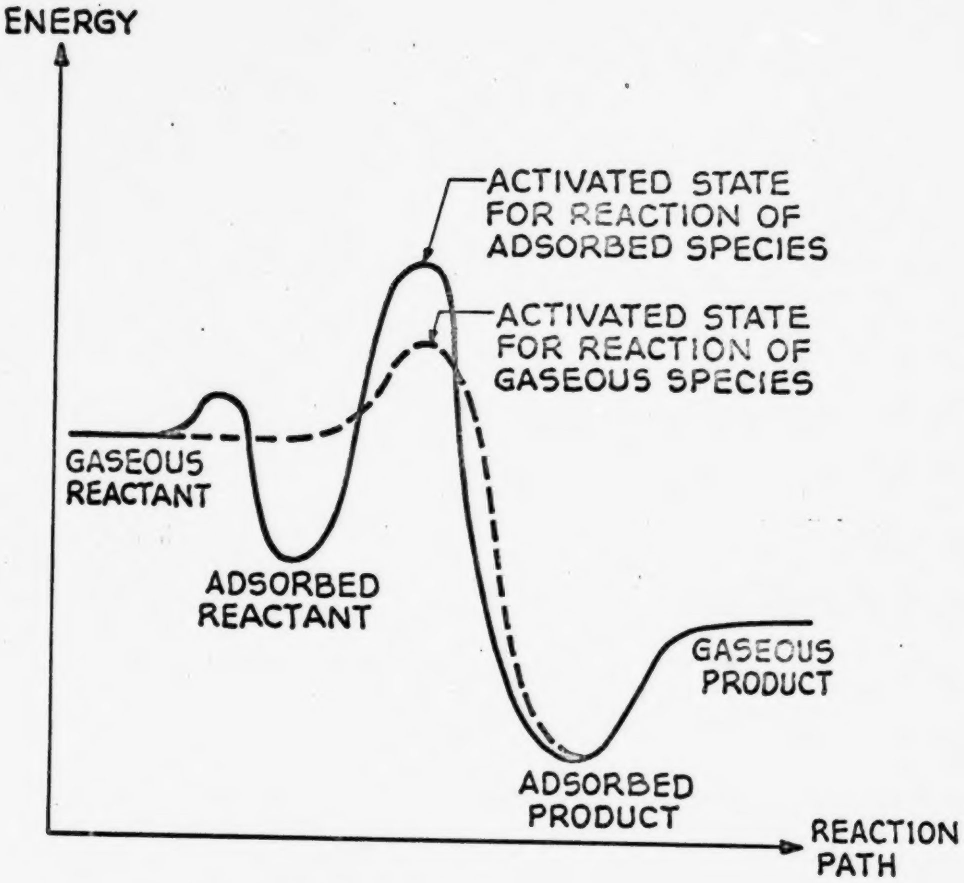
ENERGY
ACTIVATED STATE FOR REACTION OF ADSORBED SPECIES
ACTIVATED STATE FOR REACTION OF GASEOUS SPECIES
GASEOUS REACTANT
ADSORBED REACTANT
GASEOUS PRODUCT
ADSORBED PRODUCT
REACTION PATH

Figure 8. Potential energy diagram broadly appropriate to our postulated reaction model.

energy barrier than that which unadsorbed H_2S must pass over in order to react. This particular situation should be uncommon in catalysis, since it represents the case of a catalyst that does not work even though the reactants are known to adsorb.

In general, adsorption equilibrium will not exist during a run unless the adsorption and desorption kinetic constants are large with respect to the reaction kinetic constant. If adsorption is slow, reaction will begin at a high rate since the entire CaO surface is initially uncovered and free to react. As time passes, H_2S adsorbs upon the surface and the reaction slackens. The "final" rate will depend both upon the rate at which free CaO surface reacts and also upon the rates by which adsorption and desorption of H_2S govern the proportion of the CaO surface which is free.

Our model, of course, might include the hypothesis, mentioned earlier, that CaO exists in the solid at several levels of reactivity. It seemed preferable, however, to explore first the implications of the nonequilibrium adsorption model in its simplest form.

7.02.2 Derivation of Equations for Nonequilibrium Model

To express the proposed model in mathematical terms, we introduce the following notation:

C = $[H_2S]$ = concentration of H_2S, g-moles/liter,

W = weight of unconverted CaO in solid sample, any units,

W_o = initial weight of CaO in solid sample,

A = weight of unconverted CaO in solid sample which is available for reaction, any units,

B = weight of unconverted CaO shielded from the reaction due to formation of a CaO-H_2S surface complex, any units,

K_1 = adsorption rate constant, liters/g-mole H_2S-sec.

K_2 = desorption rate constant, sec^{-1}, and

K_3 = reaction rate constant, liters/g-mole H_2S-sec.

We may then write:

$$-\frac{dW}{dt} = K_3\ A\ C \tag{5}$$

$$-\frac{dA}{dt} = K_1\ A\ C - K_2\ B + K_3\ A\ C \tag{6}$$

Equation (5) is the rate of reaction of CaO with H_2S. The first term of equation (6) is the rate of adsorption of H_2S, the second term is the rate of desorption, and the last is the rate of reaction; the entire expression in equation (6) gives the rate of change in the concentration of CaO available for the reaction.

Noting that $W = A + B$, and that $-\frac{d^2W}{dt^2} = K_3 C \frac{dA}{dt}$, we may rearrange equations (5) and (6) to obtain:

$$\frac{d^2W}{dt^2} + (K_1C + K_3C + K_2) \frac{dW}{dt} + K_2K_3 C W = 0 \qquad (7)$$

The initial condition appropriate to our experiments is:

$$\left.\frac{dW}{dt}\right]_{t = 0} = - K_3 W_o C \qquad (8)$$

With this initial condition, equation (7) has the solution

$$(1 - x) = W/W_o =$$

$$= \left[(r_2 + K_3C) \exp(r_1t) - (r_1 + K_3C) \exp(r_2t)\right]/(r_2 - r_1) \qquad (9)$$

where

$$r_1, r_2 = - (\tfrac{1}{2}) (K_1C + K_3C + K_2)$$

$$\pm (\tfrac{1}{2}) \left[(K_1C + K_3C + K_2)^2 - 4 K_2K_3C\right]^{\frac{1}{2}} \qquad (10)$$

Both of the roots given by equation (10) are negative. The exponential term in equation (9) which carries the more negative root approaches zero more rapidly than does the term carrying the other root, and a plot of log (1 - x) versus time will eventually become linear for all practical purposes. The slope of such a plot will have the value of r_1, and this will be equal to the "final" rate as obtained from the data.

7.02.3 Equivalence with Equilibrium Case

One check on the validity of the derived equations is that they must produce the equilibrium model when the adsorption and desorption rates are fast compared with the reaction rate, that is, when

$$K_3C \ll K_1C, \text{ and } K_3C \ll K_2 \qquad (11)$$

Using (11) above in (10), we get

$$r_1, r_2 \cong -\tfrac{1}{2}(K_1C + K_2) \pm \tfrac{1}{2}\left[(K_1C + K_2)^2 - 4K_2K_3C\right]^{\frac{1}{2}} \qquad (12)$$

$$\cong -\tfrac{1}{2}(K_1C + K_2) \pm \tfrac{1}{2}(K_1C + K_2)\left[1 - \frac{4K_2K_3C}{(K_1C + K_2)^2}\right]^{\frac{1}{2}} \qquad (13)$$

Since for small x, $(1 - x)^{\frac{1}{2}} \cong 1 - \tfrac{1}{2}x$:

$$r_1, r_2 \cong -\tfrac{1}{2}(K_1C + K_2) \pm \tfrac{1}{2}(K_1C + K_2)\left[1 - \frac{2K_2K_3C}{(K_1C + K_2)^2}\right] \qquad (14)$$

$$r_1 \cong \frac{-K_2K_3C}{K_1C + K_2} = \frac{-K_3C}{\dfrac{K_1}{K_2}C + 1} \cong \frac{-K_3C}{1 + K_eC} \qquad (15)$$

$$r_2 \cong -(K_1C + K_2) + \frac{K_2K_3C}{(K_1C + K_2)} \cong -(K_1C + K_2) \qquad (16)$$

Since $|r_2| >> |r_1|$, the second exponential term in equation (9) approaches zero very quickly in comparison to the first term.

For the premultiplier of the r_1 exponential in equation (9), we have

$$\frac{r_2 + K_3C}{r_2 - r_1} \cong \frac{-(K_1C + K_2) + K_3C}{r_2} \cong \frac{r_2}{r_2} = 1 \qquad (17)$$

The equilibrium case, equation (4), is obtained by setting the premultiplier in equation (9) equal to unity and using equation (15) for r_1.

7.02.4 Determination of Kinetic Constants

The kinetic constants were determined in several stages. At high temperatures, we estimated K_3 directly from runs where first-order kinetics, equation (3), were operating. At lower temperatures, a first estimate of both K_3 and K_e can be obtained by considering adsorption equilibrium to be operating. Rewriting equation (4) in an integrated form, we get:

$$\text{Slope of log } (1 - x) \text{ vs. time} = s = \frac{K_3C}{1 + K_eC} \qquad (18)$$

If the value of the slope is known for several concentrations, (18) can be rearranged to give:

$$s/C = K_3 - K_e s \tag{19}$$

Plotting s/C vs. s gives a line whose slope is K_e and whose intercept is K_3.

The above procedure gives only first estimates of the kinetic constants since the adsorption is not actually at equilibrium. In addition it gives only two kinetic constants.

Our final kinetic constants were obtained by a trial and error procedure. The constants were adjusted primarily to provide a fit of the "final" rates and to maintain Arrhenius expressions. Keeping an eye on the curvature of the log (1 - x) versus time plots was sometimes helpful in making the choice between alternative adjustments of the K's which were nearly equivalent in respect to the fit of the "final" rates and the maintenance of Arrhenius expressions.

7.02.5 Testing the Model

The reaction model expressed by equations (9) and (10) must meet several requirements:

- Plots of log (1 - x) versus time should, at low temperatures, display a high initial rate which slackens to a "constant" final rate. At higher temperatures, the plot should become substantially linear.
- The predicted values of rate should match the observed data as a function of H_2S concentration.
- The constants K_1, K_2, K_3, and K_e must depend upon temperature according to the Arrhenius expression.

Our proposed model appears to be capable of substantially meeting these requirements.

Table 4 lists the coefficients for the Arrhenius expression for each of the above constants, and Table 5 gives the constants themselves for each experimental temperature. Figures 9, 10, and 11 give Arrhenius plots for K_3, K_2, and K_e respectively using the data in Table 5. The fit to the Arrhenius expression is good.

The activation energy for the reaction rate constant, K_3, is about 23 kcal/g-mole$^{\circ}$K.

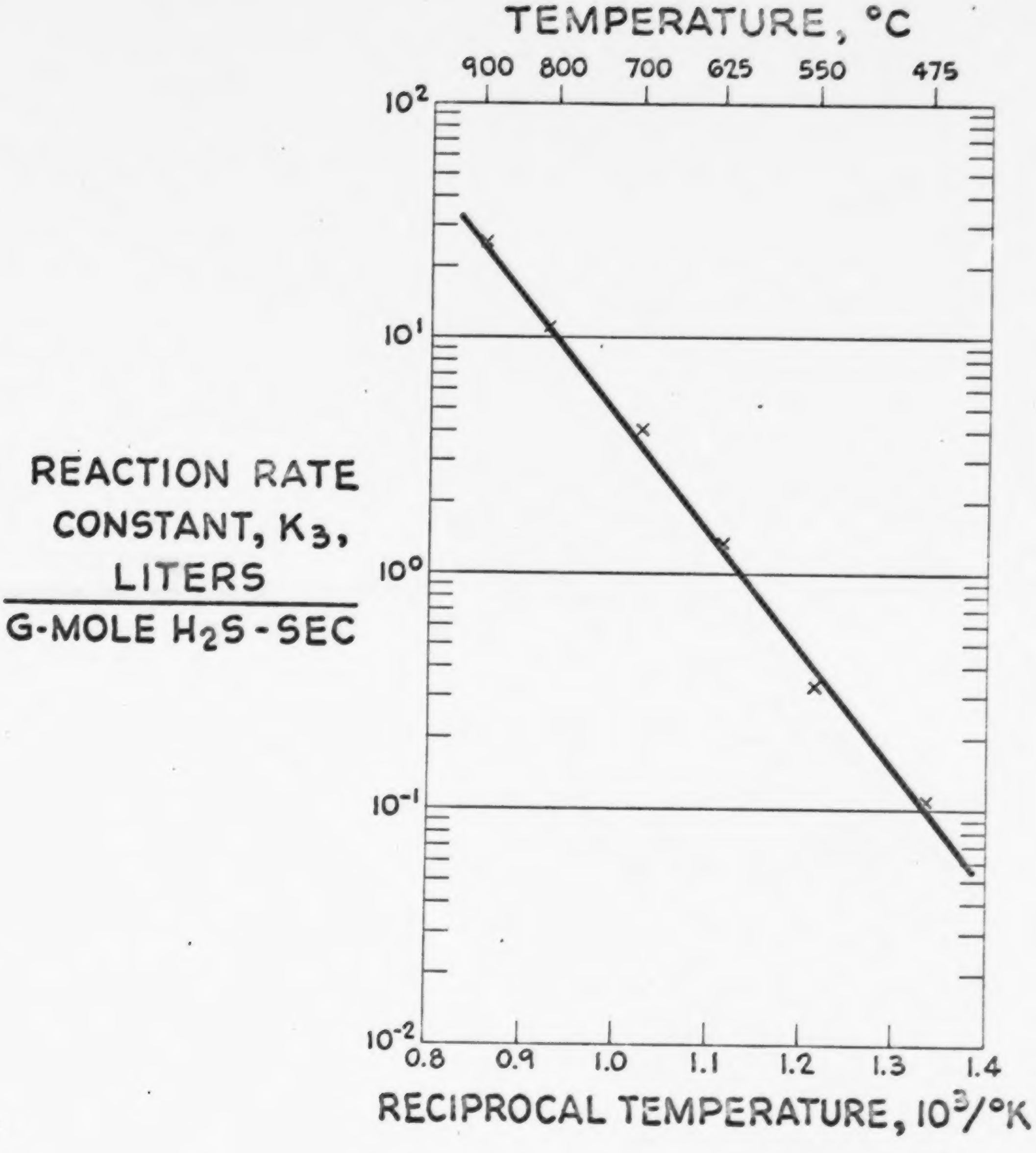

Figure 9. Reaction rate constant, K_3.

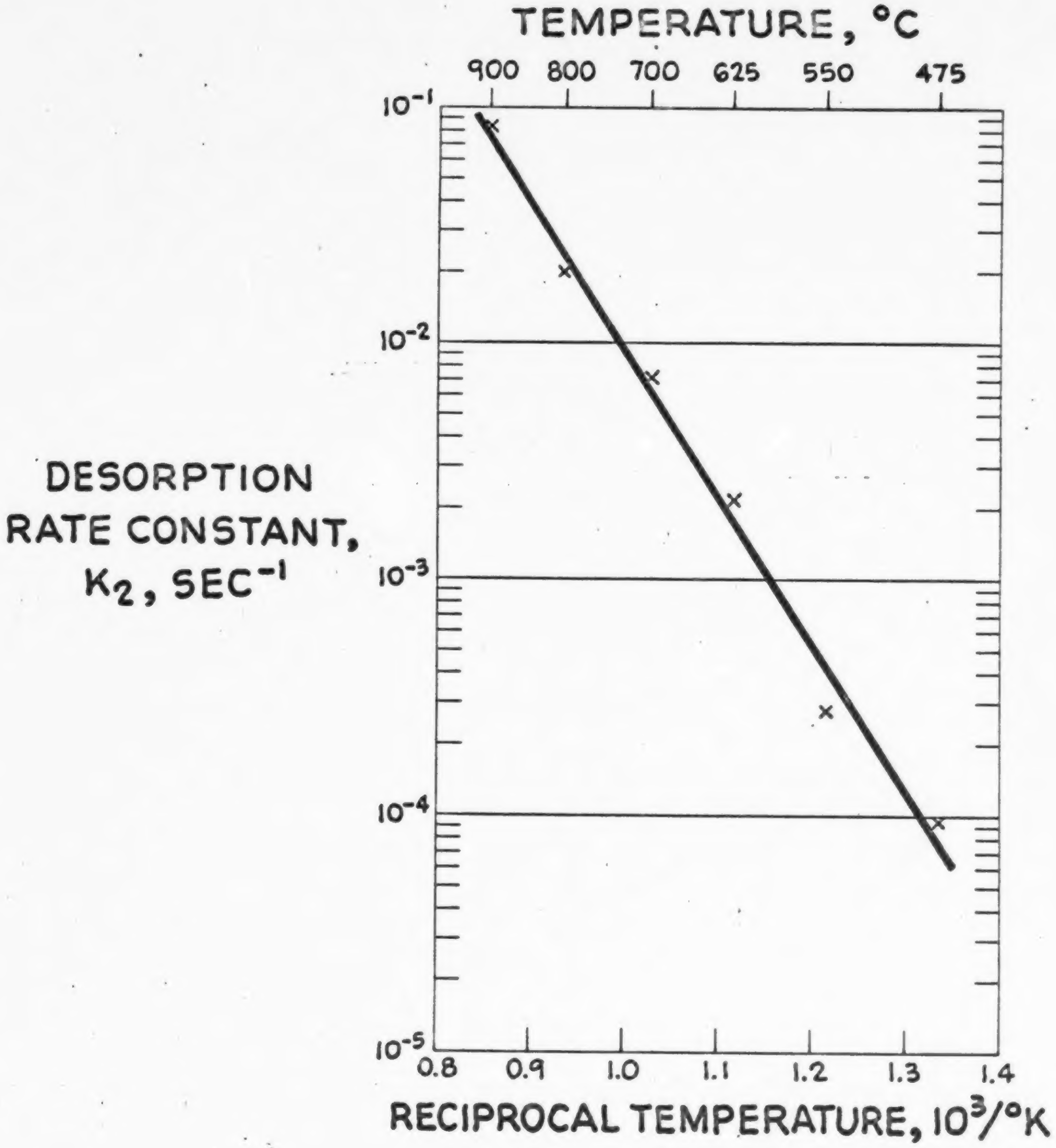

Figure 10. Desorption rate constant, K_2.

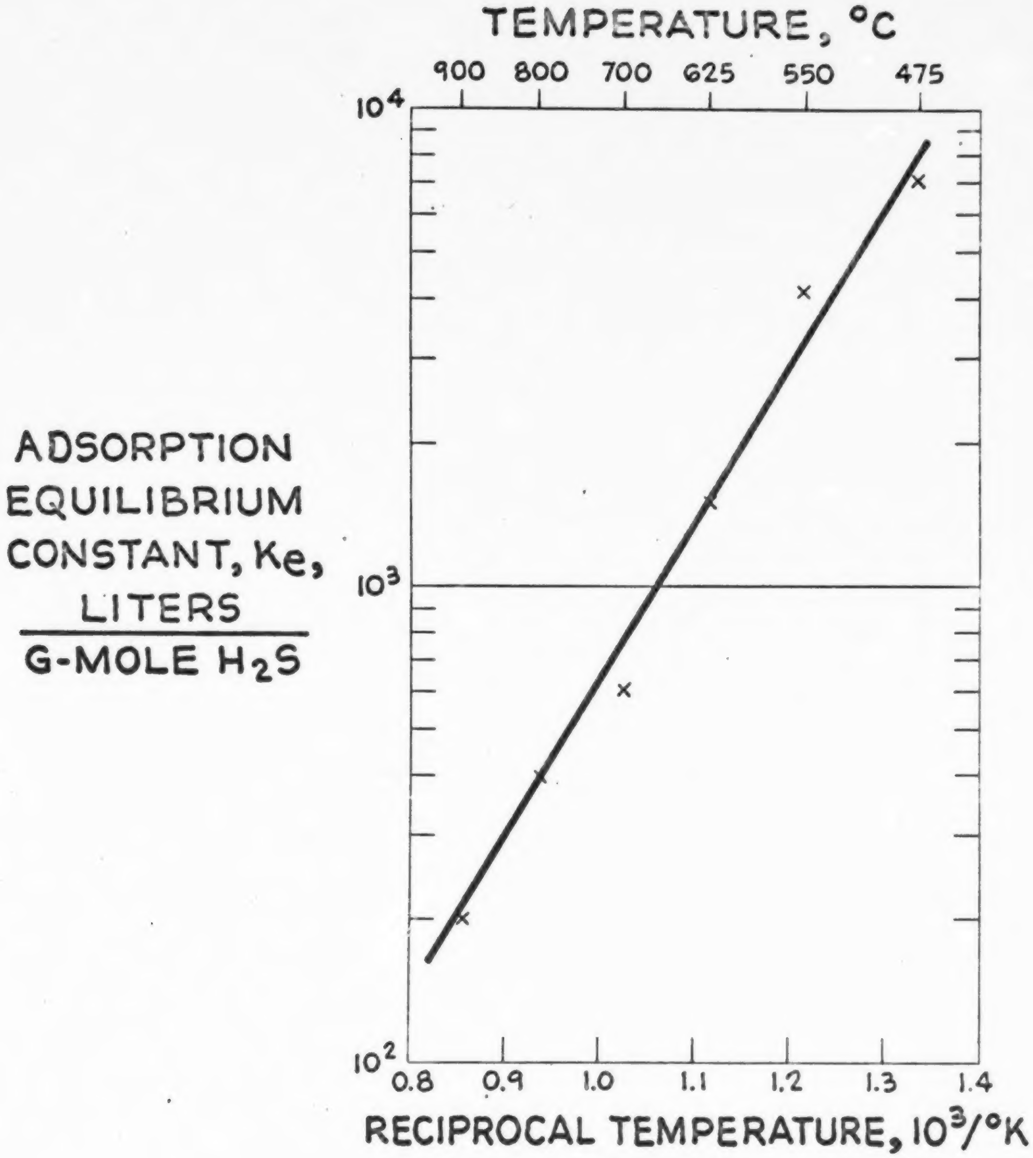

Figure 11. Adsorption equilibrium constant, K_e.

Table 4. Coefficients of Arrhenius Expressions for Kinetic Constants

$\ln K = \ln A - E/RT$

Description	Symbol	ln A	E, kcal/g-mole°K
Adsorption rate constant	K_1	8.325	13.086
Desorption rate constant	K_2	9.525	28.242
Reaction rate constant	K_3	13.114	22.917
Adsorption equilibrium	$K_e = K_1/K_2$	-1.201	-15.150

Note: The values in this table were obtained from a regression analysis on values given in Table 5, and are set down with more significant figures than the uncertainty in these values would actually warrant.

Table 5. Kinetic Constants Obtained from Trial and Error Analysis

Temperature °C	K_1 $\frac{\text{liters}}{\text{g-mole } H_2S \text{ sec}}$	K_2 sec^{-1}	K_3 $\frac{\text{liters}}{\text{g-mole } H_2S \text{ sec}}$	K_e $\frac{\text{liters}}{\text{g-mole } H_2S}$
475	6.7×10^{-1}	9.6×10^{-5}	1.1×10^{-1}	7.0×10^{3}
550	1.15	2.8×10^{-4}	3.3×10^{-1}	4.1×10^{3}
625	3.4	2.2×10^{-3}	1.35	1.5×10^{3}
700	4.2	7.0×10^{-3}	4.0	6.0×10^{2}
800	8.0	2.0×10^{-2}	1.1×10^{1}	4.0×10^{2}
900	1.68×10^{1}	8.4×10^{-2}	2.5×10^{1}	2.0×10^{2}

Figures 12, 13, 14, and 15 give plots of (1 - x) calculated from equations (9) and (10) for the conditions of some of our actual runs at 475°, 550°, 625°, and 700°C respectively. Curves drawn through the run data are plotted for comparison. In general, the curves generated from the K's reproduce the main features of the data.

The curves in Figure 7 have been calculated from the K values of Table 5, and the fit to the data is rather good. The most serious difficulty is that the "final" reaction rates at low H_2S concentrations, particularly at 900°C, tend to fall above the curves based upon K's. This difficulty will be discussed in Section 8.01.1.

7.03 Runs with Spheres

In reaction (A), a solid reacts to give a second solid product; the solid retains porosity in both the reacted and unreacted condition.

In such a situation, the rate of chemical reaction might be governed by the diffusion of gaseous species through an "ash" layer of product occupying the outer region of a particle of the solid.

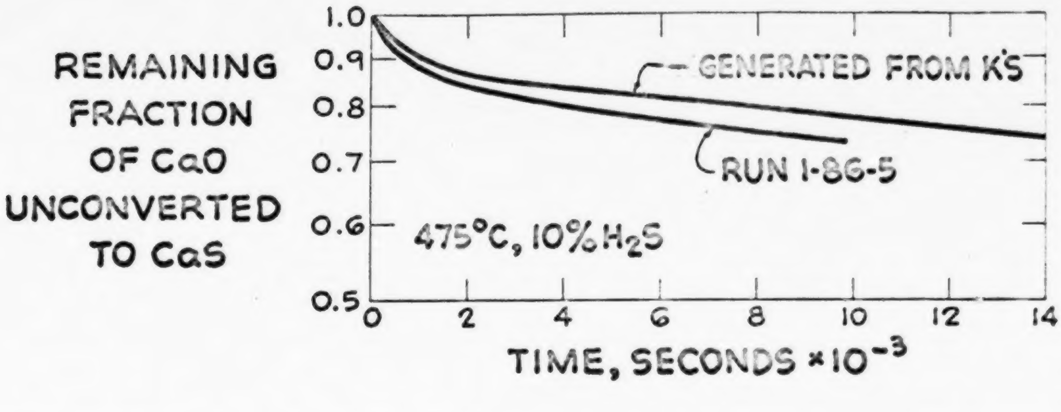

Figure 12. Comparison of log (1 - x) plot for run at 475°C with curve generated from K's.

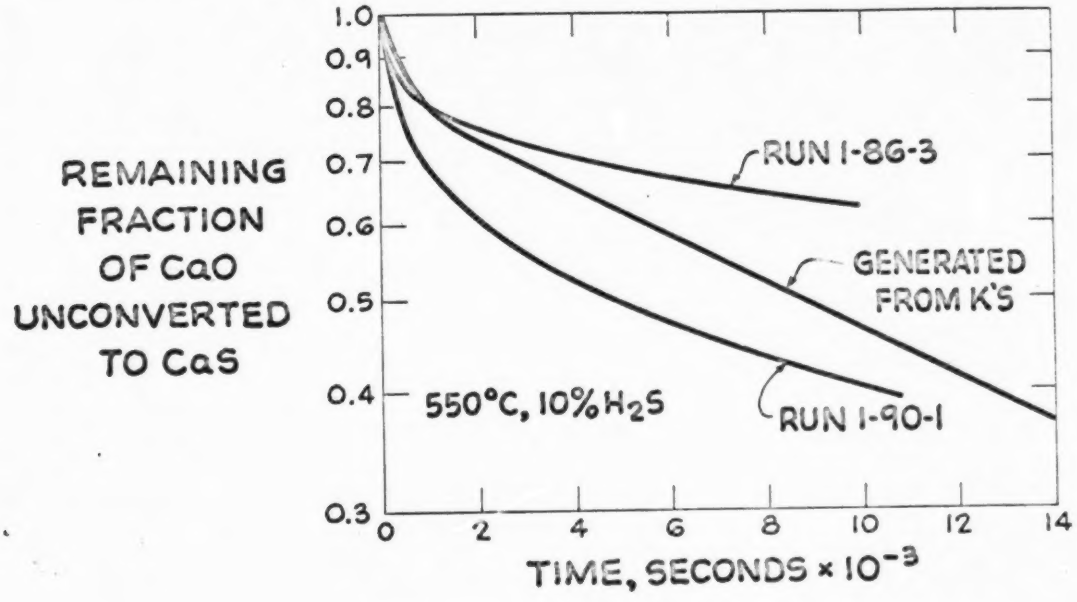

Figure 13. Comparison of log (1 - x) plots for duplicate runs at 550°C with curve generated from K's.

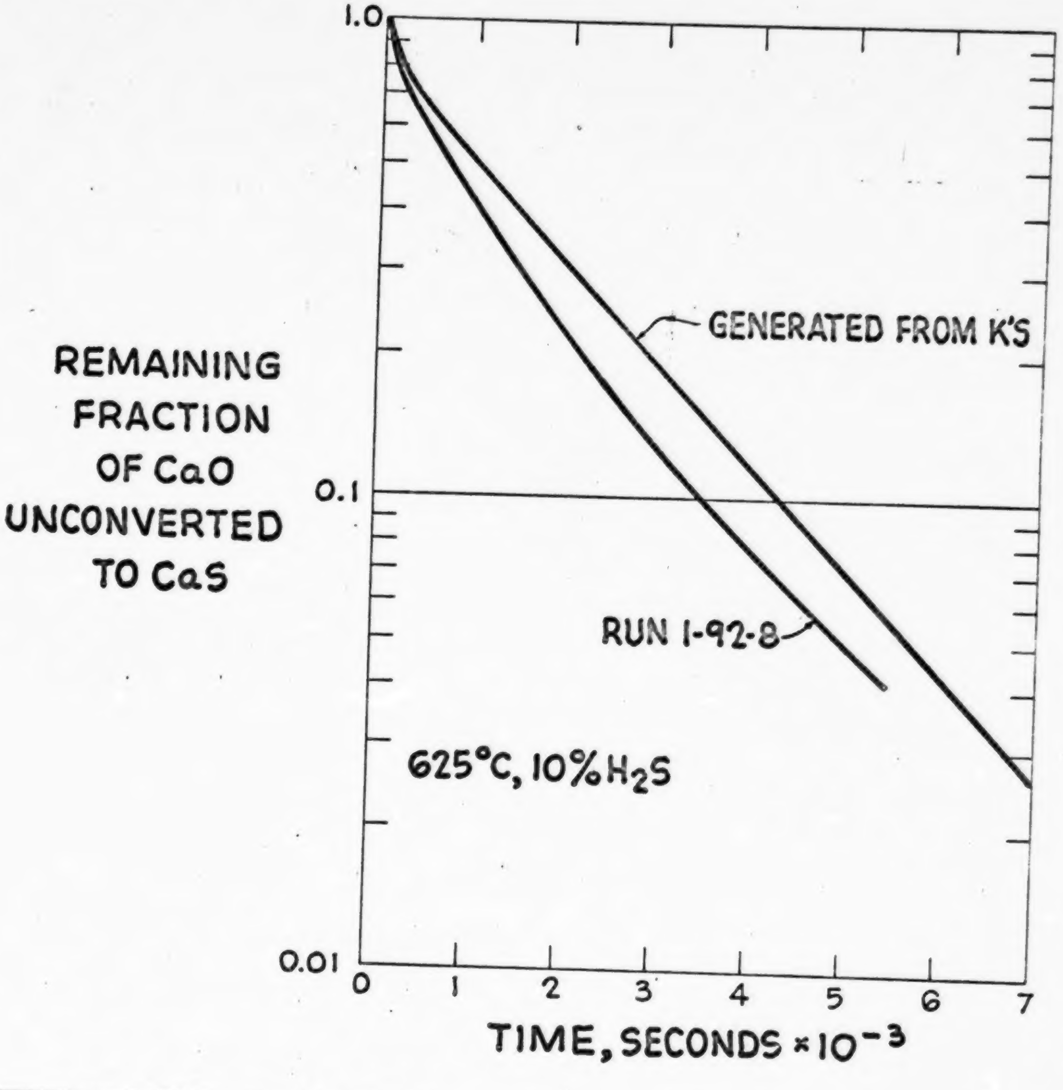

Figure 14. Comparison of log (1 - x) plot for run at 625°C with curve generated from K's.

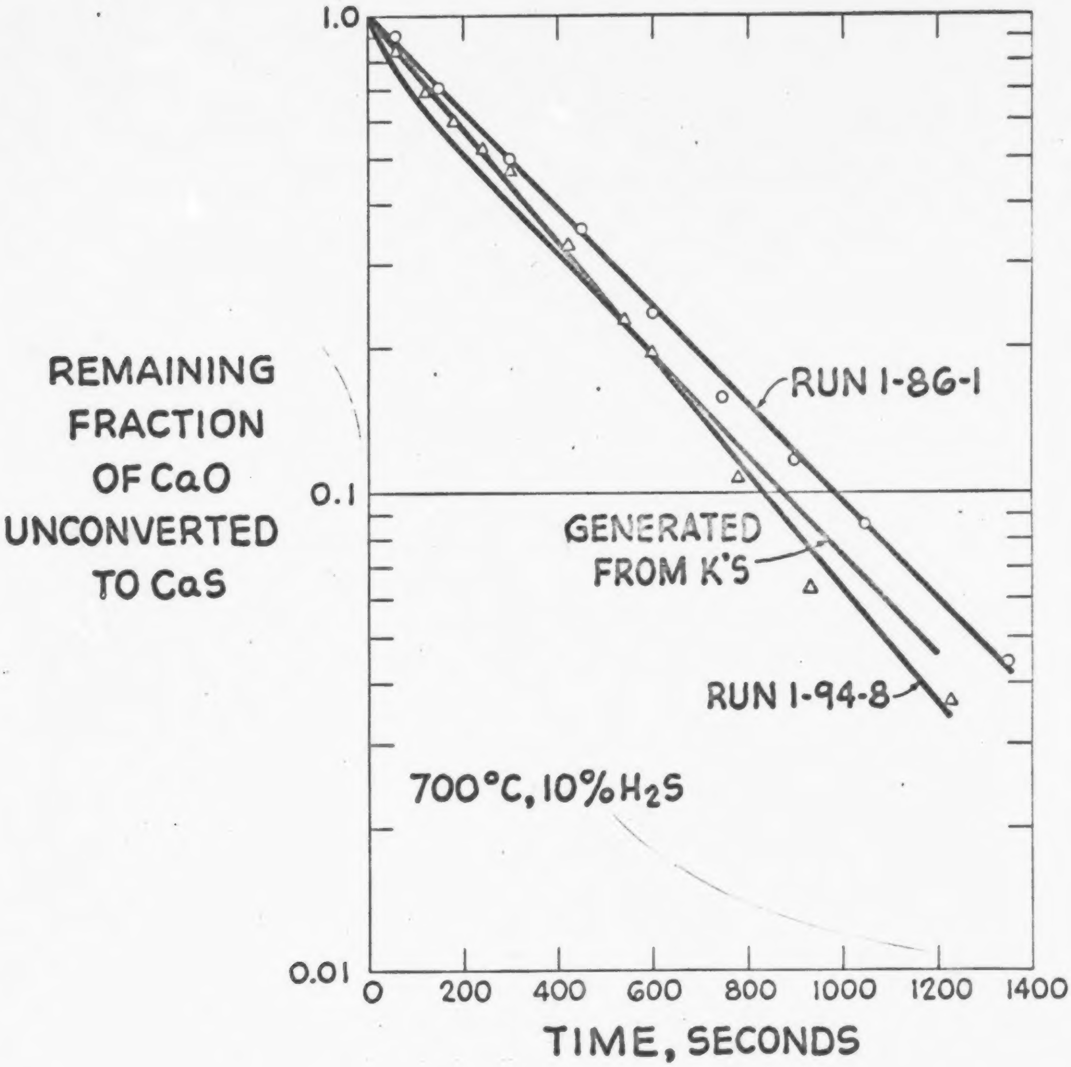

Figure 15. Comparison of log (1 - x) plot for duplicate runs at 700°C with curve generated from K's.

Another possibility would be that the reaction rate would be governed by a rate of a homogeneous reaction occurring throughout the particle, possibly inhibited by a concentration gradient within the particle brought about by diffusion of reactants to its interior. For a homogeneous reaction mechanism, the rate may be independent of solid concentration; in this case, an initial period of constant reaction rate is predicted (16). Homogeneous reactions in porous solids are also known for which the reaction rates depend upon the concentration of a reactive species within the solid; the burn-off of carbon from a catalyst shows this behavior when the carbon deposit is present simply as a monomolecular layer (17).

At the outset of this research, our first interest was to determine the reaction mechanism with respect to these questions. We chose to perform our first experiments with spheres, because spherical geometry makes the calculation of diffusional resistances easy for both the external gas film and the solid itself. We hoped in our early runs to determine the reaction mechanism independent of questions of gas-film diffusion and diffusion within the solid. Our major interest was to learn the role of solid concentration and to test the possibility, admittedly remote, that a reaction-controlled shrinking core might develop in the solid.

We thought it better to settle such questions before undertaking work to disclose the dependence of the reaction rate upon gas concentration. The concentration of H_2S was therefore held at 5% for all runs with spheres except one.

7.03.1 Dependence of Rate Upon CaO Concentration

We conducted thirteen runs for reaction (A) on seven samples of Glasshouse stone. Two samples were cycled so that reaction (A) was conducted twice, and one sample was cycled five times.

We conducted seven runs for reaction (A) on seven samples of Greenfield stone.

A reasonably straight line is obtained for all of the runs when the data are put into form of a plot of time versus the diffusion statistic, $1 + 2\ (1 - x) - 3\ (1 - x)^{2/3}$ (see Section 7.05.1). This statistic describes a diffusion-controlled, shell-progressive mechanism. As kineticists recognize well, however, approximate agreement of the data with this statistic is difficult to assess and is no quarantee that diffusion is in fact controlling. For all runs except the runs at the highest temperatures, 850° and 950°C, the values of the effective diffusivity obtained from the plots versus diffusion statistic are far too low, and the fit is poorest at high conversions. Except for the high-temperature runs, diffusion would not appear to be a major controlling factor.

Since the data showed little if any constant rate period, we can exclude a homogeneous reaction mechanism where the rate is independent of solid concentration.

A simple plot of log (1 - x) versus time provided a reasonably good it of the sphere data. Figures 16 and 17 are typical.

Before our work with powders, we did not understand why a run at a lower temperature typically began at a faster rate, and later slowed to a reasonably steady "final" rate. The run at 625° depicted in Figure 16 is typical.

Nevertheless, we adopted as a working hypothesis the assumption that the reaction proceeds throughout

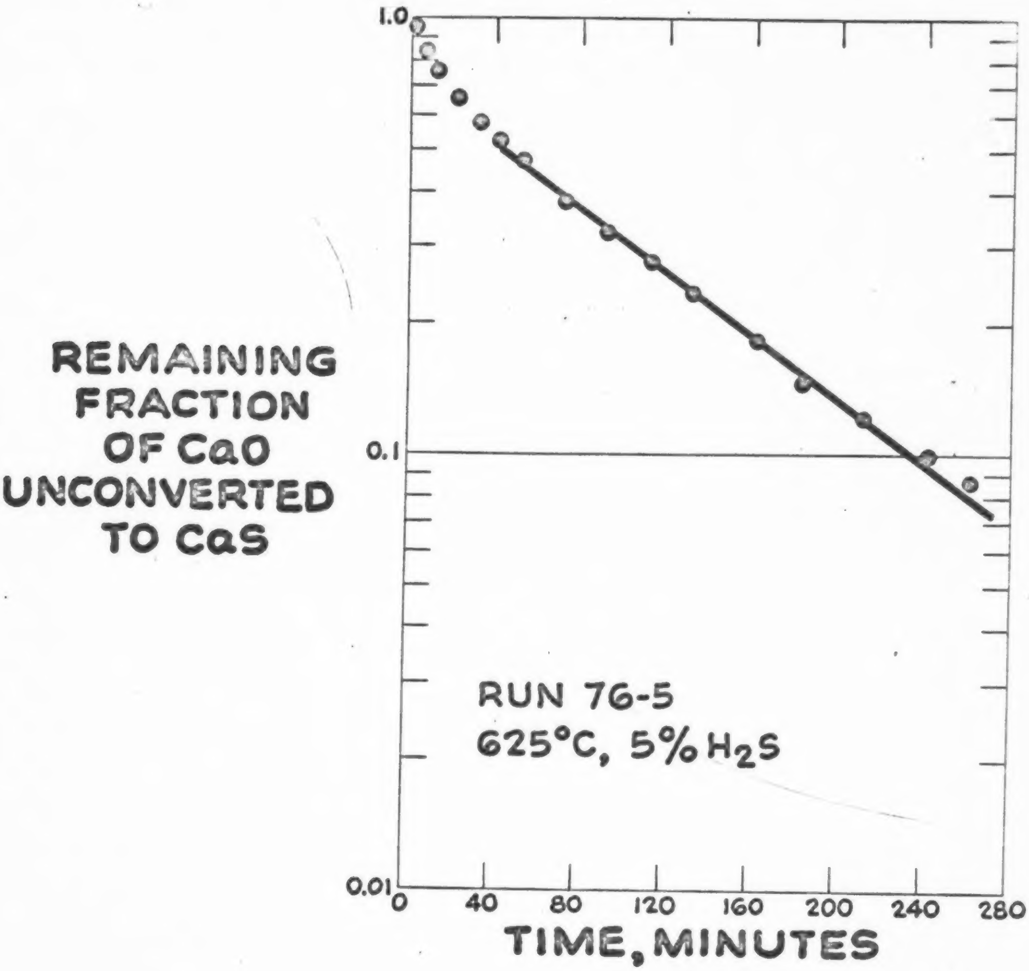

Figure 16. Data for run 76-5, conducted at 625°C on 7.6 mm sphere of Glasshouse stone.

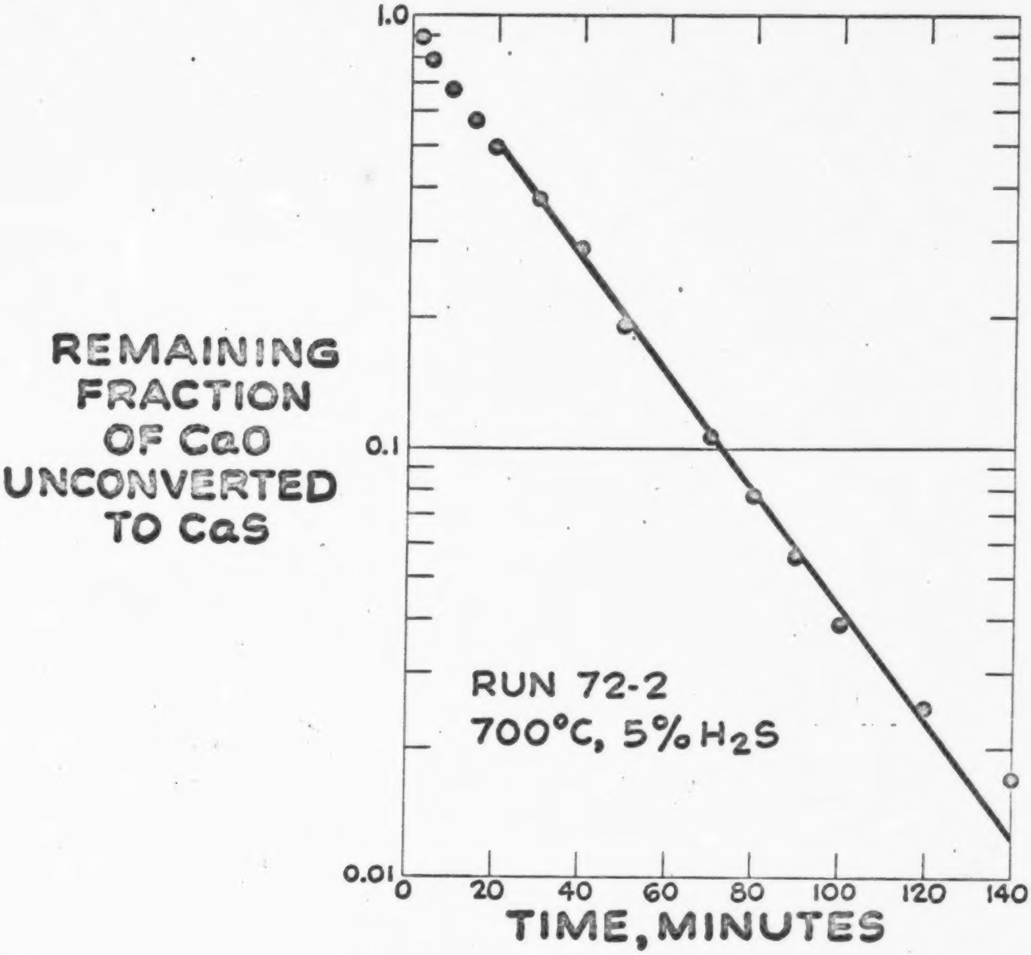

Figure 17. Data of run 72-2, conducted at 700°C on 6.5 mm sphere of Glasshouse stone.

the solid sample at a substantially uniform rate which is proportional to the quantity of unconverted CaO remaining in the sample.

We summarized the sphere data assuming the simple model in which the reaction is first order in H_2S and proportional to the unconverted CaO in the sample:

$$- \frac{1}{W} \frac{dW}{dt} = "K_3" [H_2S] \qquad (21)$$

where "K_3" is an apparent rate constant determined from the slope of the log (1 - x) plot at CaO conversion beyond 50%.

Table 6 summarizes data from all of the sphere runs, except for runs at 950°C, which were controlled by ash-layer diffusions.

7.03.2 Diffusion and Thermal Effects

Basing the apparent rate constant "K_3" in equation (21) upon data for CaO conversions beyond 50% not only excluded data for the faster rate period typical of runs at low temperature but also excluded data which might be marred by diffusion of thermal effects.

Based upon a typical observed initial reaction rate at 700°C for Glasshouse stone, an estimate of the

Table 6. Absorption of Sulfur from H_2S by Spheres of Fully Calcined Dolomite

Run Ref. No.	Sphere Ref. No.	Cycle No.	Diam. mm	Sphere Density gm/cm^3	Reaction Gas, mole % N_2	H_2	H_2S	CO_2** Evolved, moles x 10^3	H_2S Absorbed, moles x 10^3	First Order Rate Constant, liters (actual) / gm-mole H_2S-sec.	Temp. °C
64-3	68-1	1	8.4	2.9	70	20	10	4.9	4.1	0.381	700
72-1	68-1	2	8.4	2.9	85	10	5	4.1	4.1	0.040	550
72-2	68-2	1	6.5	2.8	85	10	5	2.1	2.1	1.20	700
72-3	68-2	2	6.5	2.8	87.5	7.5	5	2.1	2.0	2.64	700
72-4	68-2	3	6.5	2.8	"	"	"	2.0	2.1	0.245	555
72-5	68.2	4	6.5	2.8	"	"	"	2.1	2.2	4.66***	850
72-6	68-2	5	6.5	2.8	"	"	"	2.0	2.2	0.0316	475
76-1	74-1*	1	7.57	2.43	"	"	"	2.9	-	ca. 0.5	625
76-2	74-2*	1	7.73	2.46	"	"	"	3.1	-	0.510	625
76-3	74-3*	1	7.63	2.44	"	"	"	3.0	-	0.541	625
76-4	74-4*	1	7.49	2.45	50	45	5	2.8	-	0.292	625
76-5	74-5	1	7.62	2.74	87.5	7.5	5	3.4	3.4	0.207	625
76-6	74-5	2	7.62	2.74	"	"	"	3.0	2.8	1.27	750
80-1	79-4	1	5.90	2.61	87.5	7.5	5	1.5	.32	-	625
80-2	78-3	1	5.54	2.68	"	"	"	1.26	1.26	0.169	625
80-3	79-2	1	5.56	2.54	"	"	"	1.17	-	ca. 0.065****	625
										ca. 1.24****	756

---

*Spheres 74-1, 74-2, 74-3, and 74-4 were cut from the same chunk of rock, about 2 inches across.

**Quantity of CO_2 evolved from $CaCO_3$ during the last calcination prior to the run.

***Apparently diffusion controlled.

****Approximate values since temperature was changed during the run.

diffusion of reactants across the stagnant gas film surrounding the sphere indicates the presence of roughly a 15% drop in H_2S concentration between the bulk gas phase and the gas at the surface of the sphere.

The effective diffusivity in ⌈CaS+MgO⌉ will be developed in Section 7.05.2. Anticipating the results to be presented there, we note that the effective diffusivity in ⌈CaS+MgO⌉ prepared at 850°C from Glasshouse stone is about 14% of the bulk diffusivity, while that in ⌈CaS+MgO⌉ prepared from Greenfield stone at 950°C is about 6% of the bulk diffusivity. Based upon these values, we estimate a lower limit of 0.8 for the Thiele utilization factor at 700°C or 625° respectively for our spherical samples of the two stones. The Thiele utilization factor is the ratio of the observed rate to the true kinetic rate if the reactant concentration were uniform throughout the particle.

The reaction is exothermic by about 10 kcal/g-mole. At a typical initial reaction rate at 700°C for Glasshouse stone, the dissipation of the heat of reaction from the sphere to the gas causes a temperature difference of several degrees through the gas film.

Estimates following methods outlined by Luss and Amundson (18) show the internal temperature gradient to be negligibly small.

The foregoing diffusion and thermal effects are greatest at the outset of a run. Data for conversions of CaO beyond 50% should be relatively free of such effects.

7.03.3 Kinetic Data for Spheres

Figures 18 and 19 give Arrhenius plots of the apparent first order reaction rate constant, "K_3" in equation (21), derived from the data beyond 50% conversion of CaO.

Runs 72-2 through 72-6 were conducted on a single sample of Glasshouse stone. Figure 18 is an Arrhenius plot of the apparent rate constants for these runs. Numbers alongside the five points plotted in Figure 18 indicate the order in which the five runs were carried out.

As mentioned earlier, the run at 850°C appears to have been at least partly controlled by diffusion. Based upon the second, third, and fifth runs in sequence, an apparent activation energy of about 30 kcal/g-mole°K

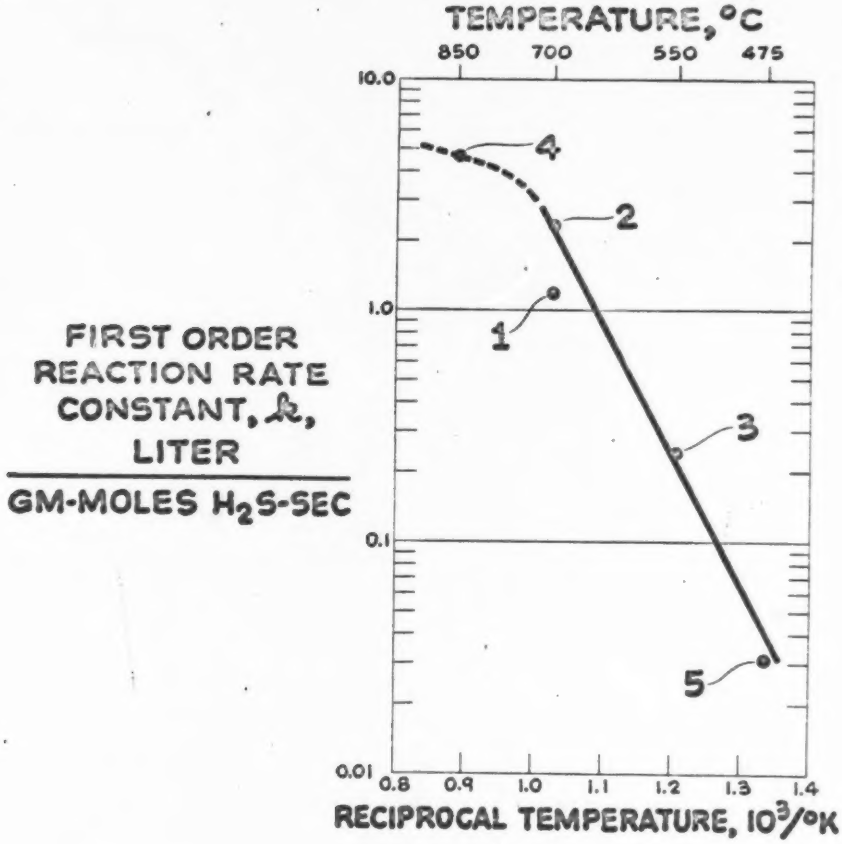

Figure 18. Arrhenius plot of data from runs 72-2 through 72-6 performed on the same 6.5 mm spherical sample of Glasshouse stone. The numbers alongside the points indicate the order of the five runs.

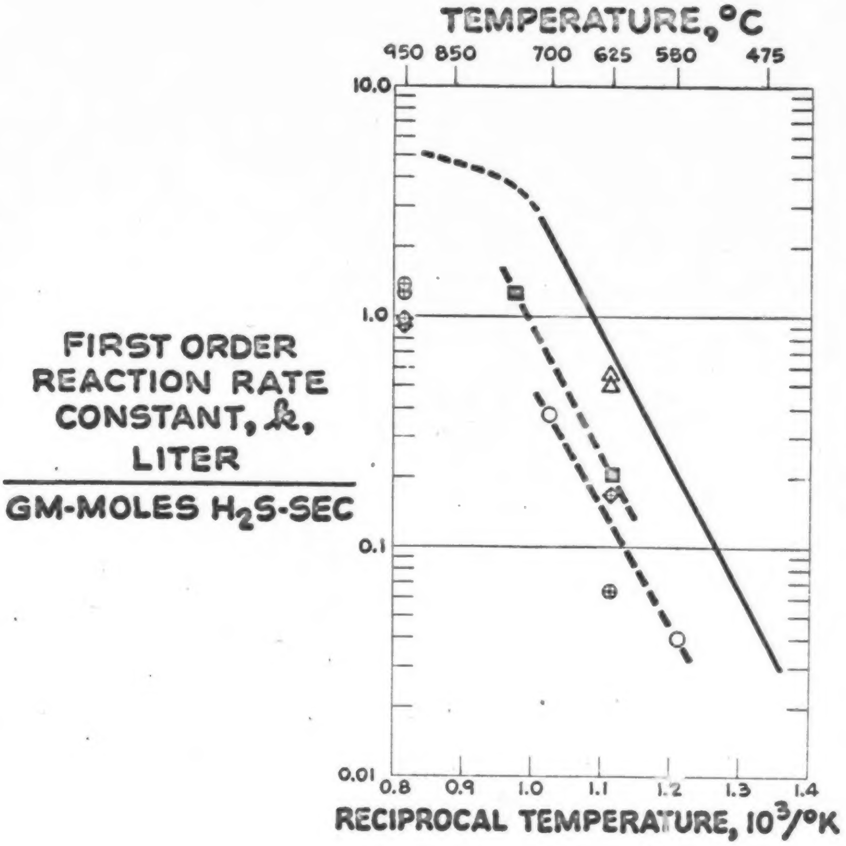

Figure 19. Arrhenius plot for data from runs on a number of spherical samples of stone. The curve without data points is reproduced from the curve in Figure 18.

△ = Runs 76-2 and 76-3 on samples cut from the same chunk of Glasshouse stone.

■ = Runs 76-5 and 76-6 on a single sample of Glasshouse stone.

○ = Runs 64-3 and 72-1 on another single sample of Glasshouse stone.

◈ = Runs 80-2, 80-4, and 80-7 on three samples cut from the same chunk of Greenfield stone.

⊕ = Runs 80-3, 80-5, and 80-6 on three samples cut from another single chunk of Greenfield stone.

would be indicated. As noted in Section 7.02.5, powder data indicate the activation energy for the "true" first order rate constant, K_3 in equation (5), to be about 23 kcal/g-mole-^{o}K. The apparent activation energy indicated by sphere data is higher because, as Figure 7 reveals, the "final" rates at lower temperatures suffer greater hindering by H_2S adsorption at the 5% H_2S level used for the data in Figure 18.

Figure 19 is an Arrhenius plot of apparent rate constants for the remaining runs listed in Table 6 (except Run 76-1). For comparison, the curve drawn in Figure 18 is repeated in Figure 19. It would appear from Figure 19 that a large variability exists among samples of stone, even when all of the samples are taken from the same quarry. The two upright triangles in Figure 19 are for Runs 76-2 and 76-3, which gave concordant results for two samples cut from the same chunk of Glasshouse rock (about 2 inches across). Run 76-1 behaved similarly, and the sample was also taken from this chunk. Two other Glasshouse stones were cycled twice (the open circles and closed squares in Figure 19), giving far lower rates than the sample cycled five times which established the curve in Figure 18.

The three diamonds in Figure 19 are for three samples of Greenfield stone all cut from the same chunk of rock. Run 80-2 was made at 625°C as a check on the kinetic activity of the stone. Runs 80-4 and 80-7 were then made to determine the effective diffusivity appliable to the stone. Similarly the three circles containing a "+" are for another three samples of Greenfield stone all cut from a second chunk of rock. Run 80-3 was made at 625°C as a test of a kinetic activity, and Runs 80-5 and 80-6 were made to determine effective diffusivity.

7.03.4 Correlation of Reaction Rate and Time for Calcination

As described in Section 6.02, calcinations were conducted nonisothermally. Although an exact history of temperature versus time is not available for each sample, in general the sample was heated at about 10 to 15°C per minute to the nominal temperature 925°C. The sample was held at this temperature until the weight became steady. Table 7 notes the time of the hold at about 925°C for each of the sphere runs.

Table 7. Variation in Time Required to Calcine Various Dolomites

Run Number	Cycle Number	Temp. of Calcination, °C Mg	Temp. of Calcination, °C Ca	Time of Calcination, Minutes Mg	Time of Calcination, Minutes Ca	Ratio of Observed Rate Given by Curve in Fig. 18
64-3	1	- 770	908 - 919	45	55	6.0
72-1	2		908 - 927		60	4.5
72-2	1		900 - 915	30	40	1.6
72-3	2		910 - 922		40	0.85
72-4	3		912 - 915		35	0.9
72-5	4		918 - 922		35	-
72-6	5		916 - 920		30	1.3
76-1	1	525 - 800	900 - 923	35	35	-
76-2	1	475 - 850	900 -	40	35	1.4
76-3	1	855	905 - 920	40	30	1.3
76-4	1		905 - 921	40	40	-
76-5	1		904 -	35	50	3.4
76-6	2		915 - 923		90	3.4
80-2	1	570 - 850	910 - 921	25	30	4.1
80-3	1	500 - 850	900 - 920	30	20	11
80-4	1	500 - 850	915 - 921	40	45	-
80-5	1		908 - 920	45	30	-
80-6	1		920	45	40	-
80-7	1	550		40	50	-

---

*Mg calcination temperatures are approximate. The lower Ca calcination temperature represents the point at which calcination was occurring rapidly and is approximate. The upper Ca calcination temperature is ± 2°C.

Table 7 also lists for each run the rate of the H_2S absorption reaction relative to the rate established for the single sample of stone in the five runs plotted in Figure 18. Comparison of the hold times at about 925°C with the relative reaction rates listed in Table 7 shows that stones which gave lower rates for absorption of H_2S also generally exhibited a lower rate for calcination. The stones varied in density from 2.4 to 2.9 g/cm^3, and they varied in color from grey to light brown, but there was no obvious relationship between these properties and rate.

7.03.5 Effect of Cycling

As mentioned earlier, Runs 72-2 through 72-6 were conducted on a single sample of stone, providing a test of the regeneration procedure using reaction (C) followed by a calcination. A column of Table 6 gives the take-up of H_2S by the sample in each run. From data in this column, we see that the capacity of the stone remained steady, all of the CaO in the stone remaining available for reaction with H_2S.

From the Arrhenius plot of the apparent rate constants for these runs, given in Figure 18, it would appear that no drastic decline in reactivity occurred betwen the second and fifth runs. The increase in reactivity between the first and second runs of this series cannot now be explained.

Two stones were cycled twice (the open circles and closed squares in Figure 19). Rates for these stones were far lower than rates for the sample cycled five times, but they indicate much the same apparent activation energy.

7.04 Inspections of Sectioned Spheres

7.04.1 Spheres Disclosing Reaction Homogeneity

For expression (21) to hold, the CaO throughout the sample of stone must be viewed as being accessible to the reaction gases.

Runs 76-1, 76-2, and 76-3 were conducted at 625°C as a preliminary test of the homogeneous mechanism implied by equation (21). Three identical samples of Glasshouse stone were prepared from a single chunk of rock, about 2 inches across. Run 76-1 was carried to 42% conversion of CaO to CaS; run 76-2 was carried to 59% conversion; and run 76-3 was carried to 94% conversion. Following the runs, each stone was mounted in a self-setting resin, sectioned, and examined under ultra-violet light at 2537 Å. Of the chemical species present, only CaS fluoresces under short wave length ultraviolet, and its presence can easily be detected under this light. An identical sample of unreacted stone was also sectioned and examined under the light. No fluorescent material could be seen on the exposed surface of the unreacted stone. Each of the reacted stones fluoresced at a substantially uniform intensity across its diameter, so far as visual observation could judge. This indicated that CaS was present throughout each of the reacted stones. Since the stone at 42% conversion showed a less intense fluorescence than the stone at 94% conversion, a sharp variation in conversion across the stone at 42% conversion would have made itself known by a gradation in the fluorescence.

At 42% conversion, a shell reaction mechanism, such as that brought about ash-layer diffusion, would call for a particle to be free of product across 83% of its diameter. The appearance of the sectioned stones under ultraviolot light was clearly not compatible with such a mechanism.

As a further test of the homogeneous mechanism, we reacted a sphere of Greenfield stone at 625°C to 21% conversion. The sphere was sectioned and submitted to electron microprobe analysis for sulfur. The lower curve of Figure 20 shows the results. As we expected from earlier examinations of the section under ultraviolet, CaS appeared throughout the solid, although there was a gradient of conversion toward the surface of the sphere. An exact mathematical analysis of the reaction kinetics in a sphere would have to take diffusion into account.

Table 8 gives the electron microprobe data for the sections, as well as data for the sectioned Glasshouse stone from Runs 76-1 and for two sections produced from spheres reacted at 950°C, to be discussed in Section 7.04.2.

7.04.2 Spheres Disclosing Control by Ash-Layer Diffusion

Sections of spherical samples of Greenfield stone partially reacted at 950°C disclosed an unreacted core of CaO when examined under ultraviolet light. Indeed, the nature of the sections is evident from an

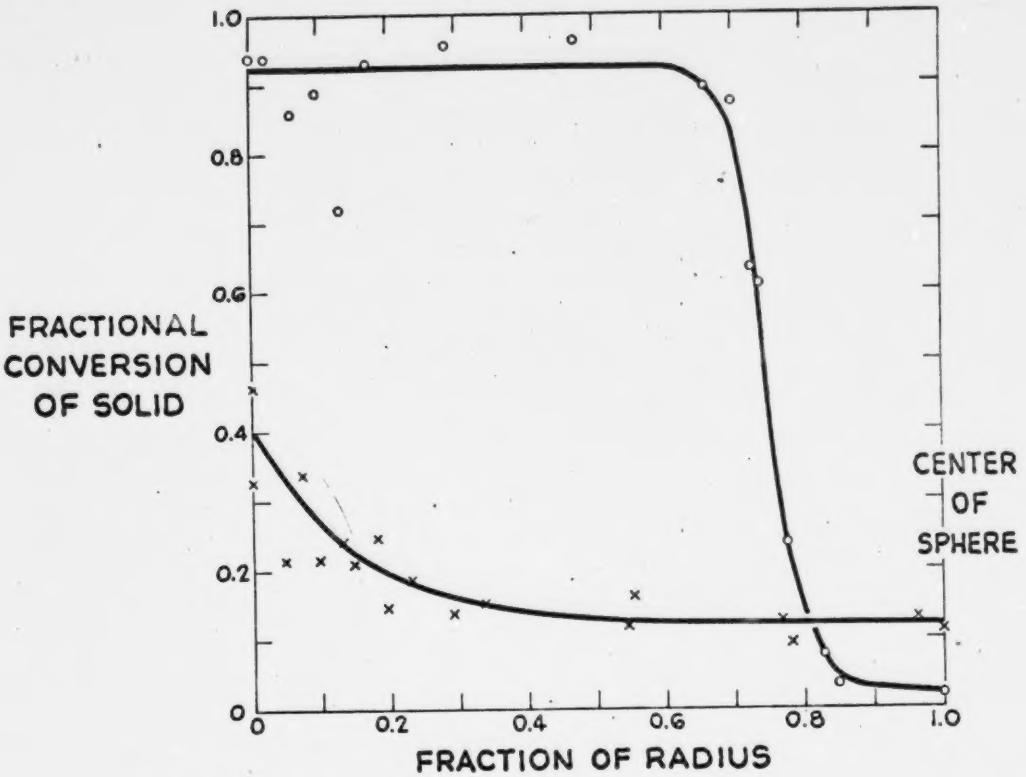

Figure 20. Fractional conversion of CaO to CaS as function of position along traverse through spherical samples of stone, as determined by electron microprobe analysis of a samples sectioned after conclusion of a run.

Upper curve is for Run 80-4, for an 8 mm sphere of Greenfield stone carried to 85% conversion at 950°C. Lower curve is for Run 80-1, for a 5.9 mm sphere of Greenfield stone carried to 21% conversion at 625°C.

Table 8. Distribution of Sulfur in Sectioned Spheres

Original analysis for sulfur performed by Advanced Metals Research Corp., Burlington, Mass. via electron microprobe

Fractional Distance, Outside of Sphere to Center	Fractional Volume of Sphere	Percentage Conversion	
0.000	0.000	46.0	Run 80-1
0.049	0.139	21.4	Traverse A
0.098	0.266	21.4	
0.147	0.379	21.0	
0.196	0.480	14.4	
0.294	0.648	13.7	
0.539	0.902	11.9	
0.784	0.989	9.5	
1.000	1.000	11.2	
0.000	0.000	32.6	Run 80-1
0.073	0.204	33.6	Traverse B
0.132	0.346	24.2	
0.181	0.450	24.6	
0.230	0.543	18.6	
0.338	0.709	15.1	
0.554	0.911	16.1	
0.769	0.987	12.6	
0.965	1.000	13.0	
0.000	0.000	52.3	Run 76-1
0.060	0.169	47.8	
0.120	0.318	36.8	
0.180	0.448	29.8	
0.270	0.611	24.9	
0.420	0.804	17.9	
0.630	0.949	11.9	
0.870	0.997	8.1	
1.000	1.000	7.0	

Table 8. Continued

Fractional Distance, Outside of Sphere to Center	Fractional Volume of Sphere	Percentage Conversion	
0.000	0.000	95.9	Run 80-5
0.014	0.041	102.5	
0.035	0.101	96.3	
0.070	0.195	95.2	
0.105	0.283	68.3	
0.140	0.363	94.0	
0.210	0.507	94.0	
0.280	0.626	95.9	
0.385	0.767	111.0	
0.490	0.867	67.2	
0.574	0.922	64.0	
0.595	0.933	62.9	
0.630	0.949	22.7	
0.805	0.992	3.1	
1.000	1.000	4.9	
0.000	0.000	93.7	Run 80-4
0.023	0.067	93.7	
0.060	0.169	85.7	
0.098	0.266	88.8	
0.135	0.352	71.7	
0.173	0.434	93.0	
0.286	0.636	95.5	
0.474	0.854	96.3	
0.661	0.961	89.2	
0.700	0.973	87.1	
0.729	0.980	63.3	
0.737	0.981	60.9	
0.775	0.988	23.8	
0.813	0.993	7.8	
0.850	0.996	3.5	
1.000	1.000	2.1	

an examination in ordinary light, since CaS has a light salmon color, easily distinguishable from white CaO.

Microprobe analysis for sulfur along the diameters of two sectioned samples of Greenfield stone, reacted to about 85% conversion at 950°C, confirmed the expectation that the reaction rate at this temperature would be controlled by ash-layer diffusion. The upper curve of Figure 20 gives the results of the microprobe analysis for one of the spheres. The curve illustrates the unreacted-shrinking-core mechanism which results when ash-layer diffusion is controlling.

7.05 Diffusion in Spheres

7.05.1 Equations for Determining Effective Diffusivity

When the reaction is controlled by ash-layer diffusion, one can use the equation given by Levenspiel (19) to describe the relationship between time and conversion:

$$t = \frac{[CaO]_c R^2}{6 D_e [H_2S]} [1 - 3 (1 - x)^{2/3} + 2 (1 - x)] \quad (22)$$

where

$[CaO]_o$ = initial concentration of CaO, g-moles/liter,

x = fractional conversion of solid to CaS, dimensionless,

D_e = effective diffusivity, cm^2/sec,

t = time, seconds, and

R = radius of sphere, cm.

A plot of time versus the diffusion statistic (the bracketed expression in x) yield a line of slope $[CaO]_o\ R^2/6D_e\ [H_2S]$, from which the value of effective diffusivity of reactant H_2S in the solid may be determined.

Equation (22) assumes that the reaction rate is very fast compared to the rate of diffusion within the sphere. If this is so, the reaction will occur within a narrow zone constituting the outer envelope of a shrinking spherical core of unreacted material. The entire gradient of concentration encountered in the reactant H_2S occurs within the reacted product layer, outside of the narrow reaction zone.

References to the upper curve of Figure 20 and to the electron microprobe data in Table 8 indicates that a Greenfield sphere data does appear to react 950^oC within such a narrow zone. We infer that diffusion in the reacted-product or ash layer is the limiting step for these reaction conditions, and that equation (22) may properly be used to estimate the effective diffusivity for H_2S within this layer.

A better evaluation of the role of diffusion in this layer can be made taking into account the resistance added by diffusion through the gas film surrounding the sphere.

The gas-film ass transfer coefficient may be estimated from the correlation (20):

$$\frac{K_g D_p}{D} = 2.0 + 0.60 \; N_{Rep}^{1/2} \; N_{Sc}^{1/3} \qquad (23)$$

where K_g = mass transfer coefficient, cm/sec,

D_p = particle diameter, cm,

D = diffusivity of reactant, cm^2/sec,

N_{Rep} = particle Reynolds number ($D_p G/\mu$), dimensionless, and

N_{Sc} = Schmidt number ($\mu/\rho D$), dimensionless.

Since the resistance of film and ash diffusion are in series, they may be combined to give the following relation for time vs. conversion:

$$t - \frac{[CaO]_o Rx}{3\ [H_2S]\ K_g}$$

$$= \frac{[CaO]_o\ R^2}{6\ D_e\ [H_2S]}\ [1 - 3\ (1 - x)^{2/3} + 2\ (1 - x)] \quad (24)$$

(Equation (24) is derived in Section 10.01.2.) This expression merely applies a correction factor to the elapsed-time side of equation (22), given earlier for pure ash-diffusion control. The left-hand side of equation (24) will be termed the "corrected time". The correction is greatest in the early part of a run. When either time or "corrected time" is plotted against the diffusion statistic, the slope obtained from either plot coincides at high conversion, indicating the same value for the quantity $[CaO]_o\ R^2/6D_e\ [H_2S]$.

7.05.2 Determination of Effective Diffusivity in [CaS+MgO]

Figure 21 displays typical plots of both time and "corrected time" versus the diffusion statistic for a run with Greenfield stone at 950°C. The fit of the data to equation (24) is excellent, and the data plotted according to this equation give a slope agreeing with the slope judged from data at high conversion plotted according to equation (22).

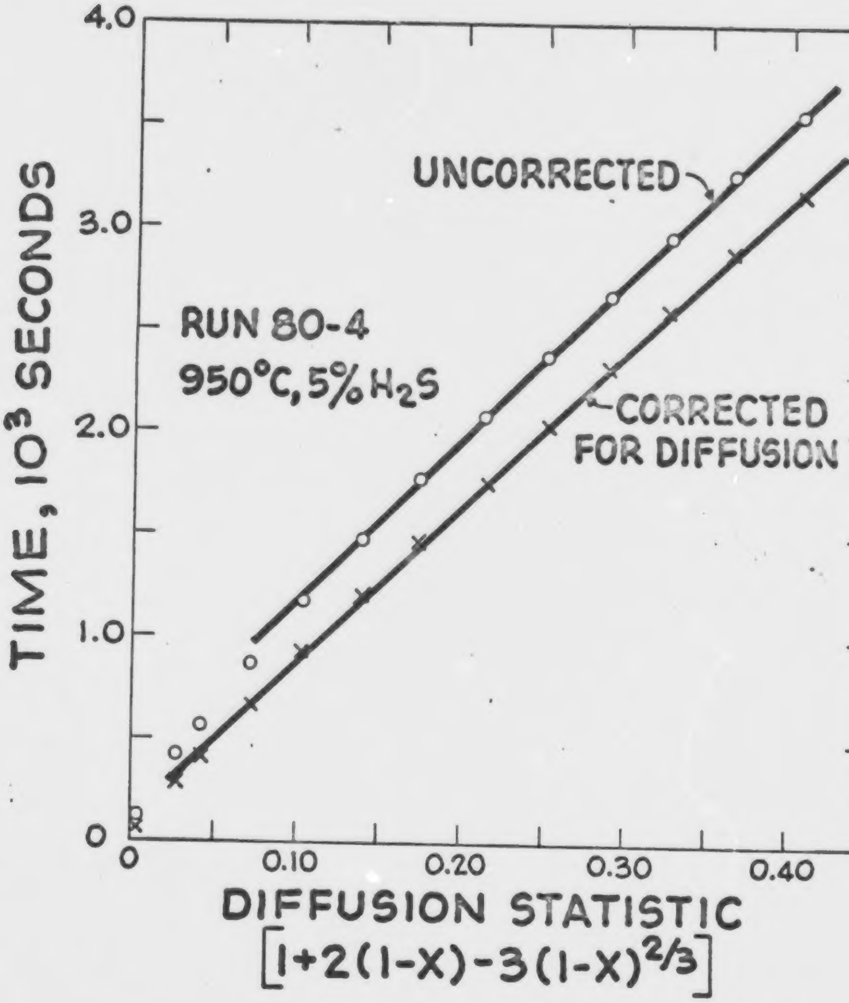

Figure 21. Run 80-4 with an 8 mm sphere of Greenfield stone, at 950°C, 5% H_2S.

Conversion data is plotted in the form of time vs. the diffusion statistic. Curves are given for both observed time and "corrected time" [see equation (24)].

Table 9 gives the effective diffusivities calculated from plots similar to Figure 21 for four runs at 950°C with Greenfield stone and one run at 850°C with Glasshouse stone.

The effective diffusivity in [CaS+MgO] produced at 850°C from Glasshouse stone is 14% of the estimated diffusivity of H_2S in the gas mixture. The effective diffusivities in [CaS+MgO] produced at 950°C from Greenfield stone range from 4.5% to 6.9% of the bulk gas diffusivity. The effective diffusivities in the four samples of Greenfield stone appear to be correlated with density.

Intrinsic differences between Greenfield and Glasshouse stones could well account for the difference in effective diffusivity. The distribution of pore size in the calcines from the two stones is not yet known, and will be obtained by others later in The City College program of study. It may be noted here that the Glasshouse stone appears to have a more open structure, marked by a few visible pores of significant size not seen in the Greenfield stone.

It is also possible that part of the difference between the effective diffusivities in [CaS+MgO]

Table 9. Effective Diffusivity of H_2S in Sulfided Calcined Dolomite

Run Ref. No.	Sphere Ref. No.	Cycle No.	Sphere Diam., mm	Sphere Density g/cm^3	Reaction Gas, mole %			Fraction CaO Converted	Effective Diffusivity cm^2/sec.	Ratio of Effective Diffusivity to Calculated Value for Open Space	Temp. °C
					N_2	H_2	H_2S				
80-4	78.1*	1	7.95	2.69	80	15	5	85	0.103	0.045	950
80-7	78-2*	1	7.64	2.69	80	15	5	86	0.107	0.047	950
80-5	78-4**	1	7.93	2.58	80	15	5	85	0.159	0.069	950
80-6	79-1**	1	8.11	2.61	80	15	5	87	0.143	0.062	950
72-5	68-2***	4	6.5	2.8	87.5	7.5	5	100	0.254	0.14	850

*Spheres 78-1 and 78-2 were cut from the same chunk of rock.

**Spheres 78-4 and 79-1 were cut from another chunk of rock.

***Sphere 68-2 was Glasshouse stone; other spheres were Greenfield stone.

prepared from the two stones was a result of some sintering of the Greenfield material when it was exposed to the 950°C temperature. The sphere diameters were not measured prior to the stones' being sectioned, but we observed no gross change in sphere diameter. Some internal sintering, not reflected by significant shrinkage, cannot be ruled out.

7.05.3 Thiele Utilization Factor in Particles Reacting Homogeneously

The extent to which the entire volume of a porous particle is utilized for reaction can be expressed by the Thiele utilization factor. This is the ratio of the observed rate to the true kinetic rate if the reactant concentrations were uniform through the particle. Weisz (21) describes how this can be calculated for a reacting sphere. His method gives a conservative estimate for the effort of internal diffusion upon the observed rate.

The fractional conversion of CaO to CaS along a traverse through a 5.9 mm sphere of Greenfield stone has been seen earlier, in Figure 20, for reaction of the sphere at 625°C. Based upon the average effective diffusivity for the four samples of Greenfield stone reacted at 950°C, an estimate of the initial Thiele factor for the 5.9 mm sphere reacting at 625° would be about 0.8. This is probably a low estimate for two reasons: some sintering may have occurred at 950°C, and the effective diffusivity in a solid in which CaO is only partially converted to CaS should be higher than in the solid at complete conversion since CaO has the smaller molecular volume.

More diffusivity data, for partially converted solid, will be required before an analysis can be given to explain quantitatively the concentration drop displayed by the electron microprobe data in the lower curve of Figure 20.

An upper estimate can be given, however, for the role played by solid diffusion in our kinetic observations made with powders and discussed in Section 7.01. Using the average diffusivity observed for the Greenfield stone at 950°C, we estimate the initial Thiele utilization factor in a particle of 80 mesh, the largest in our powder sample, to have been not less than 0.98 in runs conducted at 900°C. In all other runs, the Thiele utilization factor was greater.

We have estimated this Thiele utilization factor from the initial rate actually observed during runs at 900°C, which were affected by gas-film diffusion external to the powder sample. The role of external diffusion will be discussed in Section 10.01. For a kinetic situation in which external diffusion is reduced significantly, the Thiele utilization factor for an 80-mesh particle reacting at 900°C might be well below 0.98. The point here is that, in our actual data, homogeneity of reaction was closely approached.

7.06 Effect of Hydrogen Concentration

Having an oxide surface in contact with hydrogen, one naturally wonders whether there is any interaction between them. Runs with Greenfield powder at 700°C and runs with Pfizer spheres at 625°C showed that large increases in H_2 concentration caused moderate reductions in rate. The data are summarized in Table 10. A logical explanation is simply that H_2 adsorbs and covers part of the reactive CaO surface, thereby hindering the rate.

Our analysis is made difficult by the presence of H_2S adsorbing at the same time in a nonequilibrium

Table 10. Effect of Hydrogen on Reaction Rate

Run Number	Temp. °C	% H_2	"Final" Rate, $10^3 r$, $(sec)^{-1}$
80-8	700	7.5	1.845
80-9	700	7.5	1.94
80-10	700	7.5	1.32
86-7	700	7.5	1.253
90-2	700	7.5	1.547
84-1	700	50.0	1.290
84-2	700	50.0	1.270
76-2	625	7.5	0.346
76-3	625	7.5	0.367
76-4	625	45.0	0.1977

Note: All runs were made with 5% H_2S.

Runs at 700° were made with 82-2R Greenfield powder.

Runs at 625° were made with Glasshouse spheres.

fashion. However, one can do a crude tentative analysis with the following assumptions.

1. Either H_2 or H_2S can adsorb on the same site; this case is competitive chemisorption. Since increased H_2 does slow the reaction, it is apparently adsorbing on the CaO and excluding H_2S. An alternative mechanism would be that both H_2 and H_2S can adsorb on the same site simultaneously, either one of them inactivating this site; this alternative is unlikely.
2. Equilibrium conditions are attained in the H_2S adsorption. This is a fairly good assumption for the runs at 625°C and 700°C, since there is little initial curvature in the (1 - x) curves at these temperatures.
3. Equilibrium conditions are attained in the H_2 adsorption. The support for this is that there is little curvature in the (1 - x) curve.

With these assumptions, our rate expression becomes

$$-\frac{1}{W}\frac{dW}{dt} = \frac{K_3\,[H_2S]}{1 + K_e\,[H_2S] + K_e'\,[H_2]} \qquad (25)$$

where

K'_e = equilibrium constant for hydrogen adsorption, liters/g-mole H_2.

Using methods similar to those applied earlier in finding the H_2S adsorption equilibrium constant, we find that at 700°C, $K'_e = 77$; at 625°C, $K'_e = 380$.

These values of course must be regarded as tentative. They indicate that hydrogen is adsorbed, although not as strongly as H_2S. Further work would be needed to determine whether the adsorption is in equilibrium, and to obtain good values for the relevant constants. It is possible that the effect of hydrogen could be important in process applications where high partial pressures of hydrogen are achieved.

7.07 Effect of Water

Water is formed as H_2S reacts, and hence is indigenous to reaction (A). It is difficult to imagine the reaction being conducted where at least a trace of water is not present. However, one might not be surprised to encounter strong adsorption effects a higher concentrations.

Runs were made with Greenfield powder at 550°

and 700°C with an addition of 25% H_2O to the reacting gas mixture. Data for these runs are summarized in Table 11. Runs at 700°C are indistinguishable from runs made without water. At 550°C, water considerably increases the reaction rate, as can be seen from the (1 - x) plots in Figures 22 and 23 for runs at 10% and 0.3% H_2S respectively both with and without addition of water.

The rate constant, K_3, for 550°C is the rate which would be observed if there were no adsorption of gas upon CaO hindering its reaction. This would appear to be the highest rate attainable at any given temperature. If water merely affected the adsorption of H_2S (or any other hindering species), one would expect the first order rate constant calculated from the "final" linear portion of the (1 - x) curve for a run to which water is added to be not greater than the rate constant, K_3, determined for the nonequilibrium reaction model in Section 7.02.4.

Table 11 lists the values of the apparent first order rate constant calculated from the "final" linear portion of each of the 550°C runs to which water was added. Surprisingly, we found the "final" rate

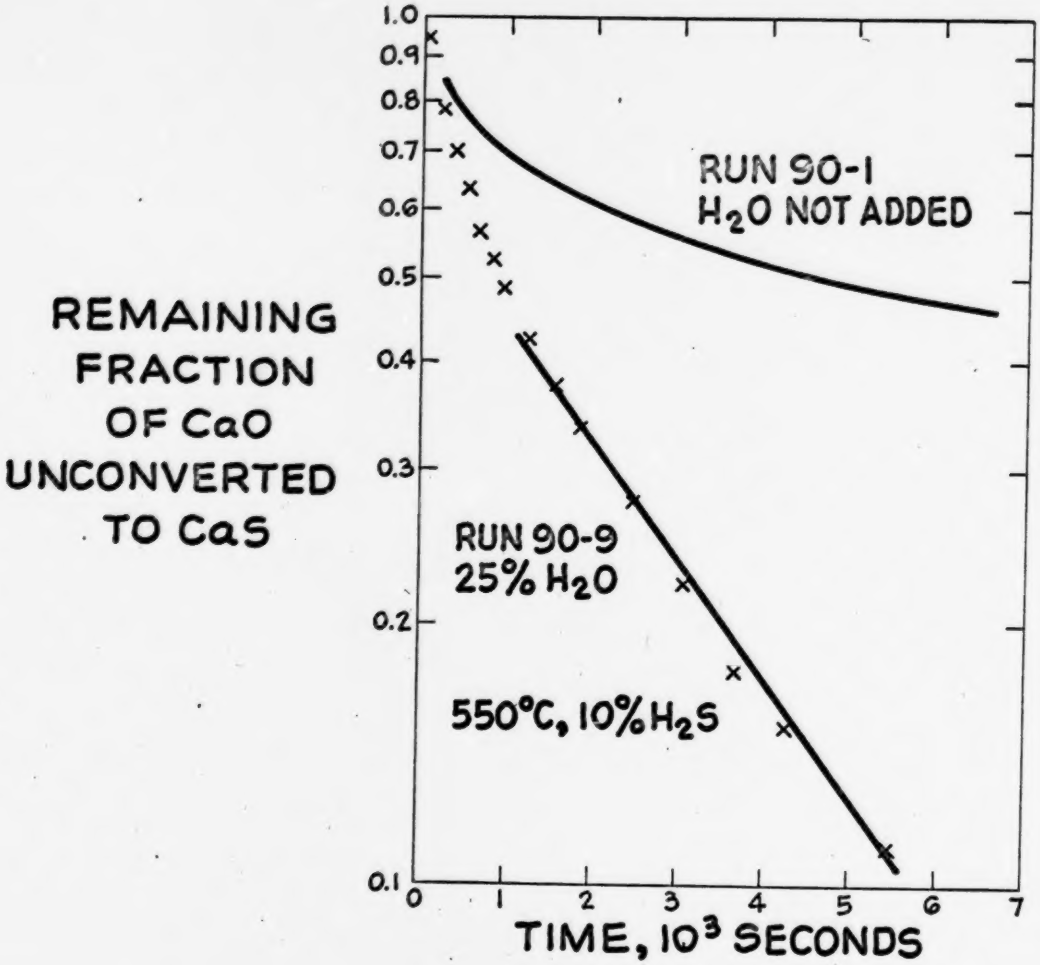

Figure 22. Runs with Greenfield powder at 550°C, 10% H_2S, with and without water added.

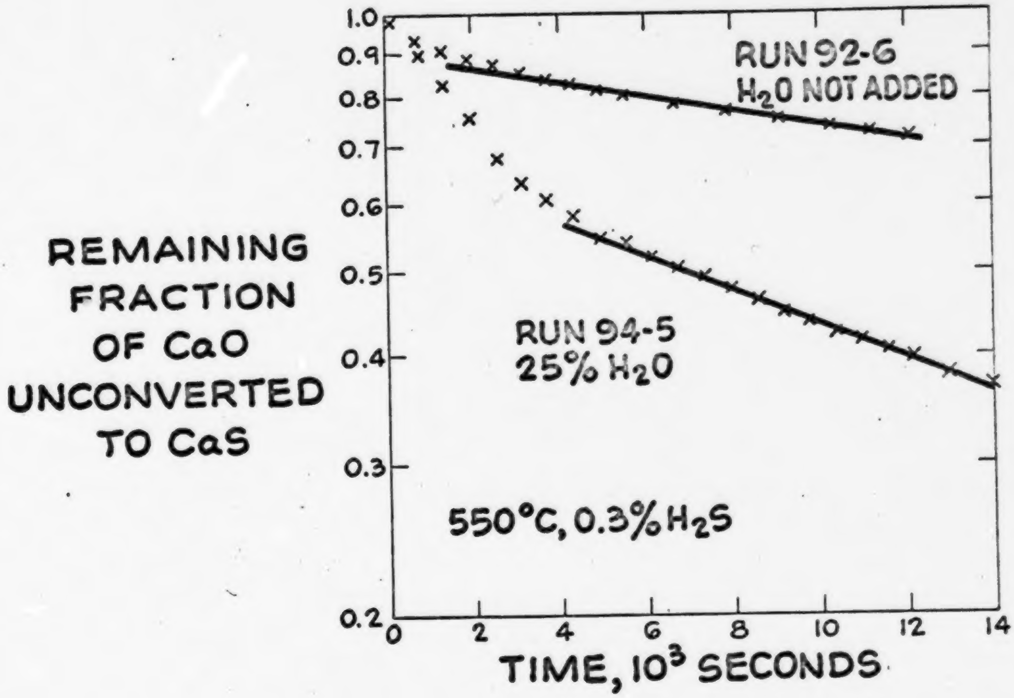

Figure 23. Runs with Greenfield powder, at 550°C, 0.3% H_2S, with and without water added.

Table 11. Effect of H_2O on Reaction Rate

					First Order Rate Constant, K_3	
Run Number	Temp. ^{o}C	% H_2S	% H_2O	r = "Final" Rate $(sec)^{-1}$	Taken From Actual Rate	Taken From all Non-H_2O Data
94-5	550	0.3	ca. 25	5.30×10^{-5}	1.18	0.33
92-9	"	10.0	ca. 25	6.19×10^{-4}	0.415	0.33
90-9	"	10.0	ca. 25	3.14 "	0.210	0.33
84-6	"	0.3	-	1.475×10^{-5}		
92-6	"	0.3	-	1.925 "		
86-3	"	10.0	-	2.14 "		
90-1	"	10.0	-	6.75 "		
94-9	"	10.0	-	6.26 "		
94-6	700	0.3	ca. 25	1.675×10^{-4}		
90-2	"	5.0	25.0	1.547×10^{-3}		
84-6	"	0.3	-	1.679×10^{-4}		
92-4	"	0.3	-	1.37 "		
86-7	"	5.0	-	1.253×10^{-3}		
80-10	"	5.0	-	1.32 "		
80-9	"	5.0	-	1.94 "		
80-8	"	5.0	-	1.84 "		

Note: Runs 94-5, 92-9, 90-9, and 94-6 used a bubbler to supply water to the reaction gas. As the degree of saturation was not independently determined, the water concentration is indicated to be approximate.

observed with water added to be the same or even greater than the rate constant, K_3. It therefore appears that water may play a catalytic role in reaction (A).

Many questions remain:

Does water itself adsorb?

If it does adsorb, does water compete with H_2S or H_2?

Why was there no effect at 700°C?

What is the effect at temperatures above 700°C and below 550°C?

The role of water in reaction (A) needs more investigation.

7.08 Effect of Calcination Conditions Upon Reactivity

As we noted in Section 4.0, the conditions under which a limestone or dolomite is calcined will affect is subsequent reactivity. For our work on the kinetics of the H_2S absorption reaction, we calcined at 925°C under one atmosphere of CO_2. We felt these conditions to be representative of those which might be encountered in a typical fuel desulfurization process.

A brief study was made to explore the effects of time, temperature, and gas environment during calcination upon the reactivity of dolomite in the recarbonation reaction. This reaction was selected, instead of the H_2S absorption reaction, because the duPont 950 thermogravimetric analyzer used in the study had not yet been fitted with baffles and purge flows to protect the analyzer's balance from H_2S. The recarbonation reaction was felt to be suitable for disclosing broadly the effects we were seeking.

The reactivity study was conducted at atmospheric pressure on samples of powder from the same supply of Greenfield stone used in powder runs of the H_2S absorption reaction, reported in Section 7.01. The duPont analyzer is controlled by a temperature programmer which permitted us to raise the temperature of a powder sample at 10°C per minute in a flowing gas stream until the desired calcination temperature was reached. The sample was then held at temperature while the gas flow was maintained. Fifteen minutes before the end of the "hold" at the calcination temperature, CO_2 was purged from the apparatus by nitrogen. At the end of the hold, the sample was cooled under flowing nitrogen to about 100° to 200°C. The cooling step generally took about 30 minutes.

Carbon dioxide was then substituted for nitrogen, and the sample was reheated in CO_2 at 10°C per minute to achieve recarbonation. The recarbonation continued until 900°C was reached, whereupon calcination would begin. Samples displaying poor reactivity for recarbonation did not achieve 100% recarbonation, since 900°C was reached before recarbonation was complete.

Figure 24 gives typical recarbonation data in form of the record of weight of sample versus temperature during the nonisothermal recarbonation. The weight record has been normalized to show the approximate percentage of recarbonation of the samples. In a nonisothermal recarbonation, the weight produces an S-shaped curve. The carbonation commences slowly, increases in rate as the temperature is raised, and finally flags as carbonation becomes nearly complete or as the equilibrium temperature for decomposition of $CaCO_3$ under one atmosphere of CO_2 is approached. In Run 82-4, the sample was calcined in CO_2, and then held in CO_2. The hold was for one hour at 975°C; it will be remembered that a N_2 purge flow was commenced 15 minutes before the end of the hold

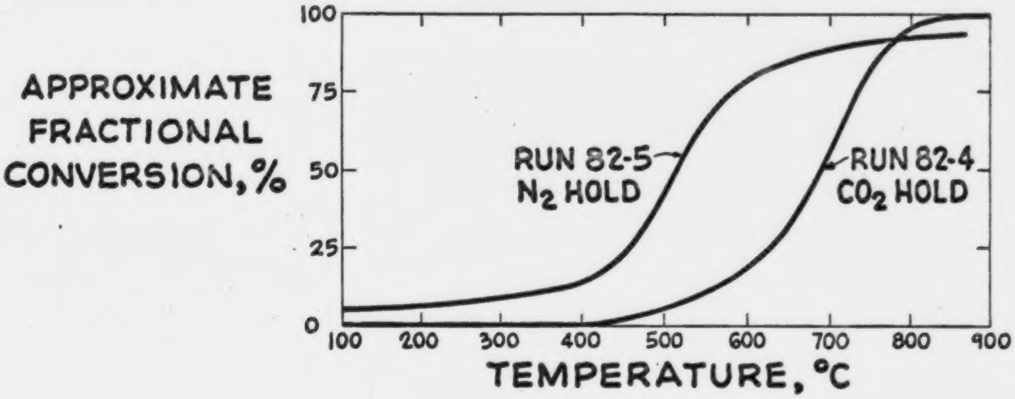

Figure 24. Typical nonisothermal recarbonation data (rate of heating = 10°C/min.).

The curve on the left is for a sample calcined in N_2 and held in N_2. The curve on the right is for a sample calcined and held in CO_2. Both holds were for one hour at 975°C.

interval. In Run 82-5, the sample was calcined in N_2 and held at 975°C for one hour in N_2. The weight records for these two runs, seen in Figure 24, reveals a striking difference in reactivity upon recarbonation, the latter run displaying markedly higher reactivity.

Table 12 and Figure 25 summarize data from nine runs performed to explore effects of calcination conditions upon recarbonation reactivity.

Figure 25 and one column of Table 12 report the temperature at which 80% recarbonation was achieved in the several runs. From Figure 25, we see that increasing either the time of the hold or the temperature of the hold causes a decrease in reactivity for recarbonation, reflected by an increase in the temperature for 80% conversion. We also see that the atmosphere during calcination and the hold can have a large effect. Calcination in nitrogen produces a solid possessing markedly higher reactivity for recarbonation.

When dolomite is calcined in nitrogen, it decomposes in one step, the decomposition of $MgCO_3$ occurring at temperatures which overlap those for the decomposition of $CaCO_3$. Calcination in CO_2 occurs in two steps. We thought that this difference in

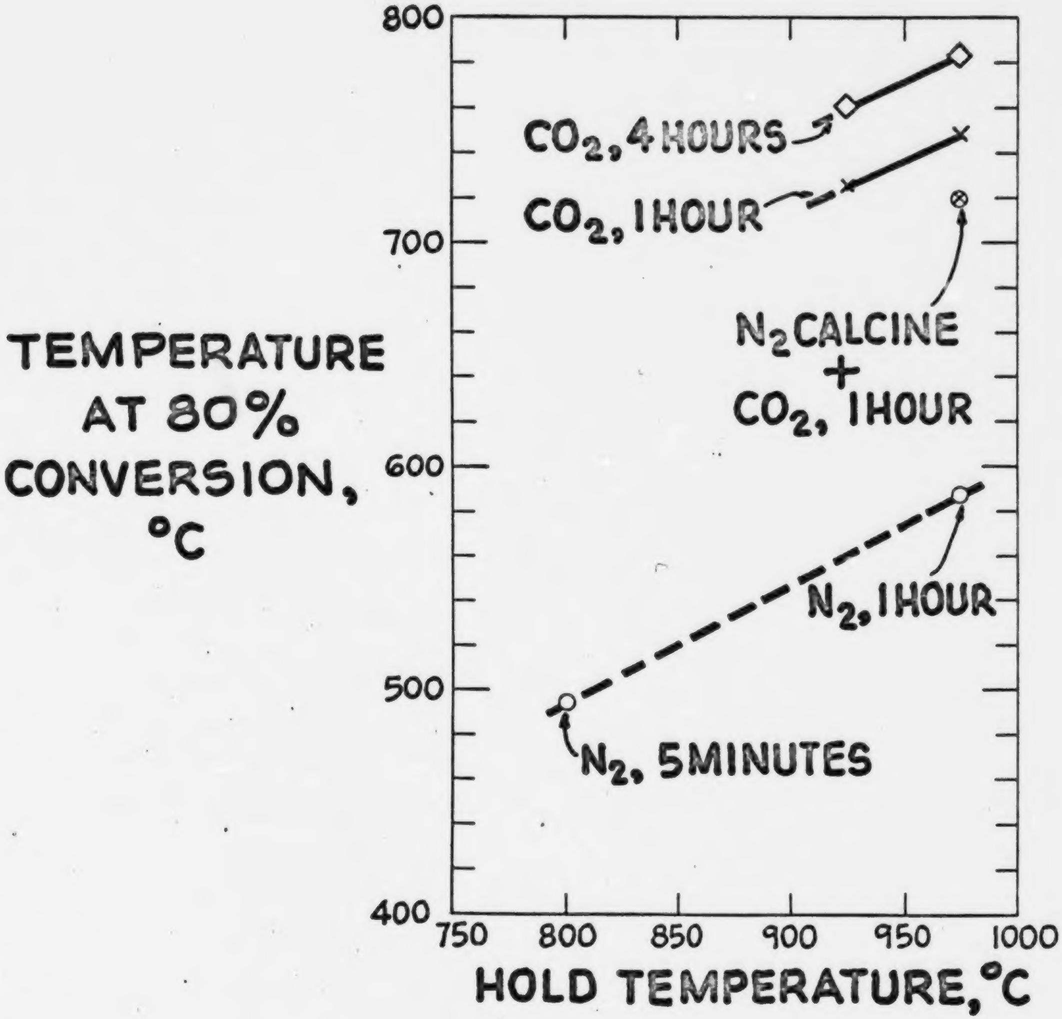

Figure 25. Temperature at which 80% conversion is attained in a nonisothermal recarbonation (10°C/min) vs. the hold temperature.

Time of hold and gas composition during calcination and hold are indicated.

More reactive stones reach 80% recarbonation at a lower temperature than less reactive stones.

Table 12. Summary of Data from Study of Sintering by Observing Rate of Recarbonation of Samples Calcined and Held under Varying Conditions

Run No.	Calcination Atm.	Hold Atm.	Hold Temp., °C	Hold Time, Hours	Final Percentage Recarbonation	Temp. at which 80% recarbonation is reached, °C	Recarbonation Rate	
							Activation Energy, kcal/g-mole	Frequency Factor, $(\text{sec-atm})^{-1}$
82-1	CO_2	CO_2	950	1.0	98	700	20	55.5
2	CO_2	CO_2	940-970	1.0	97	707	20	46.3
3	N_2	N_2	800 max.	0.0	ca. 95 (1)	495	20	1,734.0
4	CO_2	CO_2	975	1.0	94	749	20	26.7
5	N_2	N_2	975	1.0	ca. 92 (1)	588	12	1.93
6	CO_2	CO_2	925	1.0	95	725	20	38.5
7	CO_2	CO_2	975	4.0	94	783	20	21.4
8	CO_2	CO_2	925	4.0	95	761	20	41.4
9	N_2	CO_2	975	1.0	ca. 92 (1)	720	15	3.3

Note: In some cases, it would appear that 100% conversion was not reached because calcination begins before the recarbonation is complete.

(1) When calcined in nitrogen, the $CaCO_3$ calcines at the same time as the $MgCO_3$. Consequently, the weight gain required for 100% conversion can only be estimated.

the mechanics of calcination might be responsible for the different reactivities of samples calcined in N_2 and CO_2. To test this hypothesis, we conducted Run 82-9, in which the calcination was performed in N_2 and the hold was carried out in CO_2. The result of this run resembled runs for calcination and hold in CO_2 more closely than a run for calcination and hold in N_2. We may conclude tentatively that it is the presence of CO_2 which causes deactivation.

As part of his undergraduate research at The City College, Mr. Gary Weil analyzed the nonisothermal recarbonation data to obtain estimates of the activation energy and frequency factor of the recarbonation with assumption that the rate is first order in unreacted CaO. His method was crude in the respect that he took the driving force for recarbonation to be one atmosphere and constant. This is a poor assumption above about 750°C, when the equilibrium dissociation pressure of $CaCO_3$ becomes important. Furthermore, an isothermal recarbonization run at 550°C with 10% CO_2, to be discussed in Section 7.10.3, raises the suspicion that the recarbonation in affected by nonequilibrium adsorption of CO_2 according to a reaction model much like the model worked out for the H_2S absorption reaction in Section 7.02.

Nevertheless, Mr. Weil's results are worth reporting as a first attempt at a systemtic analysis of nonisothermal recarbonation data obtained to indicate reactivity of samples calcined under various conditions. Mr. Weil's results are summarized in Table 12 in columns giving frequency factor and activation energy. His results indicate that change in frequency factor probably accounts for most of the change in reactivity. Since the variation in reactivity is probably a consequence of differing degrees of sintering and loss of surface area, the variation in frequency factor may probably be attributed to variation of internal surface area.

The large effect of CO_2 atmosphere upon reactivity is an example of "activated" sintering. The sintering characteristics of a number of materials are affected by either additions of other solids or by exposure to certain gas atmospheres (22). We may reasonably postulate that CO_2 mobilizes the atoms in the calcium oxide crystal lattice and that this enhances the sintering process.

Because of its possible importance in guiding work on the process design of alternative schemes for fuel desulfurization, study of the effect of calcination conditions upon stone reactivity will be extended in further work by The City College team. The exploratory work reported here has had the value of disclosing that no "catastrophic" sintering of the Greenfield dolomite occurs at temperatures as high as 975°C for hold times as long as four hours under one atmosphere of CO_2. It would seem probable that the kinetic model developed in Section 7.03 will be valid for solids prepared at temperatures below about 975°C, although the kinetic constants may need adjustment as solid reactivity varies with calcination conditions.

7.09 Reaction of Calcium Sulfide with Steam and Carbon Dioxide

As we have already noted in Section 7.03.3, we conducted the H_2S absorption reaction five times on one spherical sample of Glasshouse stone, and two times on each of two other spherical samples of this stone. To do this, the sample was regenerated with steam and CO_2.

Data was obtained for four regenerations on one sample and for two regenerations on another. The first step in each regeneration comprised the reaction of calcium sulfide with steam and carbon dioxide:

$$[CaS+MgO] + H_2O + CO_2 = [CaCO_3+MgO] + H_2S \qquad (C)$$

This step was followed by a calcination.

At atmospheric pressure, reaction (C) proceeds at a slow rate. At relatively low temperatures, the rate is slow because of poor kinetics. At higher temperatures, the rate is slow because of poor equilibrium. For use in a process, the reaction must be conducted at elevated pressure, for which adequate kinetics have been demonstrated (7). Detailed study of the kinetics of the reaction by The City College team will be possible only after a set-up for work at high pressure, now being assembled, becomes available.

The six runs in which we conducted reaction (B) at atmospheric pressure have provided, however, some preliminary kinetic information worth reporting.

These runs encountered difficulties arising from the low rate of conversion of CaS to $CaCO_3$. Complete regeneration took as much as several days, and the runs were interrupted overnight. Problems arose from condensation of water in unwanted places, sticking of the balance, and reaction of CaS with CO_2 flowing over the sample overnight.

Figure 26 shows typical data for reaction (C) in form of a plot of log (1 - x) verus time. The data is for Run 72-4E. We began reaction (C) at 600°C. The reaction was characterized by a rapid initial rate, flagging to a slower rate, behaving much in the same manner as the H_2S absorption reaction does at low temperatures. After the rate slowed considerably and it was apparent that complete conversion would require a very long time, we raised the temperature to 750°C. At the higher temperature, the plot of log (1 - x) appears straight. The reaction would appear to be first order in unreacted CaS and to occur homogeneously throughout the solid.

Table 13 and Figure 27 summarize the data for six runs of reaction (C). At 700°C and above, the log (1 - x) plot was substantially straight.

Table 13 and Figure 27 summarize the data assuming the following hypothetical rate expression:

$$-\frac{1}{W'}\frac{dW'}{dt} = K_4\,[H_2O]\,\Delta[CO_2] \qquad (26)$$

where W' = weight of unreacted CaS remaining in the sample,

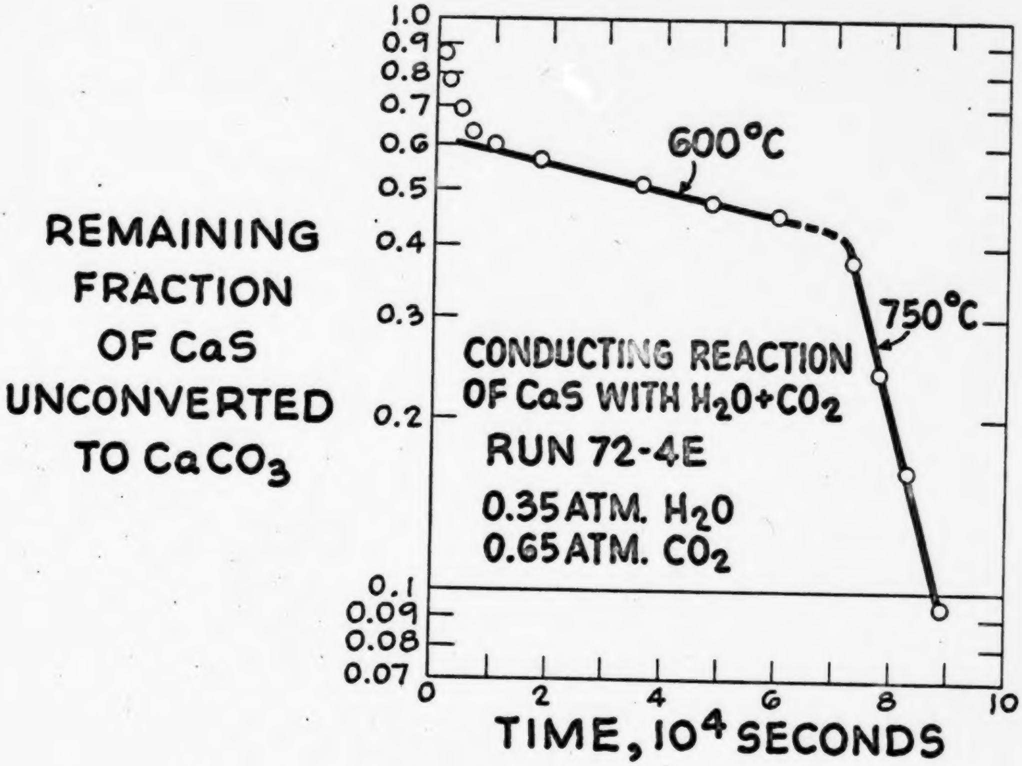

Figure 26. Plot of (1 - x) vs. time for the reaction of CaS with steam and CO_2.

When the rate slowed, the temperature was raised from 600°C to 750°C.

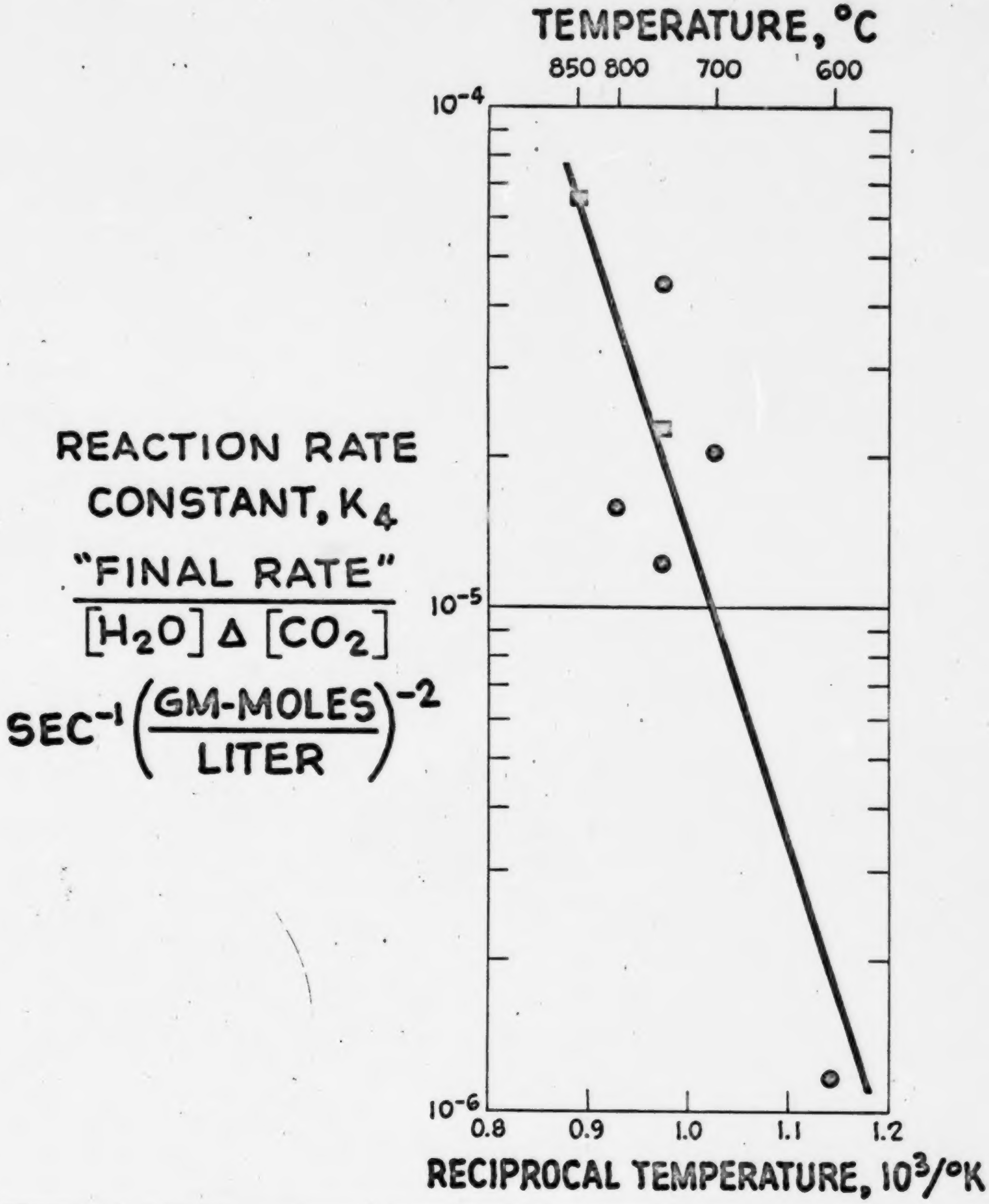

Figure 27. Arrhenius plot of rate data for reaction of CaS with steam and CO_2. Plotted are rate constants based on assumption that rate is first order in CaS and steam and proportional to difference between CO_2 partial pressure and the equilibrium decomposition pressure of $CaCO_3$.

● = regeneration runs 72-2E through 72-5E, following runs 72-2 through 72-5 respectively. Note that run 72-4E was conducted at two temperatures (see Figure 26).

■ = regeneration runs 76-5E and 76-6E, following runs 76-5 and 76-6 respectively.

Table 13. Regeneration Data

			Partial Pressure, Atmospheres				
Run Number	Temp. ^{o}C	10^5 x "Final" Rate, sec^{-1}	CO_2 in Bulk Gas	$CaCO_3$ Equilibrium Decomposition, CO_2*	ΔCO_2 $CO_2 - CO_2$*	H_2O in Bulk Gas	$K = \frac{\text{"Final" Rate}}{[H_2O]\Delta[CO_2]}$ $sec^{-1}\left(\frac{\text{g-moles}}{\text{liter}}\right)^{-2}$
72-2E	700	7.2	0.60	0.030	0.57	0.40	2.01×10^{-5}
72-3E	750	3.4	0.65	0.09	0.56	0.35	1.229×10^{-5}
72-4E	600	0.516	0.65	0.0	0.65	0.35	1.165×10^{-6}
72-4E	750	11.95	0.65	0.09	0.56	0.35	4.41×10^{-5}
72-5E	800	3.07	0.65	0.22	0.43	0.35	1.59×10^{-5}
76-5E	750	1.10	0.95	0.09	0.86	0.04	2.26×10^{-5}
76-6E	850	1.35	0.95	0.50	0.45	0.04	6.52×10^{-5}

Note: Run 72-2E followed Run 72-2, Run 72-3E followed Run 72-3, etc.

Runs 72-2E through 72-5E were conducted on one spherical sample of Glasshouse stone. Runs 76-5E and 76-6E were conducted on another spherical sample of this stone.

$\Delta[CO_2]$ = the amount by which the CO_2 concentration exceeds its equilibrium dissociation concentration over $CaCO_3$ at the temperature of the run, and

K_4 = a rate constant, $(\text{g-moles/liter})^{-2}\ \text{sec}^{-1}$.

The rates listed in Table 13 and plotted in Figure 27 are evaluated from slopes of the log (1 - x) plots. At 600°C, the "final" rate was used, i.e., the rate between about 0.6 and 0.45 on the (1 - x) scale in Figure 26.

The data points in Figure 27 do not make a good Arrhenius plot. In light of our data at 600°C, seen in Figure 26, we judge that the dependence of the reaction upon gas concentrations is complex. Equation (26) may be a poor approximation for this dependence. Still, a first approximation for the activation energy for the rate constant K_4 would be, from Figure 27, about 28 kcal/g-mole-°K. A regression analysis of the points in Figure 27 gives $\ln K_4 = 2.858 - 27.885/RT$.

As noted earlier, further work on reaction (B) will be conducted at high pressure, where the rate should be faster.

In a practicable process, reaction (C) should be conducted at as low temperature as possible, in order to achieve the highest possible concentration of H_2S

in the product gas. Squires (23) has already suggested the desirability of "staging" the reaction by carrying out the reaction in several superposed fluidized beds, the beds at higher elevation being generally at higher temperature, and the flows of gas and solids through the beds standing in countercurrent relationship. The data from Run 72-4E tend to confirm that such staging of the reaction may be desirable, so that the final conversion of CaS to $CaCO_3$ may be conducted with fresh steam and CO_2 at a relatively higher temperature, while the final conversion of steam and CO_2 may be conducted over fresh CaS at a relatively lower temperature.

7.10 Miscellaneous Observations

7.10.1 Changing Conditions During a Run

At an early stage in the work, we could not resist the temptation to try to extract data at more than one condition from a single run. Consequently, we changed conditions in a number of runs after we felt that the "final" rate had been established.

In Runs 80-3, 84-5, 84-6, 84-8, and 94-9, we began at a low temperature, where the rate was slow, and later raised the temperature. Since the time scale of the run was large compared to the time needed to effect the change in temperature, we hoped that no errors were being introduced. Unfortunately, the second half of a run conducted in this manner tended to give a result for the reaction rate which was low. We later realized that the rate was low because H_2S adsorbed at low temperature was hindering the rate at the higher temperature, this rate tending to reflect an H_2S desorption rather than an intrinsic reaction rate. With two exceptions, data from the second half of runs conducted in this manner are not reported in Table 3, nor were they used in developing values of kinetic constants reported in Section 7.02.

The first exception is Run 84-6. In this run, the concentration of H_2S was 0.3%, sufficiently low that we judged the adsorption at low temperature to have been negligible. Data for Run 84-6 appear on two lines in Table 3, corresponding to the two temperature levels used in the run.

The other exception was Run 94-9. This run was made in an attempt to test the nonequilibrium adsorption model. The run was begun at 475°C and continued at 550°C. It was felt that if the surface was indeed covered at 475°C, the data at 550°C might show no rapid initial rate period as the temperature was raised. In fact, a short initial rapid rate period was observed. The reaction rate increases with temperature more than desorption rate. If the reaction at 475°C during Run 94-9 reached a stage where H_2S adsorption was near equilibrium, the subsequent rate at 550°C would be substantially proportional to the surface left uncovered at 475°C. The rate at 550°C would first become faster, but would soon become limited by desorption just as if the run had been conducted at 550°C from its inception. Table 3 gives data for Run 94-9 at both 475° and 550°C.

In Run 84-9, conducted at 800°C where adsorption is negligible, the concentration of H_2S was changed during the run. Data for both concentrations appear in Table 3.

7.10.2 An Interrupted Run

Run 2-1-6 was conducted in an attempt to test the nonequilibrium adsorption model developed in Section 7.02. Using a reaction gas mixture containing 10% H_2S, we started the run at 550°C, stopped the flow of gas mixture and substituted nitrogen for two hours in hope of desorbing all adsorbed H_2S, and then started the run a second time. The results were not conclusive. One would expect again to see a rapid rate, appropriate to the quantity of CaO remaining in the sample, if the H_2S were completely desorbed. The reaction restarted a bit faster than just before the run was stopped, and then very soon assumed a "final" rate close to that assumed earlier.

The desorption rate constant, K_2, given in Figure 10, has units of reciprocal seconds. This constant can be considered the inverse of a time constant. At 550°C, the time constant is about 2500 seconds. The experiment should be repeated using a much longer desorption period.

7.10.3 Recarbonation of Calcium Oxide

In the hope of gaining further insight into the kinetics of reactions involving calcined dolomite, a powder sample of Greenfield stone, calcined according to our usual procedure, was recarbonated isothermally in Run 94-7 by exposing it to gas containing 10% CO_2 and 90% N_2 at 550°C. As shown in Figure 28, Run 94-7 displayed a rapid initial rate and slowed to a constant "final" rate. The data resemble data from our work on reaction (A) at relatively low temperatures.

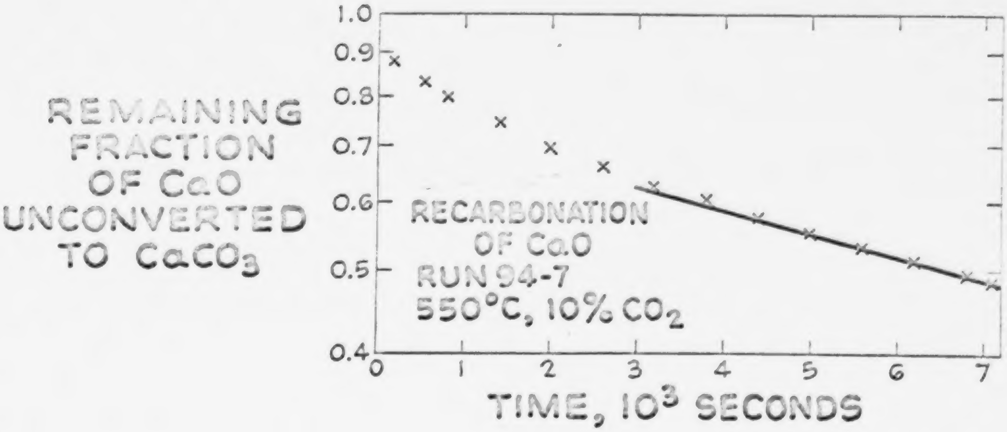

Figure 28. Recarbonation of [CaO+MgO] at 550°C, 10% CO_2, in Run 94-7. The solid was a Greenfield powder sample.

It would be speculative to draw a conclusion from this single recarbonation run. In planning future work on recarbonation, it would seem reasonable to adopt the working hypothesis that the recarbonation reaction follows a nonequilibrium adsorption model much like that presented for the H_2S absorption reaction in Section 7.02.

7.10.4 The Mysterious Wiggle

Some runs deviated slightly from a good straight line, in the plot of log (1 - x) versus time, by deviating both above and below an average line, giving a wiggle effect. Typical of this are Figure 5 and Run 94-8 in Figure 15. This wiggle was often beyond the range of known experimental error. It may be real although subtle effect, or it may be merely an unknown experimental gremlin.

7.10.5 Pan Discoloration

The patinum pan used for powder runs occasionally was discolored at the end of a run. This seems to occur most often when water was added. The discoloration was light gunmetal blue in color, and tended to disappear with further use. No weight change was observed in the pan within a fraction of a milligram out of 900.

8.0 Discussion of Results

8.01 Discussion of Model

We are keenly mindful that kinetic data alone often cannot prove the validity of a postulated reaction model beyond doubt. The history of kinetic studies provides many examples of data which appeared to obey counterfeit models, later discredited as more results became available. Nevertheless, an early attempt to model a reaction can be valuable both as a guide to further experiments and as a basis for practical design.

8.01.1 Deviation at Low Concentration and High Temperatures

Examination of Figure 7 shows a moderate positive deviation from the model for 0.3% H_2S runs at 550° and at 625° and a serious deviation at 900°. The deviation at low temperatures is small enough that it might be explained by imprecision of the model or by the fact that the feed rate of H_2S approached the lower limit of our system capability and was not as accurately known as in other runs. The deviation at 900°, however, cannot be so simply explained away. We made five runs at 900° and 0.3% due to the novelty of the result at these conditions, but the rate remained consistently high.

All of the runs at 900° were affected by diffusion in their early stages. The runs at low concentration were affected more severely since they showed a much higher kinetic rate. After correction for diffusion is made, however, the runs do not give any untoward appearance in their plots of conversion vs. time. A typical run is presented in Figure 29 showing both the corrected and the uncorrected data.

A possible explanation of the kinetic deviation may lie in the effect of CO_2 on the stone. Ruth, Squires, and Graff (24) have shown that the reaction of $CaCO_3$ with H_2S in the presence of a relatively high partial pressure of CO_2 is faster than the reaction of CaO with H_2S. One also notes the effect of CO_2 in activating dolomite for sintering phenomena. We suggest that some of our runs at low concentration which showed high rates were influenced by a trace of CO_2 remaining in the stone. This fits the observation that the greatest deviation was seen at 900° where there is the shortest time between calcination and cooling to the run temperature, and where one would accordingly most expect to find traces of CO_2 in the

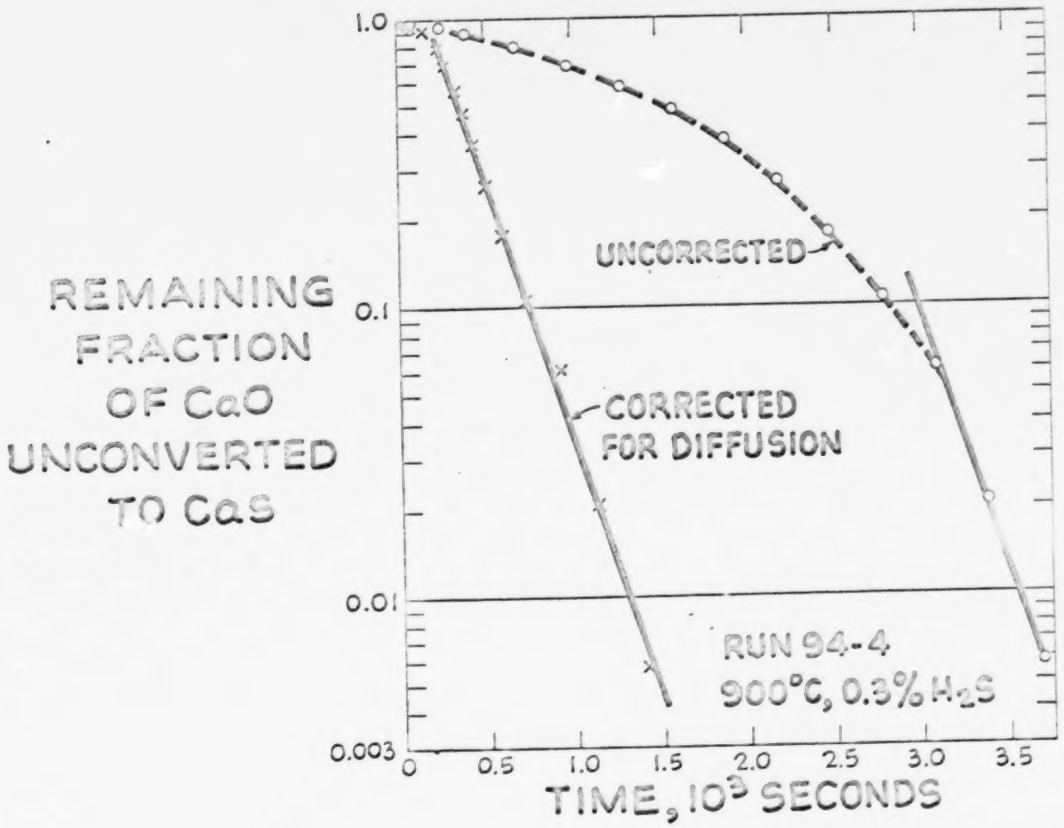

Figure 29. Run 94-4 on Greenfield powder at 900°C, 0.3% H_2S.

The original uncorrected data are presented together with data corrected for diffusion as discussed in Section 10.01.3.

solid. Runs should be made with CO_2 added to the reaction mixture in order to check this hypothesis.

Another possibility, perhaps remote but worth remembering, is that at 900°C some unknown process occurs which slowly increases the reactivity of the solid. At the long reaction times characteristic of a run at 0.3% H_2S, this process may produce an effect not observed even at 1.0% H_2S.

8.01.2 Variability of Results

A puzzle through much of our work has been variability in reaction rate between runs conducted at identical conditions on samples having calcination histories which were kept identical to the best of our ability. This behavior has been particularly striking at low temperatures. An example is shown in Figure 13, which plots results for duplicate runs at 550°C and 10% H_2S.

We suggest that such variability may be attributed at least in part to differences in the surface condition of the solid. Such differences might result from trace impurities present in different amounts in various samples, or they might result from subtle differences in our calcination procedure. When K_1 and K_2 are large in comparison with K_3, equilibrium is quickly approached on the solid surface, and the exact values of K_1 and K_2 are not critical. At lower values of K_1 and K_2, however, we get the effect illustrated in Figure 30. This figure gives plots of log (1 - x) in which values of K_1 and K_2 have been changed by an order of magnitude above and below the values we obtained in fitting our data. Increasing the values of K_1 and K_2 has relatively small effect by comparison with lowering their values. Consider the lower curve of Figure 30, in which K_1 and K_2 were reduced. Initially the surface is uncovered, and the reaction proceeds rapidly. As the H_2S slowly adsorbs, the rate flags and finally becomes substantially constant. The final rate is far slower than would be predicted from equation (4) for a simple equilibrium adsorption model, if K_e were known, since more of the surface is covered. This is because the desorption rate is too slow to replace the surface area which is being removed by reaction. Figure 30 varied K_1 and K_2 and kept their ratio constant, but there is a possibility that K_e also may depend upon surface condition.

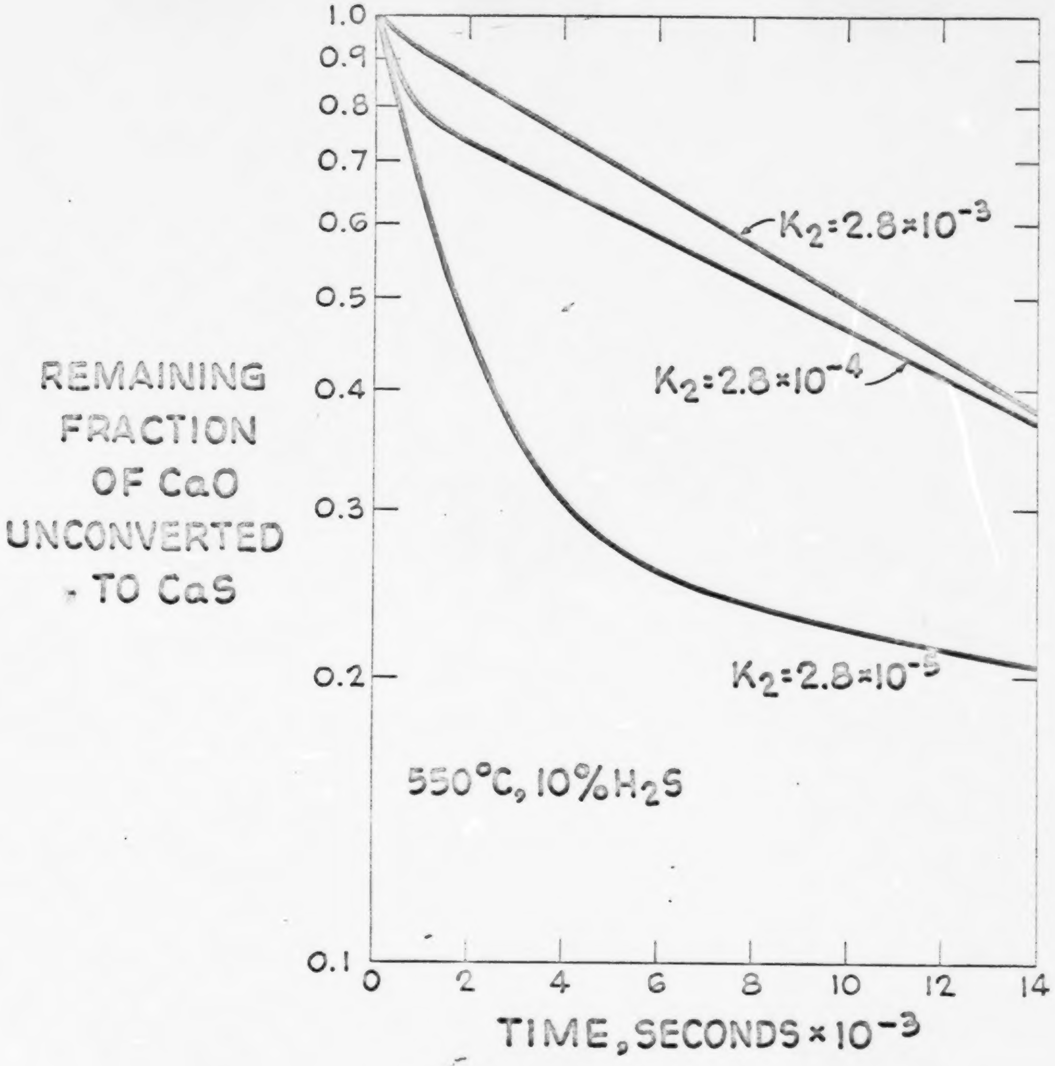

Figure 30. Comparison of a representative log (1 - x) curve generated from K's with hypothetical curves in which both K_1 and K_2 have been raised or lowered by a factor of 10.

8.01.3 H_2S Adsorption

There is little in the literature on the adsorption of H_2S in the temperature range of interest to us. Working on catalysts used in CS_2 manufacture, Thomas and Ullah (25) found that H_2S adsorbed on sulfided nickel oxide and on sulfided vanadium pentoxide. The activation energy for adsorption on sulfided nickel oxide was 12.8 kcal/mole in the range 500°-650°C, and a Langmuir adsorption model was applicable. H_2S adsorption on alumina was studied by DeRosset and collaborators between 260° and 560°C (26).

8.01.4 A Possible Model Invoking Multiple Reactivities

As we mentioned in Section 7.01, an alternate reaction model to explain the rapid initial and slower "final" rates might include the hypothesis that the solid [CaO+MgO] contains CaO with multiple reactivities. Since we know that lime may vary in activity according to both the source of the limestone and the lime's calcination history, we can logically postulate that there is a spread in reactivity within a single sample of calcined dolomite. The more active portions would react very quickly, giving a rapid initial rate, and as these portions are consumed, the rate would slow to that characteristic of the remainder of the sample.

In its simplest form, this model would assume the rate to be first order in the unreacted portions of the several respective varieties of CaO and also to be first order in H_2S. As we have noted in Section 7.01, there is a difficulty with this simple model. As Figure 6 shows, the fractional conversion occurring by a rapid reaction is typically different for a low H_2S concentration than it is for a high concentration. If the initial rapid rate were occurring simply on that fraction of the stone having a higher reactivity, one would not expect the fractional conversion occurring by a fast reaction to be dependent upon the partial pressure of H_2S. In other words, as we noted earlier in Section 7.01, one would expect the (1 - x) record for runs at several H_2S concentrations to coincide if the times were normalized by multiplying time by H_2S concentration. The simplest form of the model invoking multiple reactivities cannot fit the data.

It is clear from Figure 7 that a valid reaction model must include a role for adsorption. The data for the "final" rate, when plotted versus H_2S concentration as in Figure 7, show that this rate at low temperatures does not show simple first order dependence upon H_2S concentration. At 475° and 550°C, the "final" rate is insensitive to changes in H_2S concentration at high levels. It would appear that one must invoke adsorption to explain such a result. This is true even if the multiple reactivity hypothesis is invoked to explain the high initial rate.

Since adsorption is necessarily a factor in any model, we preferred in Section 7.02 to attempt to explain all of the results by a model invoking adsorption alone rather than a model invoking adsorption along with another mechanism.

An interrupted run, described in Section 7.10.2, did not provide an unequivocal confirmation of our nonequilibrium adsorption model. A conclusive confirmation of this model might require study of the composition of gas desorbing from a partially converted sample of solid, such as existed at the moment of interruption of this run. Before such an experiment is available, we cannot be certain whether our model should or should not also include a role for a hypothesis invoking multiple reactivities.

8.02 Other Work on the Reaction of Hydrogen Sulfide with CaO

8.02.1 Work in Russia

Russian Scientists have been experimenting with lime for removal of H_2S, but have not yet published kinetic data. Their work concentrates on limestone rather than dolomite, and their results will not be completely comparable to the results of the present research.

Al'tshuler, Klirikov, and Gavrilova (27) gasified petroleum residues with air at pressures up to 70 atmospheres and at about 1100°C. A gas containing 0.37% H_2S was completely desulfurized by limestone at 1100°C with a contact time of 0.35 seconds. The sulfurized product was mostly CaS with a small amount of $CaSO_4$.

In a series of papers (28), Al'tshuler and Gavrilova described further studies of the reaction of CaO with H_2S. The studies were carried out in a laboratory quartz reactor containing porcelain chips and CaO. The first series used 0.2 to 0.45% H_2S

in nitrogen at 500° to 1000°C. The reaction was found to be diffusion controlled with an apparent activation energy of 3,260-4,500 cal/g-mole. They stated that the reaction rate was sufficiently fast to develop a high temperature process for removal of 0.4% H_2S from a fuel gas using a contact time of only 0.2 second.

In another series of experiments, all performed at 1000°, Al'tshuler _et al_. studied the effect of adding various gases. They found that large quantities of steam lowered the reaction rate in line with equilibrium calculations. Also confirming expectations was the observation that addition of hydrogen effectively suppressed the dissociation of H_2S. Carbon dioxide had no effect at the conditions studied. Finally, the shift reaction was found to be catalyzed by CaO.

The results obtained are on the whole consistent with our observations. We found that diffusion became a factor in dolomite spheres at about 850°C. The use of limes rather than dolomite would be expected to give a less porous material, and diffusion effects would be observed at a lower temperature.

The finding that the reaction with H_2S is very fast is consistent both with our results and with the results of Consolidation Coal Company. We view the Russian finding that CO_2 has no effect on the reaction with a bit of caution. If the reaction were already proceeding at a high rate in a diffusion-controlled regime, a moderate increase or decrease in rate might go undetected.

We have not yet been able to obtain and translate the entire text of the papers from Al'tshuler's laboratory and so a detailed evaluation is not feasible. It would be interesting to know the history of the solid with respect to the calcination procedure and the maximum temperatures attained before it was reacted with H_2S.

8.02.2 Work of Vestal and Johnston

In a nonisothermal experiment, Vestal and Johnston (29) reacted calcined dolomite with a gas comprising 0.1% H_2S in helium. They first calcined the dolomite by heating it in helium at a programmed heating rate of $4^\circ C$ per minute, carrying the sample to a maximum temperature of about $750^\circ C$. Then cooled the sample, and then reheated it at the same rate in the gas containing H_2S. The reaction was followed by a mass spectrograph. They fitted their nonisothermal kinetic data to an

Arrhenius expression with the assumption that the reaction was first order in both H_2S and unreacted CaO. They obtained 1.7 x 10^{13} (atm $H_2S)^{-1}$ min^{-1} for the frequency factor and 38 kcal/g-mole for the activation energy. They thought that diffusion became controlling at temperatures above about 350°, but it seems more probable that H_2S began to adsorb at an appreciable rate at about this temperature, the adsorbed H_2S hindering the reaction.

Vestal and Johnston used the dolomite which the Air Pollution Control Office has designated BCR 1930. This is a stone taken from the same Pfizer quarry which supplied the Glasshouse stone used in most of our work with spheres. Although Vestal and Johnston published only one run, it is nevertheless interesting to compare their results with ours on the same dolomite. Our kinetic data, from Figure 19, is replotted in Figure 31 together with Vestal and Johnston's result. The agreement is remarkable considering the differences involved in experimental techniques and particularly considering that Vestal and Johnston's calcination procedure could be expected to lead to a solid of higher reactivity than ours. It would appear, however, that nonisothermal experimentation is unsuitable for obtaining kinetic data for a reaction

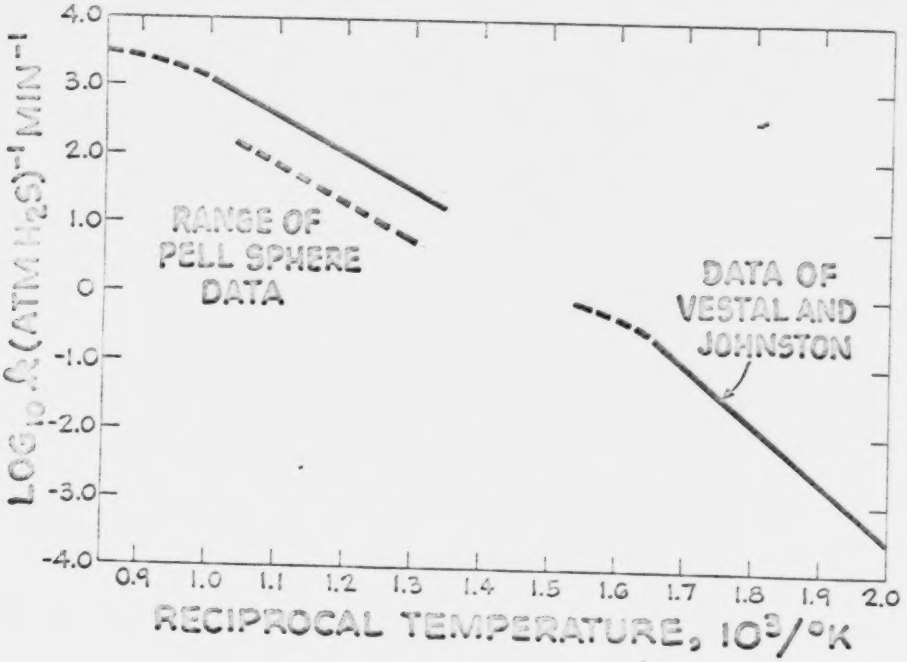

Figure 31. First order rate constant for the reaction of calcined dolomite with H_2S.

The data of Vestal and Johnston (29) are plotted together with our data for spheres. Both sets of data were obtained on a stone from Pfizer's Glasshouse quarry.

obeying a nonequilibrium adsorption model, such as the model we have developed in Section 7.02 for the H_2S absorption reaction.

8.03 Calcination and Recarbonation of Dolomite

Due to the many commercial uses of lime, there exists a huge open literature on lime and dolomite calcination. There is also a body of propriety literature sponsored by the National Lime Association which is of interest to those for whom it may be available.

8.03.1 Dolomite

Dolomite is the mixed carbonate of Ca and Mg, normal dolomite being written $CaCO_3 \cdot MgCO_3$. These carbonates are built of alternating layers of carbonate ions and cations. In dolomite, ideally, cation planes populated entirely by Mg^{2+} alternate with planes populated entirely by Ca^{2+}. Halla (30) has estimated the free energy of formation of dolomite from calcite and magnesite to be -1,720 cal/mole.

8.03.2 Calcination and Sintering of Dolomite

When dolomite is heated in the presence of CO_2, it decomposes in two steps to form an intimate mixture of crystallites of CaO and MgO. CaO sinters at temperatures close to those required for calcination, and the nature of the calcined product is related to its time, temperature, and gas-environment history during the calcination process.

A number of gaseous species are capable of affecting calcination kinetics. Carbon dioxide is naturally directly involved, since calcination slows if CO_2 approaches the equilibrium pressure for decomposition of $CaCO_3$. MacIntire and Stansel (31) found that steam catalyzes the calcination. Wist (32) reported that CO retards the calcination while the presence of H_2 hastens it.

Bryantseva and Khvosten'kov (33) calcined two high-silica dolomites and checked the influence of calcination temperature on X-ray diffraction patterns, compressive strength of molded specimens, density, and other properties. The stone was heated at 5° per minute and was held at the final temperature for twenty minutes. For samples carried to temperatures beyond $1000^{\circ}C$, they found a considerable loss of activity of both CaO and MgO as measured by heat of hydration. X-ray diffraction showed that the loss of

MgO activity was due mainly to its recrystallization to periclase, while the CaO tended to react with SiO_2, Al_2O_3, and Fe_2O_3 which were present in their dolomites. Some sintering as measured by dimensional shrinkage began at temperatures as low as 900°C, and shrinkage rapidly accelerated above 1000°C.

Scanning electron microscope pictures by Eades and Sandberg (34) provide further insight into the physical changes which occur during calcination of limestone and sintering of lime. The pictures first show the large increases in porosity and surface area which result when limestone is gently calcined. Calcination at higher temperatures produces a solid with larger crystallites. Finally, dead-burned specimens, produced at still higher temperatures, show very large crystals with low porosity.

It is apparent from the foregoing and from our own work, described in Section 7.08, that the condition of calcined dolomite depends upon its history. This will be further discussed in Section 8.04 relating to the choice of calcination conditions and the ability of the stone to withstand the fuel desulfurization reaction cycle.

The results of our work in Section 7.08 raise interesting possibilities with respect to the role of CO_2.

This gas has an activating or catalytic effect on sintering. What would be the effect of CO_2 on the reaction of CaO with H_2S? Is it possible that the presence of CO_2 could change the reaction rate, perhaps even speed it up? We again note that Ruth et al. (24) have shown that the reaction of $CaCO_3$ with H_2S is faster at higher partial pressures of CO_2.

8.03.3 Recarbonation of Dolomite

Our single isothermal recarbonation of a powder sample of calcined dolomite, described in Section 7.10.3, raises the suspicion that this reaction may follow a nonequilibrium adsorption model much like the model developed for reaction (A) in Section 7.02.

The behavior of the reaction in this run, first rapid and then slower, is consistent with results reported by others.

Dedman and Owen (35) studied the recarbonation of a lime prepared from limestone. Their CaO had a BET area of 5 m^2/g. Their study covered temperatures from $100^\circ C$ to $600^\circ C$. There was a rapid initial reaction at all temperatures causing conversions on the order of 0.4% at $100^\circ C$, 4% at $400^\circ C$, and 17% at $600^\circ C$, with signs that the conversion achieved at the end of the period of rapid reaction was levelling off at the higher temperature. They believed the reaction to occur at each temperature on all CaO surface available to CO_2, migrating along grain boundaries. The amount of the rapid reaction at 100^oC corresponded to coverage of the apparent surface, as measured by the BET method, by carbonate ions. Dedman and Owen believed that the pores expanded at higher temperatures, increasing the surface available to the migrating CO_2. They regarded the amount of CO_2 taken up rapidly at 600^oC as corresponding to coverage of 186 m^2/g by carbonate ions. The apparent activation energy for a later, slower take-up of CO_2 by the limes was determined from data between 200^oC and 600^oC to be about 9.5 ± 2 kcal/mole. Dedman and Owen regarded this activation energy to be associated with the diffusion of adsorbed CO_2 along narrow grain boundary pores, already recarbonated, to react with oxygen ions at the interior ends of the pores.

The model proposed by Dedman and Owen is a variant of the multiple-reactivity model discussed in Section 8.01.4 and used there to explain a rapid initial rate followed by a slower rate. We feel that a nonequilibrium adsorption model might be applicable to the recarbonation reaction. It would be interesting to vary the CO_2 concentration and see if any variation results in the degree of conversion achieved by the rapid reaction. Our nonequilibrium model predicts yes while Dedman and Owen's model or a multiple-reactivity model says no.

8.04 Ability of Solid to Survive the Fuel Desulfurization Reaction Cycle

The fuel treatment processes for which dolomite is being considered will require the circulation of large tonnages of dolomite through the reaction cycle which includes the H_2S adsorption reaction, the reaction of CaS with steam and CO_2, and a calcination. To avoid a solid disposal problem, the stone should be capable of surviving numerous reaction cycles before it must be discarded.

Our work is encourageing for the view that dolomite can meet this requirement if it is not exposed to a temperature much above about 1000°C.

The spherical sample which was cycled so that reaction (A) could be conducted five times did not appear to lose reactivity or capacity for absorbing H_2S. Work on this sample has been described in Section 7.03.5.

Our work to explore effects of calcination temperature, time, and gas environment upon reactivity in a nonisothermal recarbonation was discussed in Section 7.08. This exploratory work has shown that no "catastropic" sintering of the solid occurs during a hold for four hours at 975°C under one atmosphere of CO_2, a gas which apparently activates the sintering process.

This work does show a moderate loss in recarbonation reactivity when the hold at calcination temperature is increased from one to four hours or when the temperature is increased from 925°C to 975°C. This behavior is consistent with the report by Bryantseva and Khvosten'skov (33) that some sintering, as reflected by shrinkage, was observed for a high-silica dolomite at a temperature as low as 900°C.

Our findings are also consistent with the experience of Gesellschaft für Kohlentechnik (5), which observed no appreciable change in recarbonation activity after more than 20 cycles each including a calcination step at 950°C. Moreover, the MgO crystallites in the solid remained catalytic for the water-gas-shift reaction, a fact indicating that the solid preserved an appreciable surface area through a large number of reaction cycles.

Our work falls short of proving that calcined dolomite will maintain good reactivity through many reaction cycles including the reaction of H_2S with CaO. It will be important to obtain a practical demonstration of this fact, preferably by conducting the reaction cycle a number of times on a charge of solid in a fluidized-bed reactor.

There is evidence that reactivity falls drastically and rapidly in a reaction cycle which includes a roast to expel SO_2 at a temperature above 1000°C. Consolidation Coal Co. (6) has conducted a life study of calcined dolomite used in Consol's CO_2 acceptor process for gasifying coal char. The regeneration temperature was 1060°C. The measure of solid reactivity was the extent to which the stone recarbonated in a standard test at 870°C. From a fractional conversion of 0.8 in the fifth cycle, the reactivity fell to 0.4 in the twentieth cycle and to 0.2 after 40 cycles. In Consol's process, the solid make-up rate is adjusted to provide an economic balance between the cost and thermal disadvantage of circulating more stone and the cost of make-up and waste disposal.

In a recent publication (36), Consol has described an embodiment of their process for providing low-sulfur fuel for power generation. In this embodiment, Consol proposes to use a make-up of fresh dolomite amounting to 30% of the stoichiometric quantity needed for absorbing sulfur present in the coal feed. Acceptor solid is circulated at a rate more than seven times greater than the rate of coal feed.

There are good grounds for the hope that a fuel desulfurization process in which the solid is exposed to temperatures no higher than about 950°C can operate not only with a significantly smaller rate of dolomite make-up but also with a significantly smaller rate of circulation of acceptor solid.

For reasons not yet apparent, Moss (37) has reported that dolomite is unsuitable for a process in which residual oil is gasified by partial oxidation with air at 850°C. In Moss's work, conducted at atmospheric pressure, lime is used to absorb sulfur in a bed fluidized with air fed at about one-third of the stoichiometric rate for complete combustion of the oil feed. Moss conducts a regeneration step at 1050° with expulsion of SO_2. At a stone make-up rate amounting to about 30% of the stoichiometric rate for removal of sulfur from the oil, the efficiency of sulfur removal from the product gas was only about 60% after eight cycles. In order to maintain 90% efficiency absorbing sulfur, in steady operation after many cycles, the stone had to be made up at a rate of about 75% of stoichiometric.

Another requirement for an acceptor which is to be cycled through reactions conducted in fluidized beds is that the solid must resist both breakage and attrition. Consol has demonstrated that calcined dolomite can meet this requirement. There is a possibility, however, that the sintering which takes place at the high temperatures of Consol's regeneration may have strengthened Consol's stone and increased its resistance to attrition. We must consider the question whether or not a process conducted at a lower temperature might give a less favorable result.

Our experience in handling Greenfield dolomite is that is appears strong and might be expected to resist decrepitation even if calcination is conducted at a low temperature. If this stone or another stone should prove disappointing in this respect, however, there is a good possibility that a single hold at a high temperature might strengthen the stone. After such treatment, the stone should still possess good reactivity, in light of the relatively small decline in reactivity suffered by a stone in Consol's work during a first reaction cycle. Once in a process, the stone might be expected to become progressively stronger as slow sintering and shrinkage occurs.

8.05 Further Kinetic Experiments

In planning further experiments, one must be aware of the effect of both calcination conditions and the implications of the kinetic model.

Our calcination conditions were not controlled with the precision which might be desired. The hold temperature for calcination, 925°C, was set by turning a pointer to the appropriate spot on the dial of the controller indicator. The exact temperature reached varied from run to run by several degrees. Some of the variability in reactivity of our powder samples, noted particularly at low temperatures and discussed in Section 8.01.2, may have resulted from inadequate control of calcination.

After the conclusion of the present experiments, we acquired a new temperature controller, with a digital set point, for the furnace of our set-up. The controller will provide a more rapid approach to constant temperature as well as ability to reproduce a given temperature more consistently. Work within the new controller should reduce the variability in calcination conditions as a factor conducive to variability in sample reactivity.

Our calcination procedure is probably a reasonable first approximation to conditions for calcination in a practical process. It will be important, however, to explore systematically the effect of calcination conditions upon reactivity. Our exploratory study of reactivity for the recarbonation reaction, discussed in Section 7.08, provides an introduction to such work.

Studies exploring the effect of calcination conditions upon the H_2S absorption reaction might advantageously be combined with work examining the effect of cycling the stone through the reactions used in the fuel desulfurization cycle. Because of the slowness of regeneration reaction (C), this were best done at high pressure.

Unrealistic calcination conditions, such as calcination in helium as practiced by Vestal and

Johnston (29), should be avoided in work directed toward providing information for process application. Work upon stones calcined in absence of CO_2 might, however, have considerable scientific interest. We are curious to know if the nonequilibrium reaction model developed for the H_2S absorption reaction in Section 7.02 would apply to such materials.

Further experiments to verify this model are of course in order. A simple experiment would be to react a sample at 550°C and 10% H_2S for several hours, purge with nitrogen to desorb H_2S, and then switch back to the reaction gas. The desorption period should be a number of hours to be certain that thorough desorption takes place. According to our model, a rapid rate should again be observed when reaction is resumed.

An experiment of greater power would be to analyze for H_2S desorbing from a partially reacted sample. The sample should preferably be reacted with H_2S in a chamber having a short gas residence time. After a partial conversion of CaO to CaS, the flow would be switched to nitrogen and effluent gas would be analyzed for H_2S in trace quantity.

Experiments of this type would also be useful to test for the absorption of H_2, H_2O, CO, CH_4, and CO_2. These are all gases expected to appear in fuel gases produced in a practicable process. In the experiments, each gas in turn, as well as various gases in combination, should be added to the gaseous reaction mixture containing H_2S. Caution should be exercised to make certain that gaseous constituents entering into the water-gas-shift reaction, when all are present, stand at shift equilibrium at the temperatures of the solid sample.

In Section 8.01, we suggested that CO_2 might affect the kinetics of reaction (A). To test this, one can merely add CO_2 to the reacting as. The test should preferably be made at 900°C, where the effect was suspected, but at an H_2S concentration other than 0.3%. Two precautions will generally be required: The first is that the concentration of CO_2 must be low enough so that recarbonation will not take place. The second is that the presence of CO_2 will bring the shift equilibrium into play, and this will have to be taken into account in the manner just mentioned.

The role of water in reaction (A) is obviously important, but has not been thoroughly investigated in our experiments. The mechanism by which water acts on reaction (A) and its effect as a function of temperature and composition remains to be determined.

Work on the H_2S absorption reaction should be extended to a representative collection of dolomites obtained from a variety of rock formations. The City College team is acquiring such a collection of dolomites.

8.06 Process Implications

In fuel-treating processes now visualized, the initial partial pressure of H_2S might range from a few tenths of an atmosphere to perhaps 1 atm. In a practical reactor, however, the bulk of the reaction space and CaO inventory must be provided to remove final amounts of H_2S. Typically, the outlet partial pressure of H_2S might be a few thousandths of an atmosphere, corresponding roughly to the lowest concentrations studied by us. Hence, the main practical interest will lie in our data at relatively low concentrations. Here, our model may tend to predict rates conservatively on the slow side, particularly at higher temperatures.

Our work at higher concentrations has led, however, to a conclusion which the practical man should keep in view. This relates to the importance of adsorption in the kinetic model. Our rate data were taken for CaO which was relatively "fresh" and "clean". That is, it had just been produced in a calcination at 925°C under CO_2 at 1 atmosphere. We cannot yet say how different our results might have been for CaO having different histories as regards temperature or gas environment. After engineering study indicates flowsheet conditions for calcination in attractive process embodiments, it will be important to check the possibility that kinetics for absorption of H_2S may be materially different for the new calcination conditions.

The role of adsorption and the solid's history may become particularly important if the solid is used in several processing steps between calcinations. Dolomite which has been in contact with H_2S at a relatively low temperature might need some time to desorb if it is to show full reactivity at a higher temperature. This consideration might affect a gravitating-bed process, for example.

A major practical interest lies in use of calcined dolomite in fluidized beds. The history of the development of fluidized-bed processes provides many examples of the difficulty of predicting kinetic results in such beds with any precision from differential reaction rate data of the type which this research has provided. Kinetic studies of the H_2S absorption reaction in fluidized beds are now desirable, preferably in conjunction with work in which the solid is cycled through this reaction, the reaction of CaS with steam and CO_2, and a calcination. We anticipate that the studies may be usefully planned and their results regarded in light of our kinetic model.

9.0 Conclusions and Recommendations

At the outset of this research, no data were available for the kinetics of the reaction of H_2S with fully calcined dolomite. The primary aim of the research was fulfilled in that the main features of the kinetics of this reaction have been outlined and relevant kinetic constants evaluated. For a sample of powdered stone calcined under 1 atm of CO_2 at 925°C, held for 15 min under N_2 at this temperature, and cooled under N_2 to a temperature between 475° and 900°C, the progress of the reaction of H_2S with fully calcined dolomite at the latter temperature is described by equations (9) and (10) in Section 7.02.2:

$$W/W_o = [(r_2 + K_3C)\exp(r_1t) - (r_1 + K_3C)\exp(r_2t)]/(r_2 - r_1) \tag{9}$$

$$r_1, r_2 = -\tfrac{1}{2}(K_1C + K_3C + K_2) \pm \tfrac{1}{2}[(K_1C + K_3C + K_2)^2 - 4K_2K_3C]^{\frac{1}{2}} \tag{10}$$

Table 4 of Section 7.02.5 gives the Arrhenius expression for the rate constants K_1, K_2, and K_3.

The foregoing expressions (9) and (10) were derived from the hypotheses that the rate is hindered by activated adsorption of H_2S and that gas-phase H_2S molecules react with bare CaO surface.

The reaction occurs homogeneously throughout the solid provided the particle size is not too large, and diffusion in the solid will have minor importance under most anticipated conditions for applying the reaction in processes for desulfurizing fuels.

The investigation has provided kinetic information which should be useful to persons undertaking the development of processes of this type. The kinetic model, although not yet proved, can be expected to help such persons avoid difficulties which might arise from the role of H_2S adsorption in hindering the reaction rate. The importance of defining conditions for calcination early in such a development has been confirmed. The kinetic model should be useful in planning and interpreting fuel-desulfurization experiments conducted in fluidized beds.

Several related topics were investigated briefly. These are reported in Sections 7.06 through 7.10, and include examination of effects of hydrogen, steam, and calcination conditions upon reactivity and exploratory work on the reaction of CaS with steam and CO_2 and the recarbonation of CaO.

Further work is needed to confirm our reaction model; to elucidate the roles of H_2 and steam and to explore possible roles of CO_2, CO, and CH_4 in affecting the rate of the H_2S absorption reaction; to explore effect of calcination conditions upon reactivity for H_2S absorption; and to explore the behavior of dolomites of various origins.

Pilot-scale work in fluidized beds operating at elevated pressure is needed to prove the operability of a cyclic process using the H_2S absorption, the reaction of CaS with steam and CO_2, and a calcination. Such work is also needed to provide kinetic data for the reactions when conducted in fluidized beds.

10.0 Appendix

10.01 Derivation of Equations

10.01.1 Role of Diffusion

In a generalized reaction between a gas and a porous solid, both diffusion and chemical reaction occur. In order to determine rate constants from conversion data, it is necessary to reduce unwanted diffusion effects or to correct for them. The change in concentration from the bulk gas phase to the reacting solid surface is caused by diffusion through the gas film surrounding the solid, diffusion through the solid, and by reaction on the solid.

When diffusion in the solid is important, the reaction takes place on a thin interface between a core of unreacted material and a product shell. The concentration drop takes place in a product shell sometimes called the ash layer. Diffusion limitation in the solid is thus often referred to as an ash-diffusion limitation.

The concentration drop caused by external film diffusion around a sphere is

$$\Delta C = J/4 \pi R^2 K_g \qquad (27)$$

where ΔC = concentration change, g-moles/liter or millimole/ml, and

J = molar flux, millimoles/second.

Since the reaction slows as the solid is consumed, the concentration drop due to film diffusion will continually decrease as time passes.

Consider the external resistance to mass transfer, $1/(4\pi R^2 K_g)$ or $2/4\pi RD(N_{NuD})$, where N_{NuD} = Nusselt number for diffusion, $K_g D_p/D$. This may be compared to the internal diffusion resistance, $\left(\frac{1}{r_i} - \frac{1}{R}\right)/4\pi D_e$ or $\left(\frac{1}{r_i} - \frac{1}{R}\right)/4\pi(\varepsilon/\tau)D$,

where ε = porosity, dimensionless,

τ = tortuosity, dimensionless,

D_e = $(\varepsilon/\tau)D$ = internal effective diffusivity,

r_i = radius of reaction interface, cm, and

R = outside radius of experimental sphere, cm.

The ratio of external to internal diffusion resistance is seen to be

$$\frac{\text{External Resistance}}{\text{Internal Resistance}} = \frac{2\varepsilon}{\tau R\,(1/r_i - 1/R)\,(N_{NuD})}$$

The numerical value of the ratio is 0.10 for the following estimated values:

$N_{NuD} = 5$

$\varepsilon = 0.4$

$\tau = 3$

$R = 0.50$ cm

$r_i = 0.33$ cm

When diffusion is controlling, the effect of external diffusion upon results can be kept small by judicious selection of reaction conditions. In any case, the outside film resistance is expected to have a negligible effect upon data obtained in advanced stages of a run, and does not disturb the evaluation of D_e, the internal effective diffusivity, from these data.

10.01.2 Corrected Time for Control by Film Diffusion

We consider here the reaction of a sample of solid with a gaseous reactant at such rate that diffusion in the gas external to the solid sample cannot be neglected. When the sample reacts at a rate proportional to the concentration of the gaseous reactant at the interface a time correction may be applied to the data to remove the effect of external diffusion. This correction is independent of the way in which the solid reacts and is applicable, for example, to a sphere reacting by a shrinking core mechanism or to a solid reacting homogeneously by a first order reaction.

A mass transfer coefficient Kg is adopted to describe diffusion external to the sample

$$J = S K_g (C - C_i) \tag{28}$$

where J = total reaction rate of solid sample, g-moles/second,

C = concentration of H_2S in the bulk gas, g-moles/liter,

C_i = concentration of H_2S at sample-gas interface, g-moles/liter, and

S = exposed surface area of sample, cm^2.

For the rate of reaction of the solid, we adopt the general expression

$$J = V f(x) C_i \tag{29}$$

where V = volume of solid sample, cm^3

x = fraction of solid converted.

For a sphere of radius R reacting by a shrinking core mechanism equation (29) would have the form

$$J = 4 \pi D_e R C_i [(1 - x)^{-1/3} - 1] \tag{30}$$

where D_e = effective internal diffusivity.

For a sample reacting homogeneously with first order kinetics

$$J = VN_oK\ (1 - x)\ C_i \qquad (31)$$

where N_o = initial concentration of solid reactant.

Eliminating C_i between equations (28) and (29)

$$J = C/\left[\frac{1}{SK_g} + \frac{1}{V\,f\,(x)}\right] \qquad (32)$$

Using

$$J = VN_o\frac{dx}{dt} \qquad (33)$$

and integrating equation (32)

$$t - \frac{VN_ox}{SK_gC} = \int_o^x \frac{N_o}{C\,f\,(x)}\,dx \qquad (34)$$

The right hand side of this equation is independent of external diffusion. Film diffusion appears as a time correction term on the left side of the equation, and data may be plotted using a "corrected time", i.e. the entire left side of equation (34).

For a sphere reacting by a shrinking core mechanism

$$t - \frac{N_oRx}{3CK_g} = \frac{N_oR^2}{6D_eC}\left[1 + 2\ (1 - x) - 3\ (1 - x)^{2/3}\right] \quad (35)$$

For a homogeneously reacting sample

$$t - \frac{VN_o x}{SK_g C} = \frac{1}{K_c} \ln (1 - x) \qquad (36)$$

10.01.3 Corrected Time Applied to Powder Samples

For work with powders, we spread the powder to form a thin layer in a pan. This sample geometry obviated diffusion considerations in most of our powder runs.

At 900° and at H_2S concentrations of 1.0 and 0.3%, however, the runs began slowly, indicating presence of diffusional resistance. Typical data for 0.3% H_2S are seen in Figure 29, and for 1.0% H_2S in Figure 32.

For such runs, the expression in time on the left side of equation (36) was used to correct the data, a value for the product SK_g being derived empircally from the rate data. The value of this product was adjusted by trial and error for each run to give a uniform rate for the run when log (1 - x) was plotted versus the corrected time. Figure 32 gives data for a run at 900°C using corrected and uncorrected time coordinates. It is important to note that even at 900°C, the linear portion of the log (1 - x) plot

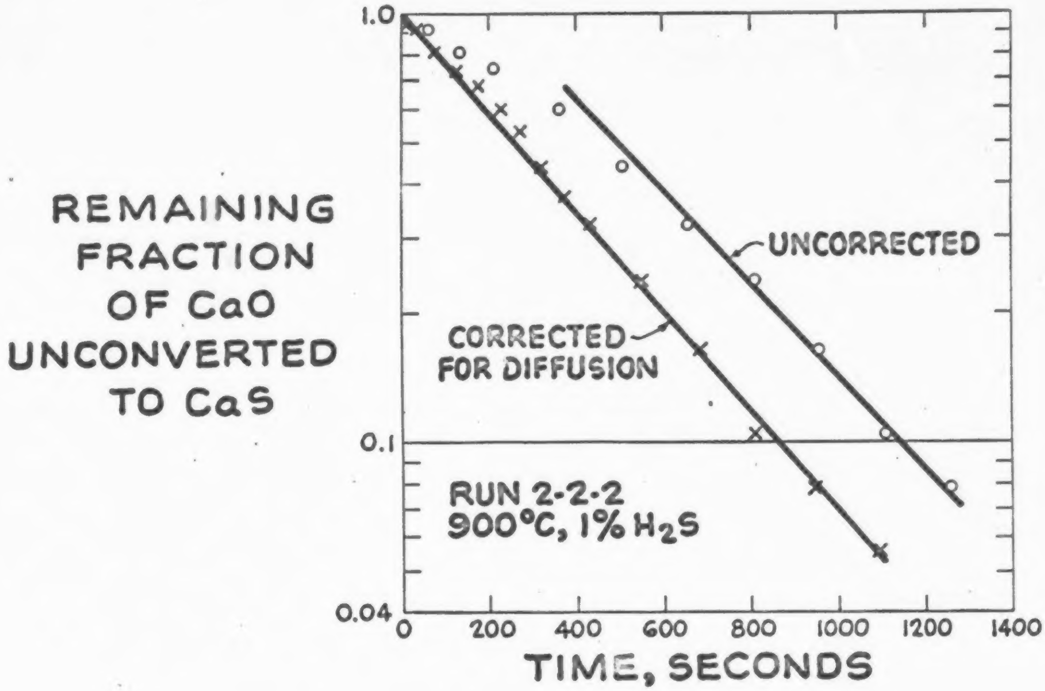

Figure 32. Runs 2-2-2 on Greenfield powder at 900°C, 1% H_2S.

The original uncorrected data are presented together with data corrected for diffusion as discussed in Section 10.01.3.

would give the same slope at higher conversions whether or not diffusion correction is applied.

The values for the product SK_g derived empirically in the manner just described are about three times larger than values for this product derived from initial rate data assuming diffusion control.

10.02 Weight of H_2S Absorbed on Dolomite

It is of interest to know the weight of H_2S which would be adsorbed on dolomite if the surface were completely covered. For interpreting our experimental data, it is important to know that adsorption of H_2S could not change the weight sufficiently to be mistaken for chemical reaction. From a process point of view, there is a question of how much H_2S might be associated with the surface if conditions are such that the H_2S desorbs slowly.

The calculation can be made by assuming an area of calcined dolomite amount to 5 m^2/g of original dolomite. The area of an H_2S molecule is taken to be 10.29 $\mathring{A}^2$. From these data one may estimate that 0.3 lbs of H_2S might be adsorbed by the calcine prepared from 100 lbs of original dolomite with assumption of complete coverage of the total CaO surface. If such a weight gain were to occur during the reaction, it would contribute only 3% to the observed conversion. This result indicates that adsorption should not invalidate the rate data based upon the solid's weight gain.

10.03 Raw Data

Tables 14 through 18 present weight-gain data on all our kinetic runs. The runs in the tables are listed in the order in which they were made. Reference may be made to the tables to be indicated for run temperatures and compositions of reaction gas mixtures.

Table 14 presents data on runs for reaction (A) conducted on the powder sample of Greenfield stone. Data for these runs are summarized in Tables 3, 10 and 11. Table 15 presents data for reaction (A) conducted on spheres of Glasshouse dolomite and on spheres of Greenfield dolomite. Data for these runs are summarized in Tables 6, 8, 9, and 10. Table 16 presents data on runs for reaction (A) during which conditions were changed in midrun. These data were not considered valid for our kinetic determinations, but they may have use for others. These runs are discussed in

Table 14. Raw Data: Time and Change in Weight for Powder

80-8, 34.4*		80-9, 36.7		80-10, 45.6	
1**	2.4***	1.5	2.9	1	2.0
2	5.1	3.0	7.25	2	5.1
3	7.4	4.5	11.0	3	7.5
4	10.4	6.0	14.2	4.5	10.8
5	12.2	7.5	17.15	7	15.8
6	14.1	9.0	19.7	9.5	19.9
7	15.9	11.5	23.5	12	23.8
8	17.5	14.0	26.8	14.5	27.0
9	19.7	16.5	29.45	17	29.8
10	20.9	19.0	31.6	19.5	32.3
11	22.25	21.5	33.2	22	34.4
13	24.6	24	34.1	24.5	36.5
15	26.7	26.5	34.9	27	38.0
17	28.9	29	35.4	29.5	39.4
19	30.3	31.5	35.7	34.5	41.2
21	31.1	34	35.9	37	42.2
23	31.95	36.5	36.05	42	43.3
26	32.68	39	36.2	47	44
31	33.44	44	36.4	52	44.55
36	33.84	49	36.55	57	44.95
41	34.15			62	45.1
46	34.35			67	45.3
				72	45.4

* Capacity of sample in mg.

** Time in minutes.

*** Observed weight change in mg.

Table 14.--Continued

84-1, 35.3		84-2, 34.9		84-3, 33.4	
1	2.5	1	1.0	1.5	2.7
2	6.6	2.5	8.8	3	4.8
3	8.8	4	11.8	4.5	6.9
4.5	12.0	6	16.5	5.5	8.3
7	16.5	7.5	18.2	8	11.8
9.5	19.8	9	19.75	10.5	14.6
12	22.4	11.5	22.2	13	16.9
14.5	25.0	14	24.6	15.5	19.1
17	26.6	16.5	26.3	18	21.3
19.5	28.1	19	27.4	20.5	23.3
22	29.2	24	29.4	23	24.8
27	31.0	29	30.7	28	27.2
32	32.2	34	31.65	30.5	28.1
37	33.4	39	31.95	33	29.0
42	34.05	44	32.9	35.5	29.8
47	34.45	49	33.2	45.5	31.75
52	34.7	54	33.55	48	32.0
57	34.9	59	33.8	53	32.4
62	35.1	64	34.0	58	32.75
67	35.18	69	34.15	63	32.95
72	35.25	79	34.45	73	33.2
		89	34.67		
		94	34.8		

Table 14.--Continued

84-4, 23.0	
0.75	1.5
2.0	4.1
3.25	6.4
4.5	8.5
5.75	10.7
7.0	13.0
8.25	15
9.5	16.55
12.0	19.2
14.5	20.9
17.0	21.8
19.5	22.2
22.0	22.4
24.5	22.45
29.5	22.8

84-5, 40.3	
4	3.5
7	4.6
9	5.2
14	6.3
24	7.9
34	9.0
44	10.0
54	10.9
74	12.4
94	13.5
104	14
114	14.55
124	15.0

84-6, 29.2	
10	0.8
20	1.6
30	2.3
40	2.9
50	3.4
60	4.0
70	4.4
80	4.9
100	5.6
120	6.3
140	6.9
185	15.9
190	16.9
200	18.6
210	20.0
220	21.4
230	22.5
240	23.6
250	24.4
260	25.1
270	25.7
280	26.2
290	26.6
300	27.0
310	27.3
315	27.4

Table 14.--Continued

84-7, 37.5		84-8, 29.1		84-9, 22.2	
2.5	1.2	0.5	0.8	5	0.5
5.0	2.2	1.0	1.3	10	1.4
7.5	3.6	2.5	2.9	15	2.2
10	5.0	6	3.9	20	3.1
15	8.0	11	5.0	25	4.0
20	11.3	16	5.7	30	4.9
25	14.3	21	6.3	35	6.0
30	17.1	31	7.1	40	6.8
35	20	41	7.6	45	7.9
40	22.4	51	8.1	50	9.2
45	24.5	61	8.6	55	10
50	26.3	71	9.0	60	10.8
55	28.2	81	9.4	65	11.9
60	29.8	91	9.7	70	12.9
		101	10.0	75	13.9
				80	14.8
				85	15.8
				90	16.4
				95	17.5
				97.5	19.7
				102.5	20.9
				105	21.2
				110	21.5
				115	21.7

Table 14.--Continued

86-1, 29.2		86-2, 36.6		86-3, 35.3	
1.0	2.8	0.75	5.7	1.0	2.4
2.5	8.5	2.0	14.2	3.5	4.1
5.0	14.7	3.25	20.1	6	5.0
7.5	18.8	4.50	26.4	11	6.2
10.0	22.3	5.75	29.3	16	7.0
12.5	24.6	7.0	32.4	21	7.6
15.0	25.8	8.25	34.0	26	8.0
17.5	26.7	9.5	34.9	31	8.45
22.5	27.9	10.75	35.3	36	8.8
25	28.2	12.0	35.5	46	9.4
30	28.5	13.25	35.75	56	9.9
35	28.8	14.5	35.8	66	10.4
40	29.05	15.75	35.9	76	10.7
		17.0	36.0	96	11.4
		19.5	36.15	116	11.9
		22.0	36.35	136	12.5
				156	13.0
				166	13.3

Table 14.--Continued

86-4, 21.8		86-5, 42.9		86-6, 15.5	
0.50	1.5	2	1.7	0.25	1.3
1.0	5.2	4	2.7	1.0	2.7
1.75	8.4	9	4.1	1.5	4
2.5	11.8	14	5.0	2.0	5
3.0	13.7	16.5	5.6	2.75	6.45
3.75	16.6	36.5	7.2	4.0	8.8
4.25	17.7	44	7.6	5.25	10.9
5.0	19.1	54	8.1	6.5	12.3
5.5	19.7	64	8.6	7.75	13.5
6.75	20.6	74	9.0	9.0	14.3
8.0	20.95	84	9.4	10.25	14.65
9.25	21.25	94	9.7	11.5	14.85
10.5	21.4	104	10.05	12.75	15
		114	10.4	14.0	15.1
		134	10.9	16.5	15.2
		144	11.2		
		164	11.6		

Table 14.--Continued

86-7, 33.1		86-8, 40.4		90-1, 38.1	
1.5	4.0	3	1.1	1	2.6
4.0	9.2	8	2.6	2	4.1
6.5	13.2	13	3.35	4	6.1
9.0	16.4	18	4	6	7.6
11.5	19.15	23	4.7	8	8.7
14.0	21.5	33	5.75	10	9.5
16.5	23.45	43	6.55	15	11.3
19	25.1	53	7.25	20	12.7
24	28	63	7.9	25	13.6
29	30.1	73	8.45	30	14.5
34	31.4	83	8.9	35	15.2
39	32.2	93	9.4	40	15.8
44	32.8	103	9.85	45	16.3
		113	10.23	50	16.8
		128	10.75	60	17.7
		143	11.23	70	18.35
		158	11.7	80	19.0
		173	12.1	90	19.65
		183	12.4	100	20.2
				110	20.64
				120	21.1
				130	21.5
				140	21.9
				150	22.2
				160	22.54
				170	22.8
				180	23.08

Table 14.--Continued

90-2, 31.6		90-4, 31.8		90-8, 35.0	
1.0	1.5	1.0	2.6	1.5	1.0
2.5	4.45	3.0	5.6	3.5	2.5
3.5	6.0	5.0	6.9	6.5	4.3
5.0	8.3	7.5	8.2	16.5	10.8
6.0	10.5	10	9.1	21.5	13.2
7.5	13.05	15	10.5	25.0	14.8
8.5	14.5	20	11.5	31.5	18
10.0	16.6	25	12.4	36.5	19.9
12.5	19.85	30	13.1	41.5	21.7
15.0	22.45	40	14.3	51.5	24.8
17.5	24.8	50	15.3	61.5	27.1
20.0	26.6	60	16.1	71.5	29.1
22.5	28.3	70	16.8	81.5	30.65
25.0	29.4	80	17.4	91.5	31.75
27.5	30.28	90	17.9	106.5	32.75
30.0	30.75	110	18.8	121.5	33.4
32.5	31.1	130	19.55	136.5	33.8
35.0	31.33	150	20.2	151.5	34.05
37.5	31.47	170	20.8	166.5	34.3
40.0	31.55	190	21.3	181.5	34.95

Table 14.--Continued

90-9, 28.2		92-1, 19.2		92-2, 39.2	
1.0	1.4	0.5	1.5	0.5	0.1
3.5	6.2	1.0	6.4	2.0	0.5
6.0	8.5	1.5	10.4	10.5	0.75
8.5	10.4	2.0	14.1	20.5	1.1
11.0	12.2	2.5	16.7	40.5	1.7
13.5	13.45	3.0	18.1	60.5	2.2
16	14.5	3.5	18.6	80.5	2.6
21	16.25	4.0	18.8	100.5	2.8
26	17.6	4.5	19.0	120.5	3.0
31	18.7			140.5	3.1
41	20.4			160.5	3.3
51	21.9			180.5	3.5
61	23.2			200.5	3.68
71	23.9			220.5	3.85
91	24.8			230.5	3.95

Table 14.--Continued

92-3, 19.2		92-4, 29.5		92-5, 38.1	
2.5	0.3	2	0.1	2	.35
5.0	0.6	12	0.7	12	2.4
10	1.25	22	1.6	22	4.3
20	2.95	32	2.65	32	5.9
30	4.6	42	3.9	42	7.4
40	6.4	52	5.3	52	8.8
50	8.3	72	8.4	62	10.15
60	10.2	82	10.05	72	11.4
70	12.3	92	11.6	82	12.5
80	14.2	102	13.15	92	13.6
90	15.7	112	14.5	102	14.4
100	17.1	122	15.9	112	15.2
110	18.05	132	16.95	122	16.0
120	18.85	142	17.7	132	16.7
130	19.1	152	18.7	142	17.45
		162	19.55	152	18.1
		172	20.35	162	18.8
				172	19.5
				182	20.1

Table 14.--Continued

92-6, 36.8		92-7, 19.8		92-8, 28.8	
1.5	.65	0.5	1.9	1	2.7
11.5	2.5	1.0	5.7	2	4.8
21.5	3.45	1.5	12.2	3	6.5
31.5	4.1	1.75	13.5	4	7.8
41.5	4.8	2.0	15	5	8.7
51.5	5.4	2.25	16.45	6	9.7
61.5	5.95	2.75	19.2	8	12
71.5	6.5	3.25	19.5	11	13.8
81.5	6.9	3.0	19.4	16	16.2
91.5	7.35	3.5	19.6	21	18.2
111.5	8	4.0	19.68	26	19.6
131.5	8.65	4.75	19.75	31	21.0
151.5	9.2			41	23.3
171.5	9.7			51	24.6
186.5	10.1			61	25.5
201.5	10.55			71	26.1
				81	26.55
				91	26.85
				101	27.05
				111	27.3

Table 14.--Continued

92-9, 31.4		94-1, 15.1		94-2, 16.3	
1	1.1	2.5	0.8	0.5	0.2
3	5.5	5	1.6	5.5	1.95
5	8.5	10	3.1	10.5	3.8
8	11.5	15	4.6	15.5	5.5
10	13.2	20	6.1	20.5	7.5
15	16.2	25	7.4	25.5	8.8
20	18.8	30	8.7	30.5	10.1
25	20.9	35	10.0	35.5	11.5
30	22.55	40	11.0	40.5	12.8
40	25.05	45	12.0	45.5	13.9
50	26.85	50	12.9	50.5	15.1
60	28.28	55	13.7	55.5	16.05
70	29.05	60	14.25		
80	29.65	65	14.6		
90	30	70	14.9		
100	30.3	80	15.0		
110	30.4				

Table 14.--Continued

94-3, 12.2		94-4, 12.4		94-5, 24.7	
2.5	0.5	1.5	0.4	3	0.6
5.0	0.9	4.0	0.85	13	2.5
10	1.6	6.5	1.3	23	4.35
15	2.5	11.5	2.5	33	6.15
20	3.4	16.5	3.9	43	7.95
25	4.4	21.5	5.2	53	9.1
30	5.4	26.5	6.5	63	9.8
35	6.45	31.5	7.8	73	10.4
40	7.55	36.5	9.1	83	10.95
50	9.6	41.5	10.2	93	11.35
55	10.5	46.5	11.1	103	11.85
60	11.25	51.5	11.65	113	12.2
65	11.8	56.5	12.14	123	12.6
70	12.05	61.5	12.33	133	12.9
				143	13.3
				153	13.6
				163	13.9
				173	14.2
				183	14.4
				193	14.7
				203	14.9
				223	15.4
				233	15.6

Table 14.--Continued

94-6, 31.8		94-8, 27.1		94-9, 31.7	
3	0.7	0.5	2.3	2	0.1
13	2.9	1.0	4.2	7	3.0
23	4.9	1.5	6.9	12	3.8
33	6.95	2.0	8.4	17	4.4
38	8.0	2.5	9.6	22	4.9
43	8.95	3.0	10.7	27	5.3
48	10.15	4.0	12.8	32	5.6
53	11.2	5.0	14.2	37	5.9
63	12.9	6.0	16.8	42	6.2
73	14.6	7.0	18.2	52	6.7
83	16.35	8.0	19.7	62	7.1
93	17.9	9.0	21.0	82	7.9
103	19.35	10.0	21.9	102	8.5
113	20.7	13.0	24.2	122	9.0
123	21.85	15.5	25.4	142	9.4
128	22.4	20.5	26.1	182	9.7
		25.5	26.4		
		30.5	26.8	242	11.4
		40.5	26.9	247	12.0
		45.5	27.0	252	12.5
				257	13.1
				262	13.6
				272	14.4
				282	15.1
				302	16.2
				322	17.2
				342	17.8

Table 14.--Continued

2-1-4, 30.3		2-1-5, 31.9		2-2-1, 23.6	
5	0.6	1	0.5	2	1.7
10	1.3	6	1.8	7	5.55
15	2.1	11	2.4	12	7.95
20	2.9	21	3.2	17	9.7
25	3.8	31	3.8	22	11.10
30	4.7	41	3.3	27	12.6
40	6.3	51	4.7	42	15.9
50	7.9	61	5.1	52	17.35
60	9.3	81	5.65	62	18.4
70	10.6	101	6.2	82	20.0
80	11.8	121	6.7	102	21.25
100	13.8	141	7.05	122	21.9
120	15.6	161	7.35	142	22.5
140	17.1	181	7.55	162	23.0
160	18.4	201	7.8	182	23.05
180	19.7	221	8.1		
200	20.8	241	8.35		
215	21.5	251	8.5		

Table 14.--Continued

2-2-2, 13.4	
0.5	0.8
1.0	1.2
2.25	2.45
3.5	3.5
4.75	4.3
6.0	5.4
7.25	6.3
8.5	7.5
9.75	8.4
11.0	9.1
13.5	10.2
16.0	11.2
18.5	12.0
21.0	12.35
23.5	12.65

Table 15. Raw Data: Time and Change in Weight for Spheres

64-3, 77.5 *		72-1, 65.7		72-2, 34.35	
2.5**	0.8***	2.5	2.5	2.5	3.75
5.0	5.8	5.0	3.8	5.0	6.95
7.5	13.6	7.5	4.8	7.5	9.27
10.0	19.7	10	5.55	10.0	11.14
12.5	24.1	15	6.98	15	14.33
15.0	26.8	20	8.17	20	17.19
17.5	29.8	25	9.19	30	21.33
20	32.7	30	10.15	40	24.68
25	36.5	40	11.79	50	27.78
30	40.4	50	13.34	60	29.43
35	43.3	60	14.75	70	30.69
40	45.8	80	17.21	80	31.67
50	50.3	100	21.24	90	32.43
60	53.9	120	21.24	100	33.00
70	56.8	140	23.03	120	33.50
80	59.2	160	24.7	140	33.77
90	60.8	180	26.3		
100	62.6	200	27.6		
120	64.4	220	28.8		
150	65.9	250	30.5		
		280	32.2		
		300	33.1		

* Capacity of sample in mg.

** Time in minutes

*** Observed weight change in mg.

Table 15. Continued

72-3, 32.4

2.5	3.25
7.5	10.20
5.0	7.3
10	13.35
12.5	16.75
15	19.6
20	22.9
25	25.85
30	27.55
35	28.8
45	30.6
50	31.3

72-4, 33.8

2.5	2.90
5.0	4.95
10	8.20
15	10.48
20	12.45
30	15.55
40	17.80
55	20.02
70	21.70
90	23.75
110	25.43

72-5, 35.8

1.0	2.05
2.0	4.4
3.5	7.6
5.0	11.4
7.5	16.2
10.0	20.5
12.5	23.6
15.0	26.7
17.5	29.55
20	31.0
25	33.55
30	34.7
40	35.55

72-6, 36.3

5	9.1
10	9.4
20	9.9
40	10.78
60	11.5
90	12.6
120	13.62
150	14.6
180	15.6
210	16.53
240	17.43
260	18.05

76-1, 46.5

1.0	1.45
2.5	3.75
4.5	5.90
6.0	9.30
8.0	11.50
10.5	13.8
14.0	16.45

76-2, 50.2

1.0	1.15
3.0	4.65
5.5	7.50
8.0	9.90
10.5	11.8
13.	13.7
15.5	15.45
20.5	18.6
25.5	21.2
30.5	23.7
38.0	26.95
40.5	28.0

Table 15. Continued

76-3, 47.7		76-4, 45.5		76-5, 54.55	
2	2.2	1.0	2.8	2	2.8
5	6.05	3.5	6.35	7	8.4
7	8.25	6.0	8.5	12	13.05
12	12.85	8.5	10.35	17	16.0
17	16.85	13.5	13.05	22	18.85
27	23.0	18.5	15.15	32	22.95
37	28.05	26.0	18.05	42	26.05
47	31.85	33.5	20.4	52	28.9
57	35.00	41.0	22.3	72	33.7
72	38.95	48.5	23.95	92.	36.9
87	41.0	56	25.55	112	39.5
10	42.77	61	26.8	132	41.7
112	43.71			162	44.65
122	44.43			187	46.6
				212	47.9
				242	49.1
				262	49.8

Table 15. Continued

76-6, 45.0		80-2, 23.5		80-3, 18.2	
2	3.4	3.5	1.75	1.5	0.7
5	9.8	8.5	3.25	6.5	2.3
10	17.2	13.5	4.75	16.5	3.8
15	22.3	18.5	5.5	26.5	4.8
20	24.7	28.5	7.15	36.5	5.4
25	29.25	38.5	8.4	51.5	6.4
30	31.9	48.5	9.45	61.5	7.3
40	36.1	58.5	10.3	71.5	8.0
50	38.98	68.5	11.15	86.5	8.45
60	41.1	83.5	11.95	101.5	8.9
70	42.55	103.5	13.05	111.5	9.2
80	43.1	123.5	14.	131.5	9.7
100	44.9	143.5	14.8	151.5	10.1
		163.5	15.4	181.5	10.7
		178.5	15.75	211.5	11.2

Table 15. Continued

80-4, 60.6		80-5, 57.0		80-6, 61.6	
2.0	6.1	1.5	5.3	1.0	2.2
7.0	16.2	2.5	8.6	2.5	7.4
9.5	19.9	5.0	14.8	5.0	13.6
14.5	25.2	7.5	20.2	7.5	18.4
19.5	29.55	10.0	23.2	10.0	22.9
24.5	23.4	12.5	26.3	12.5	26.2
29.5	36.6	17.5	31.9	15.0	29.0
34.5	39.7	22.5	36.8	17.5	32.2
39.5	42.3	25.0	38.3	20.0	34.7
44.5	44.35	27.5	40.2	22.5	37.0
49.5	46.4	30.	41.5	25.0	38.9
54.5	48.1	37.5	46.2	30.0	43.2
59.5	49.85	40.0	47.2	35.0	46.1
64.5	51.5	42.5	48.3	37.5	47.5
				40.0	48.8
				42.5	50.8
				45.0	51.8
				47.5	53.0

Table 15. Continued

80-7, 54.2

1.0	2.0
2.0	5.5
5.0	11.7
7.5	15.9
10.0	18.7
12.5	21.0
15.0	23.4
20.	27.6
25	31.2
30	33.8
35	36.1
40	38.5
45	40.55
50	42.3
55	43.95
60	45.4
62.5	46.15

Table 16. Raw Data: Time and Change in Weight for Runs in which Temperature was Changed in Midrun

80-3, 18.2*, 756°C		84-5, 40.3, 700°C		84-4, 29.1, 700°C	
231.5**	12.6***	154	28.9	126	19.2
236.5	13.8	159	31.2	131	20.5
241.5	14.7	164	32.8	136	21.4
246.5	15.45	169	34.1	141	22.3
251.5	16.0	174	35.0	146	22.9
261.5	17.1	179	35.7	156	24.0
266.5	17.35	184	36.25	166	24.9
271.5	17.6	189	36.7	176	25.5
281.5	18.0	194	37.15	186	26.1
				196	26.5
				206	26.8
				216	27.0

* Capacity of sample in mg.

** Time in minutes

*** Observed weight change in mg.

Section 7.10.1. Table 17 presents data for reaction (C), the reaction of CaS with steam and CO_2. These data are discussed in Section 7.07. Table 18 presents data for the single recarbonation run discussed in Section 7.10.3.

In these tables, the reference number of each run is followed by the capacity of the sample in milligrams. For example, the capacity of Run 80-8 in Table 14 was 34.4 milligrams. The capacity is the weight change which would occur if all of the reactant solid were to be converted. For runs which achieved high conversion, this was taken from the total weight actually gained. For runs which achieved only low conversions, the capacity was estimated from the weight change occurring in the calcination of $CaCO_3$. Following the reference number of each run and the capacity, two columns of data give the time in minutes from the start of the run, on the left, and the observed weight change in milligrams, on the right. No corrections are given.

Table 17. Raw Data: Time and Change in Weight for Regeneration

72-2E, 57.6* starting time is arbitrary		72-3E, 53.1		72-4E, 57.8	
10**	43.3***	5.0	4.05	4	2.20
30	43.75	10	4.63	12	5.4
60	44.8	20	5.1	20	8.5
100	45.4	30	6.8	32	11.9
140	48.1	50	9.04	56	16.75
180	49.8	75	11.6	80	19.7
220	51.1	100	14.0	100	21.3
260	52.0	125	16.25	140	22.65
310	52.2	150	18.35	220	23.93
		175	20.4	300	24.98
		200	23.2	400	26.1
		225	23.7	600	28.15
		250	25.4	800	30.3
		300	28.4	1000	31.7
		350	31.1	1220	36.0
				1240	38.55
				1260	39.45
				1300	43.9
				1340	46.3
				1380	48.45
				1420	50.2
				1480	52.35

* Capacity of sample in mg.

** Time in minutes

*** Observed weight change in mg.

Table 17. Continued

72-5E, 52.3		76-5E, 95.7		76-6E, 87.9	
12	1.1	20	3.3	32	2.6
40	3.6	40	6.3	52	4.8
80	6.95	60	9.3	72	6.7
120	10.3	80	11.9	120	11.0
160	13.6	100	14.3	160	14.4
200	16.35	120	16.6	200	17.7
240	19.0	160	20.2	260	22.4
280	21.25	820	52.2	320	26.9
320	23.7	1100	60.2	820	55.6
360	25.6	1200	62.4	880	57.1
400	27.35	1300	64.6	940	59.4
480	30.65	1400	66.8	1000	61.7
560	34.0	1500	68.55	1100	65.2
		1600	70.2	1200	68.9
		1800	73.6	1400	72.9
		2000	76.3	1500	75.0
		2200	78.4	1600	76.9
		2500	80.8	1700	78.5
		2800	82.4	2300	86.2
		3040	83.3	2400	86.9
				2500	87.6

Table 18. Raw Data: Time and Change in Weight for Recarbonation

---

94-7, 61.2 *

3.5**	7.1***
8.5	10.2
13.5	12.4
23.5	15.8
33.5	18.6
43.5	20.8
53.5	22.7
63.5	24.3
73.5	25.85
83.5	27.4
93.5	28.65
103.5	29.9
113.5	30.9
118.5	31.45

* Capacity of sample in mg.

** Time in minutes

*** Observed weight change in mg.

10.04 Weight Loss During Calcination of Powder Samples

Table 19 gives the weight loss during calcination of powder samples from the supply of - 80+325 mesh Greenfield dolomite used in our powder runs; see Table 2 for the chemical analysis of this supply. The weight loss during calcination of $MgCO_3$ invariably exceeded the weight loss predicted from the chemical analysis. The average weight loss from calcination of $MgCO_3$ exceeded the predicted loss by about 57 mg per gram of sample. We belive that about 6% of the sample was lost early in the $MgCO_3$ decomposition, probably by explosive ejection of ultra-fine powder from sharp edges of individual particles. This view is consistent with the average weight loss during calcination of $CaCO_3$, about 6% below the loss predicted from the analysis.

Curran, Fink, and Gorin (38) report that $CaCO_3$ in a dolomite containing silica can react with the silica at a temperature as low as 840°C under one atmosphere of CO_2, with release of CO_2.

$$CaCO_3 + SiO_2 = CaSiO_3 + CO_2$$

Table 19. Weight Loss during Calcination of Powder Samples

Note: All samples from a single supply of -80+350 mesh Greenfield dolomite No. 82-2R. See Table 2 for chemical analysis of this supply.

Run No.	Weight Loss during Calcination of $MgCO_3$, mg CO_2/g of sample	Weight Loss during Calcination of $CaCO_3$, mg CO_2/g of sample
84-1	265.7	225.7
84-2	258.3	220.2
84-3	275.6	222.1
84-4	282.8	219.5
84-5	269.5	223.3
84-6	277.5	223.4
84-7	269.4	228.1
84-8	274.4	223.8
84-9	286.3	221.8
86-1	276.8	225.1
86-2	273.2	222.5
86-3	291.1	228.3
86-4	285.2	225.2
86-5	262.0	231.2
86-6	298.8	217.9
86-7	272.2	228.9
86-8	286.7	229.9
90-1	295.5	255.1
90-2	270.3	229.9
90-3	269.2	226.4
90-4	273.6	227.2
90-5	272.1	225.9
90-6	284.5	228.0
90-7	269.1	231.3
90-8	267.9	226.9
90-9	276.0	227.1
92-1	290.7	222.1
92-2	290.4	230.0
92-3	292.7	222.6
92-4	310.8	227.5
92-5	267.3	229.5
92-6	266.5	233.8

Table 19. continued

92-7	288.4		225.6	
92-8	275.1		226.5	
92-9	269.2		230.1	
94-1	295.5		221.0	
94-2	295.7		222.0	
94-3	312.1		212.5	
94-4	303.2		215.9	
94-5	285.8		223.4	
94-6	271.5		231.0	
94-8	280.2		225.6	
Average	280.4		226.0	
Standard deviation from average		± 11.1		± 3.3
Weight loss predicted from analysis	223		242	

This reaction cannot account for the anomolous weight loss which we experienced during $MgCO_3$ decomposition. Our sample of Greenfield dolomite (see Table 2) certainly contained no more than 0.5% silica. It follows that the above reaction could account for a loss of weight amounting to no more than 0.8% of the sample.

Limestones and dolomites often contain small amounts of organic material. Calcination of a large chunk of Greenfield dolomite produced a slight tarry deposit at the outlet of a furnace tube. This deposit was dissolved in acetone, dried at 80°C, and weighed. The recovered material amounted to only 0.1% of the weight of the original chunk of stone.

10.05 Nomenclature

A = weight of unconverted CaO in solid sample which is available for reaction, any units,

B = weight of unconverted CaO shielded from the reaction due to formation of a CaO-H_2S surface complex, any units,

C = concentration of H_2S, g-moles/liter,

C_i = H_2S concentration at the solid-gas interface, g-moles/liter,

C_m = H_2S concentration throughout the solid, g-moles/liter,

D = gas diffusivity, cm^2/sec.

D_e = effective gas diffusivity, cm^2/sec.

D_p = particle diamter, cm.

G = mass flow, g/sec-cm^2

J = molar flux, millimoles/sec.

K = a generalized kinetic constant.

K_1 = adsorption rate constant, (g-moles H_2S/liter)$^{-1}$ sec^{-1}

K_2 = desorption rate constant, sec^{-1}

K_3 = reaction rate constant, (g-moles/liter)$^{-1}$sec^{-1}

K_4 = reaction rate constant for reaction (C), (g-moles/liter)$^{-2}$ sec^{-1}

K_e = adsorption equilibrium constant, (g-moles H_2S/liter)$^{-1}$

K_e' = adsorption equilibrium constant, (g-moles H_2/liter)$^{-1}$

K_g = mass transfer coefficient, cm/sec

N_{NuD} = Nusselt number for diffusion, dimensionless

N_{Rep} = particle Reynolds number, dimensionless

N_{Sc} = Schmidt number, dimensionless

P = pressure, atm.

R = Radius of sphere, cm. When premultiplier for T, R = gas constant, cal/g-mole-^{o}K

r = "final" rate, sec^{-1}

r_i = radius of unreacted spherical core, cm

r_1 , r_2 = roots of the nonequilibrium adsorption equation (10), sec^{-1}

S = exposed surface area of a reacting sample of stone, cm^2

t = time, sec.

T = temperature, ^{o}k

V = volume, cm^3

W = weight of unconverted CaO in solid sample, any units.

x = fractional conversion of solid, dimensionless

Δ = delta, indicates a difference in the value of its postmultiplier

ϵ = porosity, dimensionless

μ = viscosity, g/sec-cm^2

ρ = density, g/cm^3

τ = tortuosity, dimensionless

[...] = concentration of the material enclosed in the brackets, g-moles/liter (actual), or mole fraction in Section 5.01

Subscript o = initial value

11.0 References

1. A.M. Squires, "Air Pollution: The Control of SO_2 from Power Stacks: IV. Power Generation with Clean Fuels". Chemical Engineering, December 18, 1967, 101-109.

2. A.M. Squires, "Clean-Fuel Power Cycles", A.S.M.E. Paper, 67-Wa/PWR-3, Pittsburgh meeting, November 1967.

3. R.A. W. Haul, "Adsorptionsuntersuchungen an thermisch zersetzten Dolomitkristallen" ["Adsorption studies on calcined dolomite"], Z. anorg. allgem. Chem., 281 (1955) 199-211.

4. Reported at the Limestone Symposium sponsored by National Center for Air Pollution Control (now National Air Pollution Control Office of the Environmental Protection Agency), St. Petersburg Beach, Florida, December, 1967.

5. W.E. Gluud, E. Keller, W. Klempt, and R. Bestehorn, "Entwicklung und technische Durchführung eines neuen Verfahrens zur Gewinnung von Wasserstoff and Wasserstoff-Stickstoff-Gemischen" ["Development and operation of a new process for hydrogen and hydrogen-nitrogen mixtures"], Berichte der Gesellschaft für Kohlentechnik, 3, (1930) 211-370.

6. G.P. Curran, C.E. Fink, and E. Gorin, "CO_2 Acceptor Gasification Process - Studies of Acceptor Properties", in Advances in Chemistry Series, Number 69, "Fuel Gasification", American Chemical Society (1967) 141-165.

7. A.M. Squires, "Cyclic Use of Calcined Dolomite to Desulfurize Fuels Undergoing Gasification", in Advances in Chemistry Series, Number 69, Fuel Gasification", American Chemical Society (1967) 205-229.

8. A.M. Squires, "Gasifying Oil for Clean Power", A.I.Ch.E. New York meeting, November, 1967.

9. T. Uno, Tetsu To Hagana, 37 (1951) 14-17.

10. T. Rosenqvist, "A Thermodynamic Study of the Reaction $CaS+H_2O = CaO+H_2S$ and the Desulfurization of Liquid Metals with Lime", J. Metals Trans. A.I.M.E., 3 (1951) 535-540.

11. K.J. Hill and E.R.S. Winter, "Thermal Dissociation Pressure of Calcium Carbonate", J. Phys. Chem., 60 (1956) 1361-1362.

12. Joint Army, Navy, and Air Force Thermochemical Tables, (JANAF Tables) prepared under direction of D.R. Stull, Thermal Research Laboratory, Dow Chemical Company, Midland, Michigan (1960-65), First Addendum, August, 1966.

13. W.M. McKewen, "Kinetic of Reduction of Iron Ores", in Physical Chemistry of Steelmaking, ed. by J.F. Elliot, M.I.T. Press (1965) 141-154.

14. K. Laidler, Chemical Kinetics, 2nd ed., McGraw-Hill, New York (1965) 265-270.

15. N.L. Johnson and F.C. Leone, Statistics and Experimental Design in Engineering and the Physical Sciences, Vol. 1, John Wiley and Sons, New York (1964) 413-415.

16. I.M. Ausman and C.C. Watson, "Mass Transfer in a Catalyst Pellet During Regeneration", Chem. Eng. Sci., 17 (1962) 323-327.

17. P.B. Weisz and R.B. Goodwain, "Combustion of Carbonaceous Deposits within Porous Catalyst Particles", J. Catalysis, 6 (1966) 227-236.

18. D. Luss and R. Amundson, "Maximum Temperature Rise in Gas-Solid Reactions", A.I.Ch.E.J., 15, 2 (1969) 194-215.

19. O. Levenspiel, Chemical Reaction Engineering, John Wiley and Sons, New York (1962) 348.

20. R. Bird, W. Stewart, and E. Lightfoot, Transport Phenomena, John Wiley and Sons, New York (1965) 647.

21. P.B. Weisz, "Diffusivity of Porous Particles: I. Measurements and Significance for Internal Reaction Velocities", Zeitschrift für Physikalische Chemie, Neue Folge, 11 (1957) 1-15.

22. A.J. Shaler, "Activated Sintering - A Review", in Sintering and Related Phenomena, ed. by G.C. Kuczynski, N.A. Hooten, and C.F. Gibbon, Gordon and Breach, Science Publishers, New York (1967) 807-828.

23. A.M. Squires, "Process and Apparatus for Desulfurizing Fuels", U.S. Patent, 3,481,834, December 2, 1969.

24. L. Ruth, A.M. Squires, and R.A. Graff, "Desulfurization of Fuels with Calcined Dolomite, III. First Results for Reaction of $CaCO_3$ with H_2S", paper to be presented at Los Angeles meeting of American Chemical Society, March, 1971.

25. W.J. Thomas and U. Ullah, "Chemisorption of Hydrogen Sulfide and Carbon DiSulfide on Nickel Oxide and Vanadium Pentoxide", J. Catalysis, 15 (1969) 342-354.

26. A.J. DeRosset, C.G. Finstrom, and C.J. Adams, "Adsorption of H_2S on Alumina at Low Coverages", J. Catalysis, 1 (1962) 235-243.

27. V.S. Al'tshuler, G.V. Klirikov, and A.A. Gavrilova, "Gasification of Petroleum Residues and Removal of H_2S, Khim, Pererabotka Topliv (Khim. i Tekhnol.), Akad. Nauk SSSR, Inst. Goryuch. Iskop, (1965) 144-154; Chem. Abs., 63, 9720d.

28. V.S. Al'tshuler and A.A. Gavrilova, Gazov. Protessy, Poluch, Energ. Tekhnol. Gazov, Akad, Nauk SSSR, Inst. Goryuch, Iskop. (1967) 79-99, 105-110; Chem. Abs., 68, 81162h-4k, 69, 78961x.

29. M.L. Vestal and W.H. Johnston, "Desulfurization Kinetics of Ten Bituminous Coals", Report number SRIC 69-10 from Scientific Research Instruments Corp. to Public Health Service, National Air Pollution Control Administration (1969).

30. F. Halla, "Thermodynamics of Formation of Dolomite", J. Phys. Chem. 69, 3 (1965) 1065.

31. W.H. MacIntire and T.B. Stansel, "Steam Catalysis of Dolomite and Limestone Fines", Ind. Eng. Chem., 45, 7 (1953) 1548-1545.

32. A.O. Wist, "Determination of the Activation Energy Change of $CaCO_3$ Under the Influence of Various Environmental Gases", in Thermal Analysis, ed. by R.F. Schwenker, Jr. and P.D. Garn, Academic Press, New York (1969) 1095-1110.

33. N.F. Bryantseva and S.I. Khvosten'kov, "Influence of Calcination Conditions of the Physiochemical Properties of Dolomites", J. Applied Chemistry USSR, 41, 6 (1968) 1128-1133.

34. J.L. Eades and P.A. Sandberg, "Scanning Electron Microscope Study of Development and Distribution of Pore Space in Calcium Oxide", in Scanning Electron Microscopy/1969, IIT Research Institute, Chicago (1970) 383-388.

35. A.J. Dedman and A.J. Owen, "Calcium Cyanamide Synthesis: Part 4. The reaction $CaO+CO_2 = CaCO_3$", Trans. Faraday Soc., 58 (1962) 2027-35.

36. G.P. Curran, C.E. Fink and E. Gorin, "Production of Low-Sulfur Boiler Fuel by Two-Stage Combustion: Application of CO_2 Acceptor Process", paper presented at Second International Conference on Fluidized-Bed Combustion", Hueston Woods, Ohio, October 4-7, 1970, sponsored by Air Pollution Control Office, Environmental Protection Agency [revision of December 2, 1970].

37. G. Moss "The Fluidized Bed Desulfurizing Gasifier", paper presented at Second International Conference on Fluidized-Bed Combustion, Hueston Woods, Ohio, October 4-7, 1970, sponsored by Air Pollution Control Office, Environmental Protection Agency.

38. G.P. Curran, C.E. Fink, and E. Gorin, "Phase II, Bench-Scale Research on CSG Process: Operation of the Bench-Scale Continuous Gasfication Unit", R and D. Report No. 16, Interim Report No. 3, Book 3, from Consolidation Coal Company to Office of Coal Research, no date [reporting on work in period: Dec. 1, 1965, to July 1, 1968].

12.0 Vita

Melvyn Pell was born in New York City on July 11, 1942. He received his elementary and secondary education in the New York City Yeshiva School System. He entered the City College in September 1959 and graduated in January 1964 as a Bachelor of Chemical Engineering.

He then worked for Halcon International Inc. doing process research in organic chemicals until August 1966. During this time, he earned his Master of Engineering (Chemical) from The City College of New York. He worked for Yardney Electric Co. from August 1966 to Septmeber 1967 studying battery preparation methods.

In September 1967, he returned to The City College to pursue doctoral studies in the field of fuel desulfurization. The author is currently employed by Consolidation Coal Company in their research center at Library, Pennsylvania. He lives in Bethel Park, Pennsylvania, with his wife Ellen and son Craig.